Assessment of Long-Term Losses in Prestressed Concrete Structures

Application for Nuclear Reactor Containments

Elforsk rapport 12:74

Peter Lundqvist

2012

ELFORSK

Assessment of Long-Term Losses in Prestressed Concrete Structures

Application for Nuclear Reactor Containments

LUND
UNIVERSITY

Peter Lundqvist

Doctoral thesis

Copyright © Peter Lundqvist

Lund University, Division of Structural Engineering
P.O. Box 118, SE-221 00 Lund, Sweden
Internet: www.kstr.lth.se
Report TVBK-1043
ISSN 0349-4969
ISRN LUTVDG/TVBK-1043/12-SE(161p)
ISBN 978-91-979543-4-1

Printed in Sweden by Media-Tryck, Lund University
Lund 2012

Preface

The work presented in this thesis has been carried out at the division of Structural Engineering at Lund University during the period 2007 to 2012. The project has been financed by ELFORSK, the Swedish Electrical Utilities R&D Company, with contributions from Vattenfall, EON, Fortum, Skellefteå Kraft and Karlstad Energi the power producing companies owning and operating the Swedish nuclear power plants, the Swedish Radiation Safety Authority and TVO, Teollisuuden Voima Oyj in Finland. Their financial support is gratefully acknowledged. I am also very grateful to the post-tensioning company Internordisk Spännarmering who assisted me with the post-tensioning of the test beams studied in this thesis.

I would like to express my gratitude to several of people which have helped me during these years:

To my supervisor Prof. Sven Thelandersson for his skillful guidance and encouragement during the entire project, especially in times of troublesome research results, which have not been few. Dr. Nils Rydén at Engineering Geology for his all help and supervision of the dynamic measurement part of this work, I have really enjoyed working with one of the best in this field. Dr. Patrick Anderson for his guidance and help during the first year of my PhD-studies. Per-Olof Rosenkvist for all the assistance and help with the laboratory work performed in this project and of course all other colleagues at the division who have contributed to making these years very enjoyable, especially Oskar, my fellow roommate.

Finally, I am grateful to my family and friends for their support both before and during my PhD-studies.

Abstract

Most nuclear reactors, both in Sweden and worldwide, are enclosed by a prestressed concrete containment. The main purpose of the containment is to prevent any radioactive discharge to the environment in the event of a major internal accident. The performance and structural integrity of the containment depends on the compressive stresses induced in the concrete by the prestressing system. However, due to shrinkage and creep in the concrete and relaxation in the tendons the prestress will decrease with time, significantly reducing the safety and accidental performance of the containment. The corrosion protection of tendons are for Swedish containments arranged in two different ways, either by cement grouting (bonded tendons) or e.g. by grease injection (unbonded tendons). The disadvantage with bonded tendons is that no possibility of assessing their status, e.g. measuring tendon forces, is possible as is the case for containments with unbonded tendons.

The objective of this thesis is to investigate different methods for determining the remaining tendon forces in prestressed concrete structures with an emphasis on the conditions inside nuclear reactor containments. The work has been divided into three different parts, the first in which prestress losses have been modeled using existing prediction models for creep and shrinkage of concrete and relaxation of the prestressing steel and compared to measured prestress losses in both test beams and losses measured in-situ in reactor containments. The test beams stored inside reactor containments showed very high losses compared to bridge beams of similar age, this difference was attributed to the climate in which the test beams were stored, i.e. around 30°C to 50°C and low relative humidity. For the test beams the prediction models significantly underestimated the measured losses. However, when applied for Swedish containments with unbonded tendons the models were in relatively good agreement with the measured prestress losses, a slight tendency for overestimating the losses was observed. In addition, it was shown that the accuracy of the models increased when modified by taking the actual drying conditions into account.

In the second part a first step in the development of a nondestructive method for monitoring the prestress losses based on resonant ultrasound spectroscopy in the context of acoustoelasticity is presented. Several previous studies have shown that the resonance frequencies of concrete structures are stress dependent, i.e. they

increase with the applied compressive stress. However, based on linear elasticity this behavior has been difficult to explain. In this work short-term dynamic measurements on prestressed concrete beams have confirmed this stress dependency and also explained this behavior through the theory of acoustoelasticity, which in short states that the elastic constants of a material, and hence the resonance frequencies, are stress dependent. A finite element model based on Murnaghan's third order elastic theory confirmed this stress dependency. Long-term measurements on the same beams showed that the resonance frequencies can be measured continuously over a longer period of time and that by taking the development of the modulus of elasticity with time into account the decrease in resonance frequencies follows the loss of tendon forces. These results show that a change in the state of stress in a simple concrete structure can possibly be monitored by measuring the resonance frequencies of the structure.

The third part consists of an investigation on the influence of an elevated temperature on the prestress losses in prestressed concrete test beams. Six of these beams were subjected to a climate similar to that of reactor containments and two were subjected to a normal indoor climate for a period of almost three years. The prestress losses in the beams subjected to the elevated temperature were approximately 25 % higher than the ones subjected to the normal indoor climate. In addition, there was no significant difference between the prestress losses in beams with bonded and unbonded tendons. The prestress losses in the beams were determined using the co-called crack re-opening method, in which the load required to reopen a flexural crack in the bottom of the beam is determined. Since the stress in the bottom fiber of the beam is zero at the instant the crack reopens, the remaining tendon force can easily be calculated. It was found that the normal procedure for determining the crack reopening load underestimates the tendon forces and that the accuracy for determining the crack re-opening load can be greatly increased by using a simple two-dimensional finite element model of the testing procedure.

Keywords: Nuclear reactor containments, prestressed concrete, prestress losses, bonded tendons, creep, shrinkage, relaxation, prediction models, resonance frequency, acoustoelasticity.

Sammanfattning

En kärnkraftsreaktor är försedd med flera separata skyddsbarriärer, varav den viktigaste är den så kallade reaktorinneslutningen vars primära syfte är att förhindra radioaktiva utsläpp till omgivningen i samband med en allvarlig olycka. I både Sverige och Finland är inneslutningen utformad som en betongcylinder vilken är spännarmerad både vertikalt och horisontellt. Syftet med spännarmeringen är att motverka de dragspänningar som uppstår i betongen på grund av det inre övertryck som uppstår i inneslutningen vid en allvarlig olycka i reaktorn. Vilket betyder att säkerheten i reaktorinneslutningen är direkt beroende av spännkraftsnivåerna i spännstålet. Det stora problemet med spännarmerade konstruktioner är att spännkraften minskar med tiden på grund av krypning och krympning i betongen och relaxation av spännstålet, vilket påverkar säkerheten i konstruktionen negativt. Korrosionsskyddet av spännkablarna i de svenska reaktorinneslutningarna är utformat på två principiellt olika sätt, antingen är foderrören ingjutna med cement och därmed hopgjutna med konstruktionen eller så injekteras foderrören med till exempel rostskyddsfett eller ventileras med torrluft. Nackdelen med de cementinjekterade spännkablarna är att spännkraften inte går att mäta efter injekteringen, något som utförs regelbundet på de inneslutningarna som har fria spännkablar.

Det primära syftet med denna avhandling är att undersöka olika metoder för att uppskatta spännkraftsförluster i spännbetongkonstruktioner, med fokus på de förhållanden som råder för en reaktorinneslutning. Arbetet är indelat i tre olika delar, i den första delen jämfördes uppmätta spännkraftsförluster i både gamla testbalkar och i reaktorinneslutningar med förluster beräknade med olika modeller för att prediktera krypning, krympning och relaxation. Som en del av detta arbete utfördes tester av gamla spännarmerade balkar som förvarats i två finska reaktorinneslutningar i mer än 30 år. Resultaten från försöken visade att förlusterna i dessa balkar var väldigt höga jämfört med resultat från försök på gamla brobalkar. Förklaringen till detta antas vara klimatet som testbalkarna förvarats i, det vill säga temperaturer mellan 30°C och 50°C och en låg relativ fuktighet. Modelleringen av spännkraftsförlusterna visade att samtliga prediktionsmodeller kraftigt underskattade de uppmätta förlusterna. När samma modeller användes för att beräkna spännkraftförlusterna i svenska reaktorinneslutningar med icke injekterade spännkablar, där spännkraften mäts kontinuerligt vid schemalagda inspektionstillfällen, var överensstämmelsen god

mellan beräknade och uppmätta förlusterna. För att förbättra noggrannheten i modellerna modifierades de genom att ta hänsyn till de faktiska klimatförhållandena som råder i inneslutningarna.

Den andra delen av arbetet handlade om att försöka utveckla en icke-förstörande provningsmetod baserad på en konstruktions dynamiska respons för att detektera spännkraftsförluster. Flertalet studier har visat att resonansfrekvenser för betongkonstruktioner är spänningsberoende, det vill säga att de ökar med nivån på tryckspänningarna. Dessa resultat har inte gått att förklara teoretiskt då resonansfrekvenserna bör minska med ökad spännkraft enligt en linjärelastisk modell. I den första studien i denna del utfördes dynamiska mätningar på ett antal spännarmerade betongbalkar under uppspänningen vilka bekräftade de tidigare resultaten. En teoretisk modell baserad på akustoelasticitetsteorin som förklarar resonansfrekvensernas spänningsberoende presenterades också i denna studie. Enligt akustoelasticitetsteorin är ett materials elastiska konstanter, till exempel elasticitets- och skjuvmodul, spänningsberoende och detta spänningsberoende beskrivs av tre ickelinjära elastiska konstanter, i litteraturen benämnda Murnaghans elastiska konstanter. En finita element modell baserad på Murnaghans konstanter bekräftade resonansfrekvensernas spänningsberoende. I den andra studien i denna del utfördes resonansfrekvensmätningar på samma balkar under en period av drygt 17 månader. Resultaten visade att efter att ha korrigerat för elasticitetsmodulens tillväxt på grund av cementets hydratation, minskade resonansfrekvenserna för balkarna på ett liknande vis som förlusten av spännkraft. Resultaten från dessa två studier visar att det är möjligt att uppskatta en ändring av spänningstillståndet i en spännarmerad betongkonstruktion genom att mäta en eller flera av konstruktionens resonansfrekvenser.

I den tredje delen av arbetet undersöktes påverkan av det klimat som råder inuti en reaktorinneslutning på spännkraftsförlusterna i ett antal spännarmerade betongbalkar. Sex balkar förvarades i ett klimatrum i en temperatur av cirka 42°C under en period av 33 månader. De övriga två balkarna förvarades i normal rumstemperatur, cirka 20°C. Fem av balkarna injekterades med cement, varav en förvarades i rumstemperatur. Spännkraftsförlusterna för balkar med injekterade spännkablar bestämdes genom ett trepunkts böjprov med syftet att bestämma den kraft som krävs för att åter öppna en befintlig böjspricka i underkant av balken. Vid denna last är spänningen i underkanten av balken noll och den kvarvarande spännkraften kan då enkelt beräknas. Resultaten från försöken samt mätningarna på de icke injekterade balkarna visade att spännkraftsförlusterna var cirka 25 % högre i de balkar som förvarats i den förhöjda temperaturen. Det var heller ingen mätbar skillnad i spännkraftförlust mellan balkar med injekterade och icke injekterade spännkablar. Utvärderingen av trepunktsböjproven visade att den allmänt vedertagna metoden för att bestämma den kraft som krävs för att åter öppna sprickan i balken leder till en överskattning av den kvarvarande

spännkraften, det vill säga att metoden underskattar spännkraftsförlusterna. Dock visade det sig att med hjälp av en enkel tvådimensionell finita element modell över försöket så kunde den kvarvarande spännkraften bestämmas med betydligt högre noggrannhet.

Sökord: Reaktorinneslutning, spännarmerad betong, spännkraftsförluster, cementinjekterade spännkablar, krypning, krympning, relaxation, prediktionsmodeller, resonansfrekvens, akustoelasticitet.

Table of Content

Appended papers

Paper I

Lundqvist P., Rihiimäki J., 2010, Testing of five 30-year-old prestressed concrete beams, PCI Journal, Vol. 55, No. 4, pp. 50-58.

Paper II

Lundqvist P., Nilsson L-O., 2011, Evaluation of prestress losses in nuclear reactor containments, Nuclear Engineering and Design 241, pp. 168-176.

Paper III

Lundqvist P., Rydén N., 2012, Acoustoelastic effects on the resonance frequencies of prestressed concrete beams – short-term measurements, NDT&E International, Vol. 50, September, pp.36-41.

Paper IV

Lundqvist P., Rydén N., 2012, Acoustoelastic effects on the resonance frequencies of prestressed concrete beams – long-term measurements, submitted to NDT&E International.

Paper V

Lundqvist P., 2012, Thermal effects on long-term loss in prestressed concrete, submitted to Construction and Building Materials.

1. Introduction

1.1. Background

In Sweden, approximately half of the electrical power is produced by nuclear power plants. In total, the Swedish nuclear power industry operates ten reactors, located at the three nuclear power plants Forsmark, Oskarshamn and Ringhals. Forsmark and Oskarshamn are both located on the east coast and have each three reactors in operation. Ringhals is located on the west coast and operates four reactors. Two types of reactors are used in Sweden, the boiling water reactor (BWR) and the pressurized water reactor (PWR); these are both of the generation 2 type reactors and are the most common types of reactors in the world. In Sweden, the most common is the BWR which is used in all three power plants, except for three of the reactors at Ringhals which are of the PWR type.

In case of a severe internal accident, several independent safety systems prevent any radioactive discharge to the environment. The most important of the barriers is the reactor containment enclosing the reactor. Both in Sweden and worldwide the most common design of the containment is a concrete structure which is prestressed by both horizontal and vertical steel tendons. The corrosion protection of the tendons is accomplished either by cement grouting (bonded tendons) or by injection of, for example, grease (unbonded tendons). In Sweden, both of these systems are used: unbonded tendons are used in six of the reactors (Forsmark and Ringhals) and the remaining four have bonded tendons (Oskarshamn and one at Ringhals). Worldwide, the most common of the two systems are the unbonded tendons, for example used in the U.S, bonded tendons are for example used in Finland and France.

The main accident scenario which the containment is designed to withstand is the so-called LOCA, loss of coolant accident. A LOCA can be initiated by e.g. a pipe rupture in the cooling system discharging hot steam into the containment. The release of steam increases both the temperature and pressure inside the containment, which induces tensile stresses in the concrete walls. The purpose of the prestressing system in the concrete walls is to counterbalance these tensile forces, i.e. maintain the concrete in a compressive state of stress and prevent any cracking of the concrete. To further increase the leak tightness of the containment

it is a common practice to provide the inside of the containment wall with a steel liner. Even though the main purpose of the containment is to protect the ambient areas from nuclear contamination it is also designed to withstand external actions, for example earthquakes, explosions and air craft crashes.

One of the major problems with prestressed concrete structures is that the prestress forces will decrease with time due to long-term effects in both the concrete and the prestressing steel. As described earlier, both the safety and structural integrity of the containment depend on the compressive stresses in the concrete and it is therefore important to be able to measure these prestress losses. In containments with unbonded tendons the tendon forces are monitored by measurements performed at regular intervals. However, for containments with bonded tendons no method for measuring the tendon forces exists.

1.2. Objectives

The objective of this thesis is to investigate different methods for predicting or estimating the prestress losses in prestressed concrete structures with bonded tendons. The main focus is on the bonded tendons in the Swedish and Finnish nuclear reactor containments and the influence of the unusual climatic conditions on the prestress losses that these structures are subjected to. This is also the topic of three of the appended papers, i.e. paper I, II and V. In the remaining two papers, paper III and IV, a non-destructive testing method has been used to investigate the influence of compressive stresses on the resonance frequencies of prestressed concrete beams by applying the theory of acoustoelasticity.

1.3. New research

The most important new research findings in this thesis are given below:

- Tests on five 30-year-old prestressed concrete beams stored inside one of the Finnish reactor containment showed that the prestress losses in the beams were greater than those obtained from tests of bridge beams in the literature. The reason for the high losses was attributed to the ambient climate in which the beams were stored (Paper I).
- The accuracy of the most commonly used prediction models for creep and shrinkage of concrete can be increased by taking the actual drying conditions into account. Further, it was also found that the difference between the models mostly depends on the prediction of creep (Paper II).

- A change in the state of stress in a concrete structure can be estimated by measuring the resonance frequencies of the structure. This observed stress dependency of the resonance frequencies of prestressed concrete structures can be described by the theory of acoustoelasticity. (Paper III).
- Long-term measurements over a period of 17 months of resonance frequencies on the prestressed concrete beams described in paper III were performed. It was found that it is possible to measure the resonance frequencies continuously over a longer period of time with good accuracy and reliability and that after correcting for the development of the modulus of elasticity with time, the change in resonance frequencies correlates with changes in tendon forces. The results also show that resonance frequencies are affected by the ambient temperature and relative humidity. (Paper IV).
- Measurements and testing of eight prestressed concrete beams subjected to similar climatic conditions as that of reactor containments showed that elevating the temperature from 20°C to 40° increased the prestress losses with approximately 25 %. Further, the testing of the beams using the so-called crack re-opening method showed that there are uncertainties attached to the normal procedure for interpreting the remaining tendon forces. A new method for determining the crack re-opening load based on a FE-analysis is proposed. (Paper V).

1.4. Outline of thesis

This thesis consists of five appended research papers, of which three are peer-reviewed and published and two are submitted for publication, concerning prestress losses in concrete structures, with an emphasis on the special conditions inside Swedish and Finnish nuclear reactor containments. Four chapters in this thesis will provide the reader with additional background information describing the treated subjects more thoroughly. In the final chapters the appended papers are summarized and the major conclusions from this work are provided separately along with some suggested further research needs in this field.

2. Nuclear reactor containments

2.1. The nuclear reactor

The two most common electricity generating nuclear reactors are the boiling water reactor (BWR) and the pressurized water reactor (PWR), which both are of the generation 2 type of reactors. In Sweden, the most common is the BWR which is used in all three power plants, except for three of the reactors at Ringhals which are of the PWR type. In Finland, four reactors are currently in operation, two BWR´s at Olkiluoto nuclear power plant and two PWR´s at Loviisa nuclear power plant. The similarities in design between the Swedish and Finnish power plants are many, especially regarding the containment, which means that the main part of the descriptions given in this chapter applies to both the Swedish and Finnish power plants.

Boiling water reactor

Approximately 25 % of the reactors worldwide are of the BWR type and it is the second most common type of nuclear reactor. The principal outline of the BWR type of reactor is shown in figure 2.1. The nuclear energy which is produced in the BWR through nuclear fission is used to generate steam by boiling the cooling water inside the reactor tank, (1) in figure 2.1. The produced steam is used to drive the turbines (2) which in turn power the generators (3). The electricity produced in the generators is sent to the power grid through a transformer (4). After the steam has escaped the turbine it is passed through a condenser (6) thus being converted back to water and returned to the reactor tank. Usually sea water (5) is used to cool the steam in the condenser, but cooling towers can also be used. The circuit in the reactor is closed and the cooling water never comes in contact with the sea water.

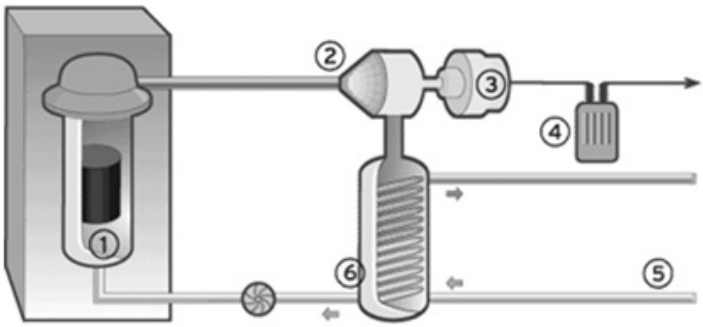

Figure 2.1. Principal outline of the BWR, www.vattenfall.se.

Pressurized water reactor

The PWR is the most common reactor type and more than 50 % of the reactors worldwide are of this type, CEB-FIP Bulletin 13 (2001). The principal outline of the PWR type of reactor is shown in figure 2.2. In a PWR the cooling water is prevented from boiling due to the high pressure inside the reactor tank (1) which is controlled by a pressure vessel (2). The heated cooling water is then delivered to the steam generator (3) causing the water in the steam generator to boil. This steam is then used to drive the turbines (4), which power the generators (6). The electricity produced in the generators is sent to the power grid through a transformer (5). The steam is then converted back to water in the condenser (7), as for the BWR, the condenser is cooled by sea water (8). Both the circulatory systems, i.e. the steam generators and the reactor tank, are closed and no exchange of water occurs.

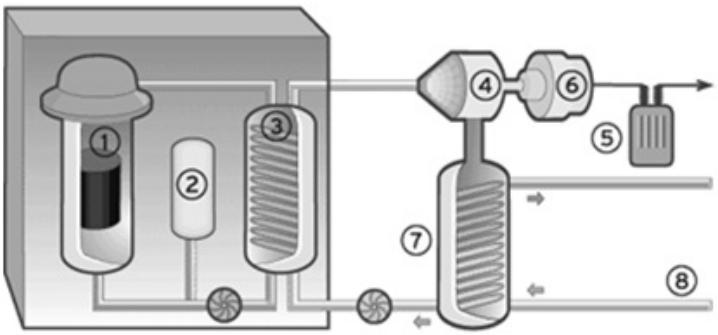

Figure 2.2. Principal outline of the PWR, www.vattenfall.se.

2.2. Nuclear safety, the defense in depth

The safety of a nuclear power plant is based on the concept of defense in depth, which means that accidents are prevented and mitigated through the use of several independent levels of protection, IAEA (2006). The concept is that if one of the protection levels fails, then the subsequent levels will prevent any harmful effects to the environment or to people in surrounding areas. This means that all of the protective levels must fail before an accident will have any impact on people or the ambient environment and these events have a very low probability to occur. The defense in depth is divided into five different levels of protection, where the first four levels concern the prevention and mitigation of radioactive release, e.g. through the physical safety barriers and the last level concerns off-site emergency measures to protect the environment and the public in case of a major radioactive discharge IAEA (1996).

The function of the different levels is described in Defense in depth in nuclear safety published by IAEA in 1996. Level 1 regards the prevention of abnormal operation and failures through conservative provisions in e.g. design, construction and operation of the nuclear power plant. Examples of such provisions are education and training of the operating staff and the choice of appropriate materials and construction processes during the design state. Level 2 regards the control of abnormal operation and failures, for example through automatic control systems. In-service inspections and testing of the safety systems are measures which also are included in the second level of protection. The third level comprises the control of accidents within the design basis, i.e. the engineered safety systems which prevents the progression of an ongoing accident. The main focus is on preventing damage on the reactor core, which e.g. can be fulfilled by emergency cooling systems. The main purpose of the fourth level is to minimize both the probability of a severe damage on the reactor core and the release of radioactive material to the environment in case of a serious internal accident. A very important safety system is the reactor containment, which encloses the reactor core and is designed to withstand a severe internal accident and thus the discharge of any radioactive material. The fifth and final level regards the off-site emergency plans, i.e. if all the other levels of protection have failed and radioactive material has been released. This comprises the collection of information regarding exposure and the actions which the authorities take to minimize the harmful effects of the accident.

2.3. The safety systems in the nuclear power plant

One of the most severe failure modes in a nuclear power plant is the co-called loss of coolant accident (LOCA), e.g. both the accidents in the nuclear power plants at Three Mile Island in 1979 and Fukushima in 2011 were caused by the loss of cooling water. A LOCA can for example be initiated by a pipe rupture in the cooling system or by a complete electric power cut-off. If the coolant system is damaged, e.g. reduced flow of coolant, the emergency shutdown system will stop the chain reactions in the core, it will, however, still continue to produce heat which needs to be removed. A failure to remove this surplus heat can result in damage on the reactor core or in worst case causes a core melt accident. During a severe LOCA the temperature in the core will increase and thus also the internal pressure inside the reactor vessel, which is referred to as the design pressure since this is the overpressure which the safety systems are designed to withstand. For containments worldwide the design pressure normally varies between approximately 0.1 and 0.6 MPa depending on the design of the containment, CEB-FIP Bulletin 13 (2001). For the Swedish containments the design pressure is 0.45 to 0.6 MPa, Barslivo et al. (2003).

Several different and independent safety barriers prevent the discharge of any radioactivity to the ambient areas in case of a severe internal accident, see figure 2.3. The first barrier is actually the fuel itself which melts at a temperature of 2 800°C. The second barrier is the fuel rods encapsulating the fuel which are made of Zircalloy and are completely air tight. The reactor vessel is the third barrier which is made of approximately 20 cm thick steel. The fourth barrier is the reactor containment enclosing the reactor vessel. This is a very important barrier and the design is usually that of a concrete cylinder, approximately 1 m thick and prestressed both horizontally and vertically. The reactor containment is designed to withstand the increased internal pressure caused by a LOCA. It also protects the reactor vessel from any outer actions, such as airplane crashes and explosions. The reactor containment is described in more detail in the following sections of this chapter. For a BWR the containment is enclosed by a secondary structure shielding it from the ambient climate, as can be seen in figure 2.3, and is considered as the fifth safety barrier.

In Sweden, all of the reactor containments are provided with two additional safety systems, which are intended to reduce the pressure inside the containment in case the internal pressure exceeds the design pressure, i.e. system 361 and 362, Barslivo et al. (2003). System 362 relieves the pressure in the containment by discharging the surplus air through a filter and out into the atmosphere, the filter removes more than 99 % of the radioactive particles in the air. For the Swedish containments the systems 362 is designed to relieve the containment at an internal

pressure of around 0.65 MPa, Barslivo et al. (2003). In case the capacity of system 362 is insufficient, i.e. unable to lower the pressure rapidly enough, system 361 will discharge the radioactivity directly to the atmosphere for a maximum of 20 minutes. In addition, several other safety systems also exist, such as emergency cooling systems, which e.g. can flood the reactor in case of a severe LOCA, and reserve electrical power units.

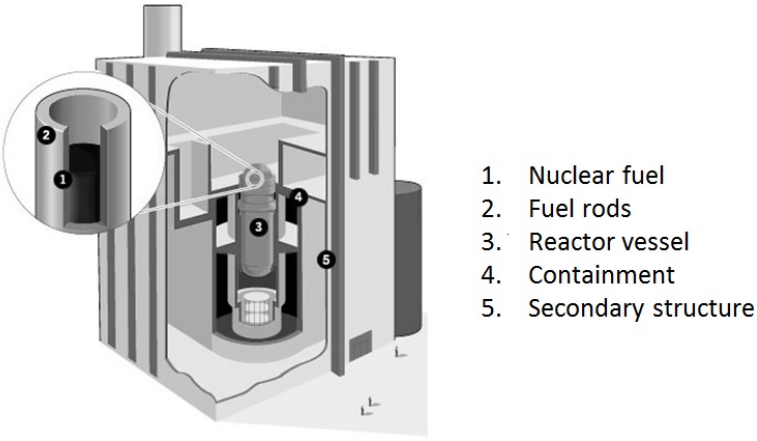

Figure 2.3. The different safety barriers in a boiling water reactor, www.vattenfall.se.

2.3. Function of the containment

A nuclear containment system should fulfill the following safety functions according to the IAEA Safety guide NS-G-1.10 (2004):

- Confine radioactive materials during both operational and accidental conditions
- Protect the reactor against external events, both natural and those caused by humans
- Shield off radioactive radiation during both operational and accidental conditions

These functions are not met by the containment alone, especially during the operational state when e.g. ventilation systems with filtration capability prevent the release of radioactive material from the reactor core. The main function of the containment structure is to prevent any radioactive discharge in case of a severe accident, i.e. it should both maintain its structural integrity and provide sufficient

leak tightness. The acceptance criteria which should be considered during the design are divided into three levels for both the leak tightness and the structural integrity of the containment structure, IAEA (2004). During a severe accident the structural integrity should not exceed level 3 which corresponds to the ultimate load bearing capacity. At level 3, large permanent deformations of the containment are expected along with some minor local damage. Even though the ultimate load bearing capacity is the upper limit for the structural integrity, the leak tightness is limited to level 2, which means that only a very limited leakage is allowed.

To assure that the structural integrity and leak tightness of the reactor containment are adequate before start of operation and during its entire service life inspections are performed before start of operation and at regular intervals throughout the structures entire service life, so called in-service inspections. The in-service inspections include both pressure tests and inspections of the tendons, which are further described in section 2.5.2. Before the start of operation and just after the completion of the construction work the initial structural integrity test is performed to evaluate the elastic behavior and bearing capability of the containment, CEB-FIP Bulletin 13 (2001). The test is performed by increasing the air pressure inside the containment up to the design pressure in order to verify that e.g. the strains and deformations at the design pressure are within the limits of the design calculations and also that the deformations are reversed after completion of the test. Just prior to the start of operation the preoperational leakage test is performed in steps up to the design pressure which is maintained for 24 hours. The objective is to verify that the leak tightness of the containment is satisfactory, especially at critical points such as penetrations and valves. In service surveillance leakage tests similar to the preoperational one are performed at regular intervals during the entire service life of the containment, the first after approximately three years and then every ten years, in order to verify that the leak tightness of the containment is satisfactory.

2.4. Outline of the containment

The main design of the containments is that of a concrete cylinder topped either by a steel lid or concrete dome. The thickness of the concrete walls varies between 0.8 to 1.2 m, depending on the type of containment. A thin steel liner, approximately 5 to 10 mm thick, is mounted on the inside of the walls, securing the leak tightness of the containment in case of an accident. The inside of the steel liner is protected by a reinforced concrete wall, with a thickness of approximately 0.3 m. The outline of the containments for the two different types of reactors in Sweden is described below.

High quality water tight concrete was used for the containments with a characteristic compressive strength varying between 25 and 35 MPa. Typically slow hardening cement was used with a cement content varying between 250 up to 450 kg/m3, the water to cement ratio varied between 0.4 and 0.5. For the ordinary steel reinforcement, the quality Ks40s was primarily used, which has characteristic yield strength of 390 MPa. The diameters of the bars varied between 16 and 40 mm.

Pressurized water reactor

The containment of a PWR encloses not only the reactor vessel but also auxiliary systems such as steam generators and pressurizers and is therefore a large structure, the cylindrical concrete walls have a diameter of approximately 35 m and the height of the structure is around 60 m, Roth et al. (2002). Due to the size of the containment it is not enclosed by a secondary containment building, as is the case for the BWR, and the outer parts of the containment is therefore in contact with the outdoor climate. The walls are prestressed both horizontally and vertically with hundreds of tendons and also supplied with large amounts of ordinary steel reinforcement. The total thickness of the walls is 1.1 m, where the outer load bearing part is 0.76 m thick, which is the part which is prestressed. On the inside of the outer wall a steel liner with a thickness of approximately 10 mm secures the leak tightness in case of a severe accident. The inside of the steel liner is protected from missiles by a reinforced concrete wall which is 0.33 m thick. The main outline of the PWR containment of Ringhals unit 3 is shown in figure 2.4.

The cylindrical walls are topped with a prestressed concrete dome which is 0.8 m thick. The steel liner in the dome is not protected by an inner concrete wall. At the top of the vertical wall a ring beam with a height of 7 m and a thickness of 1.8 m constitutes the connection between the wall and dome. The concrete cylinder is founded on a 3.5 m thick reinforced concrete slab, where the leak tightness is secured by a 5 mm steel liner placed on the top of the slab. The steel liner is in turn protected by a 0.2 m thick layer of clay aggregates submerged in water, on top of this there is a 0.3 m thick reinforced concrete slab.

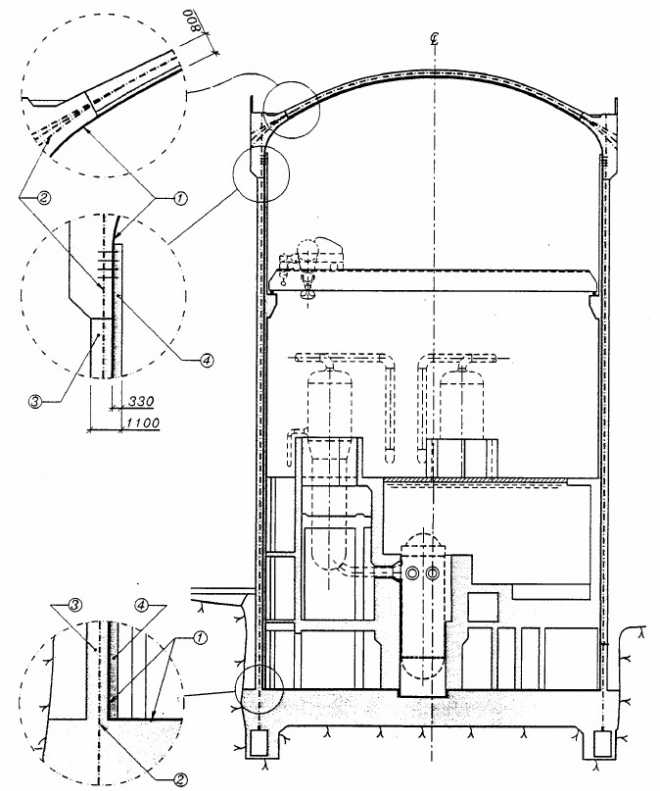

Figure 2.4. Main outline of a PWR containment. Number 1 points to the steel liner, number 2 to the tendons, number 3 the outer wall and number 4 to the inner wall, Roth et al. (2002).

Boiling water reactor

Unlike the PWR containment, the BWR containment only encloses the reactor vessel which, along with all the auxiliary systems, in turn is enclosed by a second containment. The BWR containment consists of two parts, the wet well and the dry well, respectively. In case of a LOCA the hot steam will be forced down to a suppression pool in the wet well where it condenses, which lowers the pressure inside the containment. This internal pressure suppression system allows the volume of the BWR containment to be significantly smaller than that of a PWR, the inner diameter varies between 18 to 25 m and the height is around 27 m, Roth et al. (2002).

As for the PWR containment, the cylindrical concrete walls of the BWR are prestressed horizontally and vertically and also supplied with large amounts of ordinary reinforcement, e.g. the reinforcement ratio for the walls at Forsmark is between 2.2 and 3.5 %, Roth et al. (2002). Leak tightness is secured by the steel

liner on the inside of the walls and is in turn protected by a reinforced concrete wall. The total thickness of the walls varies between 1 and 1.5 m for the different Swedish containments. The design of the top of the containment varies between the different containments, the most common design is that the concrete cylinder is topped by a reinforced or prestressed concrete slab with the shape of a ring beam, see figure 2.5. Independent of the design of the top part, a steel lid covers the top of the reactor vessel. The steel lid allows access to the reactor vessel e.g. for maintenance work. The designs of the foundations for the BWR containments vary between the Swedish containments depending on the geological conditions at the sites.

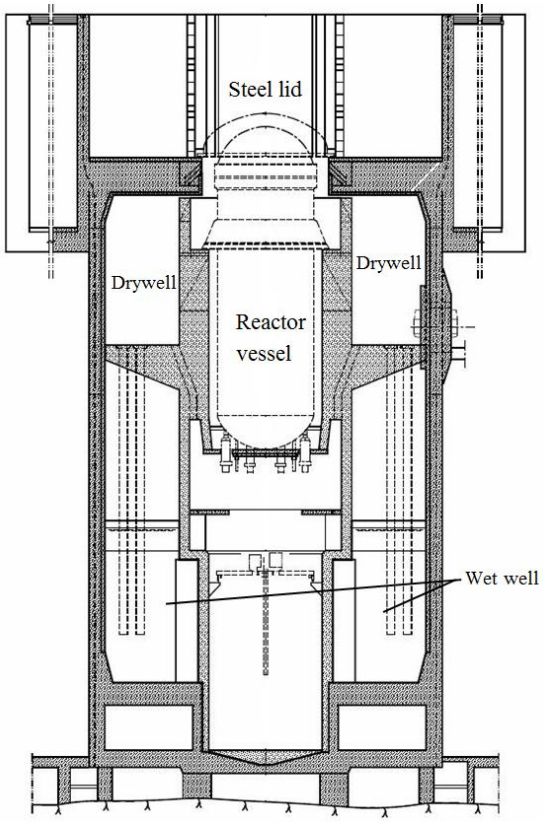

Figure 2.5. Main design of the BWR containment at Forsmark unit 1, (partly from Roth et al., 2002).

2.5. Tendons

2.5.1. Arrangement and outline of the tendons

The containments are prestressed both in the horizontal and vertical direction using the post-tensioning technique, the main features of the prestressing system for the different types of containments are shown in figure 2.6. The vertical tendons are nominally straight and the horizontal tendons are more or less curved, in some cases with a total accumulated curving angle of more than 360°.

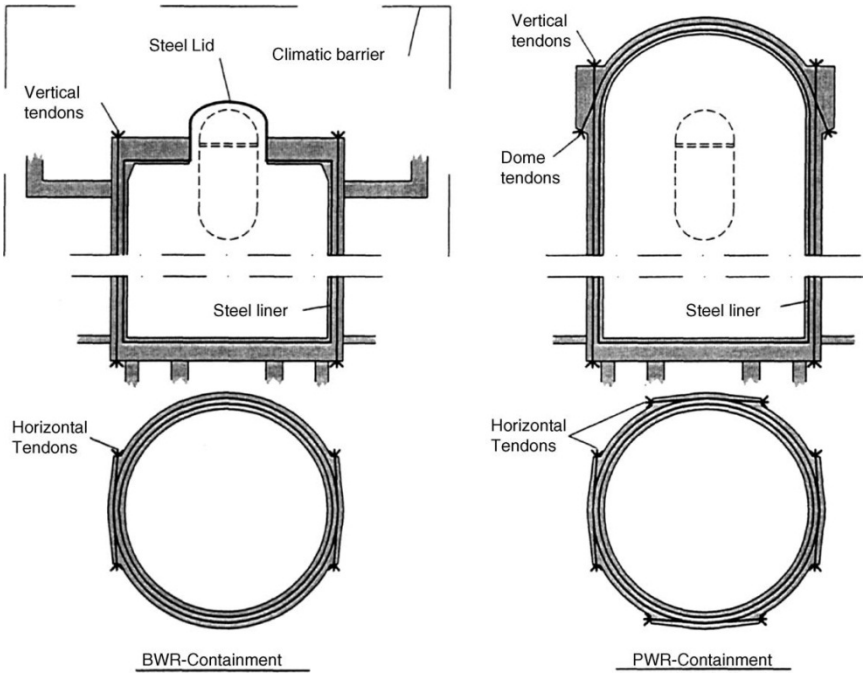

Figure 2.6. Main features of the prestressing system for the different types of containments, Anderson (2005).

In the Swedish containments two different types of post-tensioning systems have been used, BBRV (Birkenmaier, Brandestini and Ros type V) and VSL (Vorspann System Losinger). In both systems, the anchorage system consists of a bearing plate with split holding rings cast in the concrete. The post-tensioning force is transferred from the tendons to the bearing plate through a circular anchor head. The most frequently used VSL system is the 19x13, i.e. each tendon consist of 19 strands each with a diameter of 13 mm and each of these strands in turn consists of 7 wires. The strands of the tendons are attached to the anchor head using wedges,

see figure 2.7. In the BBRV system each tendon consists of a bundle of 72 individual wires each with a diameter of 6 mm. The ends of the wires have cold formed studs through which the tendon forces are transferred to the anchor head, see figure 2.7.

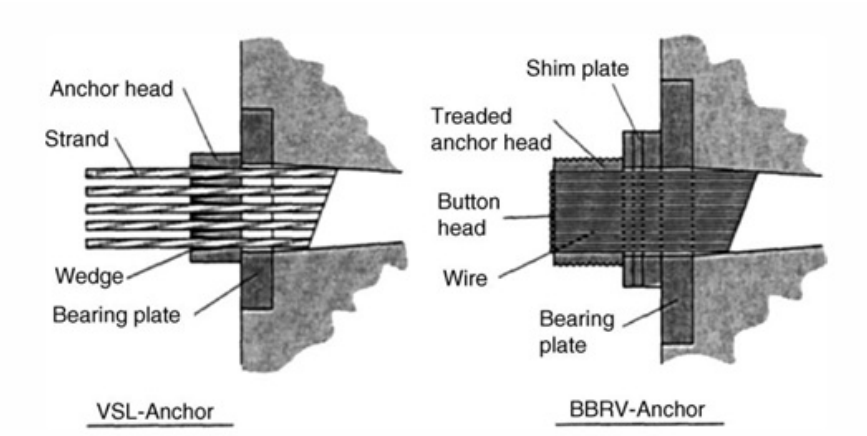

Figure 2.7. Details of the two prestressing systems used in the Swedish nuclear containments, VSL (to the left) and BBRV (to the right), Anderson (2005).

In the Swedish and Finnish reactor containments two different methods have been used for the corrosion protection of the tendons, bonded tendons where the ducts are injected with cement grout and unbonded tendons where the ducts are either injected with grease or ventilated with dry air. Bonded tendons are provided with a very robust protection from corrosion and are also well protected from local damages, for example if an anchor fails the tendon forces will be transferred from the tendons to the concrete through the bond between tendon and cement grout. Furthermore, due to the bond the tendon forces can be transferred to the concrete along the entire length of the tendon and not just at the anchors. The disadvantage with bonded tendons is that there is no possibility to assess the condition of the tendons or to measure the tendon forces. Even though the corrosion protection system for unbonded tendons is less reliable than that for bonded tendons, the advantage is that each tendon can be dismantled and inspected for corrosion or other defects and most importantly the tendon forces can easily be measured at any time. Table 2.1 lists the post-tensioning systems and corrosion protection systems which have been used in the Swedish and Finnish containments.

Table 2.1. Post-tensioning systems and corrosion protection systems used in the Swedish and Finnish nuclear containments.

Swedish containments	Post-tensioning system	Corrosion protection
Forsmark 1	VSL	Dry air ventilation
Forsmark 2	VSL	Dry air ventilation
Forsmark 3	BBRV	Dry air ventilation
Oskarshamn 1	BBRV	Cement grout
Oskarshamn 2	BBRV	Cement grout
Oskarshamn 3	VSL	Cement grout
Ringhals 1	BBRV	Cement grout
Ringhals 2	BBRV	Grease injection
Ringhals 3	BBRV	Grease injection
Ringhals 4	BBRV	Grease injection

Finnish containments	Post-tensioning system	Corrosion protection
Olkiluoto 1	VSL	Cement grout
Olkiluoto 2	BBRV	Cement grout

2.5.2. Measuring tendon forces

In Sweden, the tendon forces in the containments with unbonded tendons are inspected at regular in-service inspections (ISI) according to the United States Nuclear Regulatory Commission (U.S. NRC) Regulatory Guide 1.35 (1990). According to this guide the in-service inspections shall be performed 1, 3 and 5 years after the initial tensioning of the tendons and thereafter every 5th year. The tendons are divided into four groups depending on their shape, i.e. vertical, dome, hoop (horizontal) and U-shaped tendons. At each inspection the forces in 4 % of the total number of tendons in each group are measured using the so-called lift-off technique. The same type of hydraulic jack that is used for the tensioning of the tendons is used to lift the anchor head, see figure 2.8. In this case, the tendon force is defined as the force that is transmitted from the anchor head to the bearing plate, i.e. the force that causes the anchor head to lift off from the anchor plate. During the lift both the force applied by the hydraulic jack and the displacement of the anchor head are recorded. The lift-off force is then estimated from the force versus displacement diagram as the force as shown in figure 2.8. This procedure is very similar to the testing procedure for determining the tendon forces in prestressed concrete beams and according to the findings in the appended paper V it is probable that the true lift-off force corresponds to the point on the curve where it initially deviates from the linear behavior.

Apart from measuring the forces in the tendons at the ISI, some of the strands or wires from some of the tested tendons shall be dismounted and inspected for

corrosion or other material defects. Further, the anchorage of all tested tendons shall be inspected visually for damages or defects.

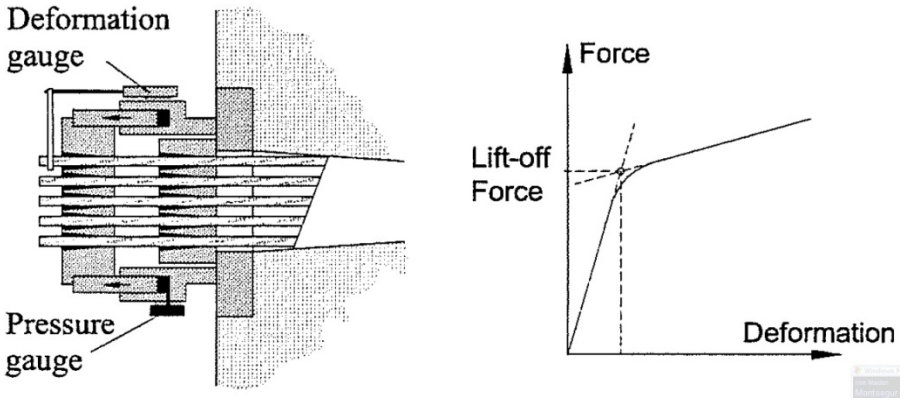

Figure 2.8. Principle of the lift off technique, Anderson (2005).

For containments with grouted tendons, where direct measurements of the tendon forces are impossible, two alternatives are presented in the U.S. NRC Regulatory Guide 1.90 (1977) for the monitoring of this system. In the first alternative the prestress levels are measured either by strain gauges attached to the tendons or by stress meters or strain gauges embedded in the concrete. The problem with this method is the long-term reliability of the sensors which must be embedded in the structure and can thus neither be calibrated or replaced. Other problems are also the influence of temperature changes on the sensors and that the prestress losses due to the relaxation of the tendons cannot be captured by strain gauges. However, embedded sensors, vibrating wire type in combination with temperature sensors, are used extensively in French containments with bonded tendons, CEB-FIP Bulletin 13 (2001), with positive results for evaluating the creep strains in the concrete. In the second alternative the elastic response of the containment is measured during the in service surveillance leakage tests and compared to the results from measurements performed at earlier pressure tests.

Pandey (1997) proposed a method for monitoring the prestress losses for containments with bonded tendons, where a number of post-tensioned test beams with identical properties as the containment walls are tested at regular intervals during the containments design life. The purpose of the beams is to verify that the prestress losses and material properties are within acceptable limits. In addition, the results from these tests are also used for distribution updating of the mechanical properties of the concrete in the containment, e.g. the tensile strength. This method is very similar to the purpose of the prestressed concrete beams tested in the appended paper I. These beams were manufactured with the same concrete

that was used for the containment walls of unit 1 and 2 at Olkiluoto nuclear power plant and were post-tensioned simultaneously as the walls. A total of nine beams were manufactured for each unit and the purpose of the beams was to, under the assumption that the behavior of the beams closely resembles that of the containments, monitor the prestress losses and degradation of the materials by testing one beam every third year. For a more detailed description of the properties of the beams see the appended paper I. Since the ducts of the beams were grouted the tendon forces could not be measured directly and the remaining tendon force were determined by a destructive test where a length of the tendon was exposed, instrumented with strain gages and then cut. From the contraction recorded by the strain gage the tendon force was calculated. Several other methods for estimating the prestress losses were also used, strain gages mounted on the ordinary reinforcement bars and vibrating wire strain gages embedded in the concrete, the strains in the concrete were also monitored using a deformometer measuring the distances between fixed points on the surface of the beams continuously. In addition, testing of the material properties, i.e. compressive strength and modulus of elasticity, were performed on specimens extracted from the beams as well as cylinders cast simultaneously as the beams. One strand of each tendon was also removed from the beams and subjected to a tensile strength test, it was also inspected for corrosion and other defects. However, the results from first couple of tests showed unreasonably high loss of tendon forces in the beams, which were deemed unreliable and the testing program was cancelled. One explanation for the high losses is that the development of both drying creep and shrinkage is size dependent, i.e. proportional to the drying rate of the structure. Due to the large difference in size, the drying rate and thus the development of prestress losses will be much faster for the test beams compared to reactor containments and the losses in the beams will therefore not be representative for those in a containment wall.

3. Prestress losses

3.1. Introduction

The major disadvantage with the prestressing systems in the nuclear reactor containments is that the tendon forces will decrease with time due to various long term mechanisms in both the concrete and the tendons. The long term prestress losses are due to contraction of the concrete, i.e. creep and shrinkage, and relaxation of the steel tendons. In addition, initial losses occur during the post-tensioning process, these are the elastic shortening of the concrete, friction between tendon and duct and slip in the anchor head when the post-tensioning force is transferred from the hydraulic jack to the anchor head. The losses due to slip in the anchor head are usually accounted for during the post-tensioning process by inserting thin steel plates between the anchor plate and anchor head.

In this chapter the different mechanisms causing the prestress losses are described along with methods for estimating and measuring losses in concrete structures, with an emphasis on the conditions inside a nuclear reactor containment.

3.2. Initial losses

3.2.1. Elastic shortening

The initial elastic shortening is the elastic response of the concrete during the post-tensioning process. Since the deformation is elastic it depends on the modulus of elasticity of the concrete and the contraction of the concrete will recover if the load is removed. Due to the large number of tendons in the containment, the elastic shortening will only add to the prestress losses for some of the tendons, i.e. the initially tensioned tendon will experience the highest losses and the tendon which was tensioned last will not be affected by elastic shortening. The contribution from the elastic shortening to the total prestress losses for a single tendon can be estimated according to equation 3.1.

$$\varepsilon_{el} = \frac{(N-n)}{N-1} \cdot \frac{\sigma_c}{E_c} \tag{3.1}$$

where:

ε_{el} = strain due to elastic shortening
σ_c = concrete stress, MPa
E_c = modulus of elasticity of concrete, GPa
N = number of tendons
n = the order in which the tendon was tensioned (for the initially tensioned tendon n is equal to 1)

3.2.2. Losses due to friction

Friction between the tendon and the duct can lead to prestress losses and uneven force distribution along the length of the tendon. Usually the losses due to friction are considered to originate from two different parts; the curvature of the tendon and wobbling, Collin and Mitchell (1991). The curvature losses are due to the change in bending angle of curved tendons introducing a normal force acting on the duct and thus multiplying this normal force with the friction coefficient between tendon and duct yields the loss of tendon force. Since the bending angles usually are quite small the friction losses are obtained as a function of the change in angle. Losses due to wobbling is caused by unintentional changes of the angle of the tendon, see figure 3.1, and depends mainly on the properties of the duct e.g. type and diameter of the duct and the spacing of the duct supports but also on the type of tendon and the form of the structure. The influence of wobbling is described by an empirically determined wobble coefficient k describing the unintentional changes in angle per unit length. The wobble losses over the length of the tendon are then obtained as the wobble coefficient multiplied with the length of the tendon. In Eurocode 2, the total losses due to friction are estimated as:

$$\Delta P_{\mu}(x) = P_{\max}\left(1 - e^{-\mu(\theta + kx)}\right) \tag{3.2}$$

where:

$\Delta P\mu(x)$ = loss due to friction, N
P_{max} = the initial tendon force at the active end, N
x = the distance along the tendon from the active end, i.e. where the tendon force is equal to P_{max}, m
μ = coefficient of friction between tendon and duct

θ = sum of the angular displacements over the distance x along the length of the tendon
k = coefficient accounting for the unintentional angular displacement

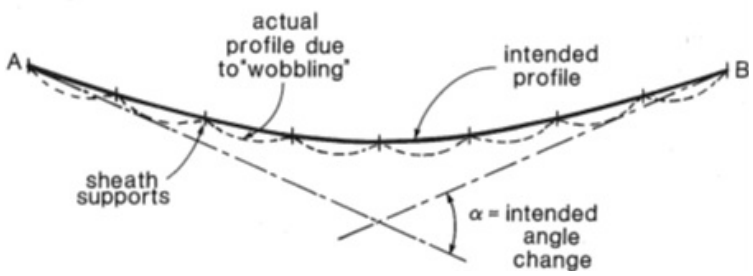

Figure 3.1. Influence of wobbling on tendons according to Eurocode 2, Collins and Mitchell (1991) (Note that sheath = metal duct)

The influence of friction will affect the prestress losses in reactor containments, especially for the horizontal tendons which are curved, some have an accumulated bending angle of over 360°. According to Anderson et al. (2005) an accumulated bending angle of 360° will result in prestress losses of approximately 40 % due to friction.

3.3. Long-term losses

The phenomena which contribute to the long-term loss of prestress force are creep and shrinkage of concrete and relaxation of the steel tendons. In figure 3.2, the principal contribution from the different mechanisms on the total long-term deformation of concrete that is allowed to dry out is shown, Brown and Hope (1972).

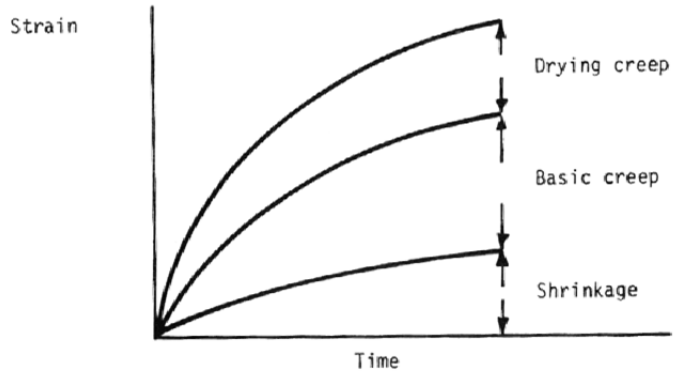

Figure 3.2. The different mechanisms which cause long-term deformations of a loaded concrete specimen subjected to drying, Brown and Hope (1972).

3.3.1. Shrinkage of concrete

Shrinkage can be defined as “the time-dependent strain measured in an unloaded and unrestrained specimen at constant temperature”, Kovler and Zhutovsky (2006), and includes both drying shrinkage and chemical shrinkage. Drying shrinkage is the contraction due to moisture losses in the concrete and includes both the shrinkage due to loss of moisture to the ambient medium, i.e. drying, and the autogenous shrinkage which is the shrinkage due to the self-desiccation of the concrete, and is approximately proportional to the moisture loss in the concrete. The drying shrinkage is partly irreversible, i.e. upon rewetting the swelling strains will be less than the preceding shrinkage strains. Chemical shrinkage is the resulting contraction due to various chemical reactions in the cement paste, such as carbonation shrinkage and hydration shrinkage.

The chemical shrinkage is very difficult or even impossible to predict since the cement reactions are impossible to estimate, even though the mineral composition of the cement could be well known, Kovler and Zhutovsky (2006). The influence

of chemical shrinkage on the total shrinkage of the concrete is relatively small, e.g. the carbonation shrinkage (which is due to the chemical reaction between the calcium hydroxide in the concrete and the atmospheric carbon dioxide) which takes place at the surface of the concrete and will therefore not influence the entire structure. From a structural point of view the drying shrinkage is the more important of the two and the contribution from the chemical shrinkage is often included in the drying shrinkage.

With time, it is assumed that the drying shrinkage approaches a final value, i.e. reaching the state of moisture equilibrium with the ambient medium, which means that the lower the relative humidity of the surrounding air, the greater the shrinkage. The shrinkage strain at an arbitrary point in time, $\varepsilon_{cs}(t)$, can be expressed as:

$$\varepsilon_{cs}(t) = \varepsilon_{csu} \cdot f(t) \tag{3.3}$$

Where:
ε_{csu} = final value of shrinkage, -
$f(t)$ = time-function, approaches the value 1 with time

Several different factors influence shrinkage of concrete, below are some of the most important factors influencing shrinkage presented, with an emphasis on those factors which are most important for the concrete in nuclear reactor containments.

Properties of the concrete

Since it is the seat of the phenomenon, the properties of the cement paste is the most important factor which influences shrinkage and generally the higher the water-cement ratio the greater the shrinkage. The influence on shrinkage by water cement-ratio, cement content and water content is illustrated in figure 3.3 and it can be seen that the water-cement ratio and especially the water content of the concrete have the greatest influence since these properties determine the amount of water which can leave the pore system of the concrete. From figure 3.3., it can further be seen that an increase in cement content at constant water-cement ratio increase shrinkage, this is due to the increased amount of cement paste in the concrete. Another factor which influence the shrinkage is the aggregate content, since the aggregate is unaffected by the moisture changes in the concrete it does not shrink and thus has a restraining effect on the concrete. Pickett (1956) performed tests on concrete specimens with different aggregate contents and the results showed that the shrinkage of a concrete with an aggregate content of 50 % was several times lower than that of neat cement paste with the same water-cement ratio. Increasing the size of the aggregate reduces the shrinkage to some extent;

according to Nasvik (2006) an increase of the aggregate size reduces shrinkage by approximately 16 %. In addition, the stiffness of the aggregate also has a great influence on the shrinkage behavior of concrete. Finally, tests performed by Kockal and Turker (2007) showed that the use of different types of cement does not influence shrinkage.

It is common to add different admixtures to enhance or add different properties to the concrete, for example, superplasticizers is used to increase the workability of the fresh concrete and to reduce the amount of mixing water. The results from a variety of tests on the effect of plasticizers and superplasticizers on shrinkage of concrete are summarized in Brooks (1989). It was found that the mean increase in shrinkage of concrete containing superplasticizers was 17% compared with plain concrete. The influence of plasticizers on shrinkage was relatively small, with an increase in shrinkage of only a few percent. The use of air entraining admixtures increases the shrinkage of the concrete which is due to that an increase of the air content corresponds to a similar increase of the water content Burström (2001).

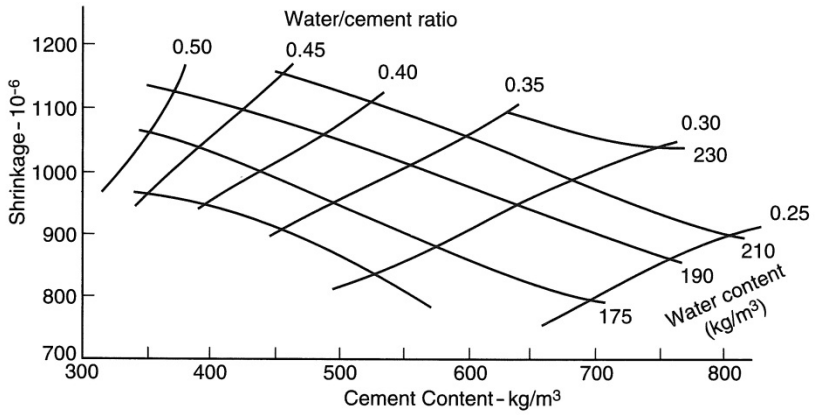

Figure 3.3. Influence on shrinkage by the composition of the cement paste (Neville 1995).

The properties of the concrete used in reactor containments are summarized in paper II, the water-cement ratio varies between 0.4 and 0.5, the cement content varies between 340 kg/m^3 and 470 kg/m^3 and the aggregate content was around 1800 to 1900 kg/m^3, the type of aggregate was usually gneiss or granite. In some cases a super plasticizer was added to the mix. This is more or less standard mixes used for large civil engineering structures, which means that the properties of the concrete will not have a major influence on the shrinkage behavior of the containments.

Reinforcement

Similarly to the effect of aggregate, reinforcement has a restraining effect on the shrinkage of concrete. Oh et al. (1995) performed tests on concrete specimens with different reinforcement ratios and it was found that reinforcement ratios of 0.64 % and 1.78 % reduced the contraction of high-strength concrete due to shrinkage by 14 % and 30 % respectively, see figure 3.4 below.

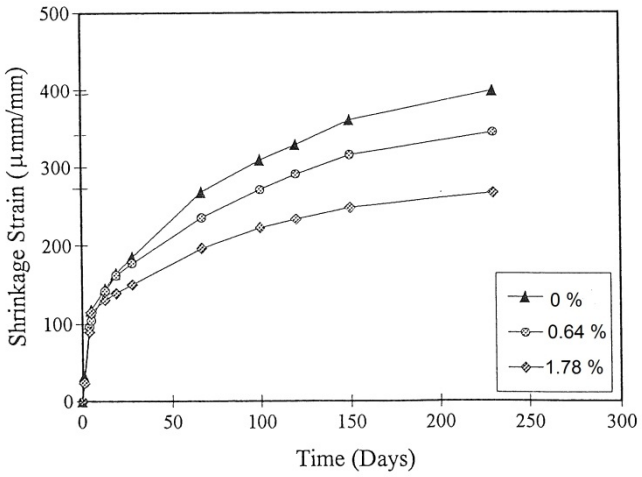

Figure 3.4. Influence of different reinforcement ratios on the shrinkage of concrete, (Oh et al. 1995).

Size

The size of a concrete structure mainly influences the drying rate and hereby the shrinkage rate significantly, but it also has an effect on the final shrinkage value. The most important factor regarding the influence of size on shrinkage of a concrete structure is the volume to surface ratio, i.e. the ratio of the volume of the structure compared with the surface in contact with the surrounding air, Ross (1944). Tests performed by Hansen and Mattock (1966) showed that the lower the volume to surface ratio the faster the development of the shrinkage. Another interesting result indicated from their study is that the final shrinkage value decreases with increasing volume to surface ratio, see figure 3.5, which means that the final shrinkage value is size dependent. However, this size dependence was questioned by Campbell-Allen and Rogers (1975) mainly because of the limited duration of the tests. The drying rate is much slower for larger specimens and it is probable that the final shrinkage values are greater than indicated by e.g. the results in figure 3.5.

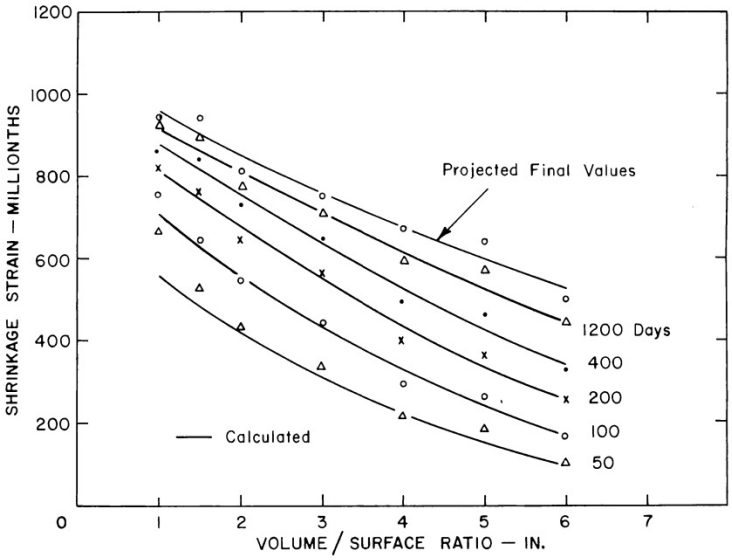

Figure 3.5. Influence of size on the development of shrinkage, Hansen and Mattock (1966).

The drying and hereby the shrinkage rate of nuclear containment structures is extremely slow, measurements of the climatic conditions inside two Swedish reactor containments have been performed during operation, namely at reactor 3 at Ringhals (PWR) and reactor 2 at Barsebäck (BWR), Nilsson and Johansson (2006) and (2009). For both types of reactors it was found that the concrete in the walls are still drying, the RH in the wall of a BWR closest to the steel liner is above 80 %, to be compared with the RH of the ambient climate which is between 5 % and 10 %, which indicates that less than 20 % of the final shrinkage has occurred. For the PWR the mean RH in the concrete was 75 %, which was almost equal to the average RH of the outdoor climate, however, due to the temperature gradient over the wall the drying process is ongoing. The explanations for this slow drying are that the walls are massive and subjected to one sided drying due to the steel liner. The low RH inside the containments will also affect the magnitude of the final value of the shrinkage strain.

3.3.2. Creep of concrete

The definition of creep is the time dependent increase of strain under constant load. Creep is usually expressed in the form of a creep coefficient, which is defined as the ratio of creep deformation to elastic deformation, but can also be expressed as specific creep or creep compliance, defined as creep per unit stress,

for instance MPa^{-1}. Creep of concrete can be divided into two different parts; basic creep and drying creep. The basic creep is the time dependent increase in deformation without any moisture exchange with the ambient climate, i.e. under more or less sealed conditions. The drying creep is the additional creep due to moisture exchange with the ambient climate, i.e. due to the drying out of the concrete. Typically the contribution from the drying creep is equal or greater than that from both the shrinkage and the basic creep. This additional effect of drying was first documented by Picket (1942), where concrete beams were subjected to different climatic conditions while loaded in deflection. Some of the results from this study are presented in figure 3.6 and as can be seen the deflection increases significantly for beams loaded during drying than for those submerged in water.

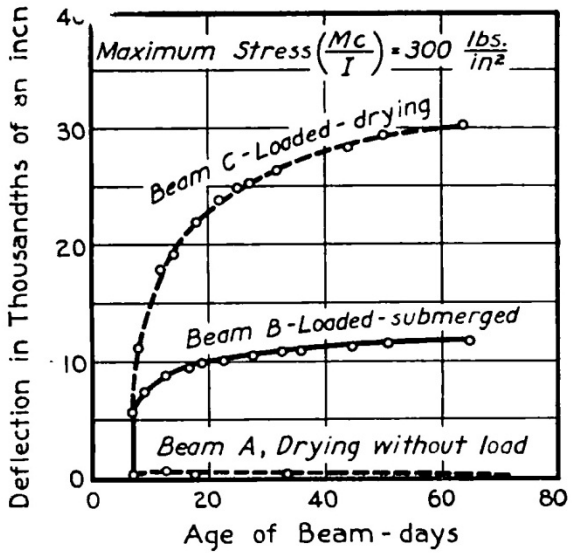

Figure 3.6. The effect of the drying-creep, Picket (1942).

Several different factors influence the creep of concrete, below are some of the most important factors influencing creep presented, with an emphasis on those factors which are most important for the concrete in nuclear reactor containments.

Stress-strength ratio and age at loading

These two factors are closely connected since the strength of the concrete increases with time due to the hydration of the cement, which means that creep will decrease with the age at loading, see figure 3.7, where the total creep strains of concrete loaded at different ages are presented, Parrot (1973). Interesting to note is that the difference in creep strains between concrete specimens loaded for 1 and 7 days decrease with the age at the time of loading. Further, creep tests

performed on concrete specimens with similar mix design as those in the Korean nuclear reactor containments showed that the creep of those specimens loaded at the age of 28 days was approximately three times that of specimens loaded at the age of one year, Song et al. (2002). Similar results were found in a study by Niyogi et al. (1973) where the influence of age at loading on both the drying and basic creep of concrete was investigated. It was found that the creep decreases significantly with the age at loading, except for those specimens loaded at a very early age, up to 20 days, where both the basic and total creep strains increased with the age at loading. For specimens loaded at an age of 20 days or more the creep strains decreased with the age at loading.

For stress levels in the concrete up to approximately 40 to 60 % of the ultimate strength the increase in creep is linear with the applied compressive stress, see figure 3.8. The proportionality between stress and strength is not valid at higher stress levels in the concrete, where creep increases with stress at an increasing rate.

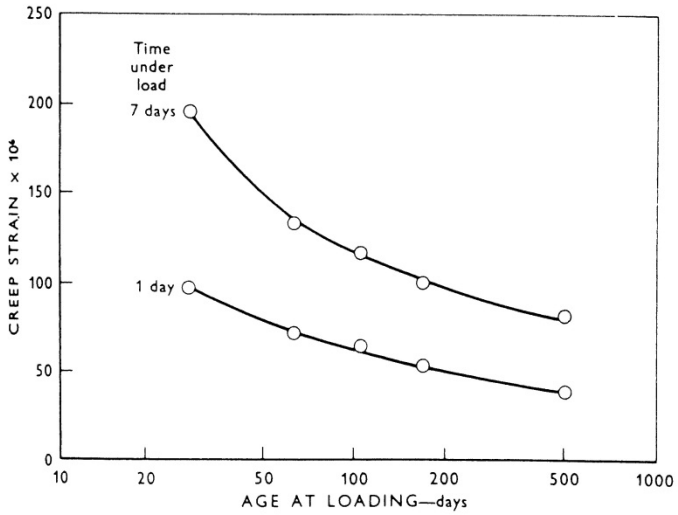

Figure 3.7. Influence of the age at loading on the creep of concrete, Parrot (1973).

The main influence on creep of the age at loading is due to the hydration of the cement, i.e. both the degree of hydration and the strength of the concrete increase with time. Creep is inversely proportional to the degree of hydration, which e.g. means that the type of cement used will influence the creep. For instance, at the same age of loading, the use of slow-hardening cement will increase creep compared with the use of standard Portland cement. In addition, other factors which influence the hydration of the cement, such as water/cement ratio, moisture conditions and temperature, will also affect the influence of age at loading. Assuming a constant stress state in the concrete, the gain in strength with time

reduces the creep since the stress-strength ratio will decrease. The influence on creep of the increase in strength with time was shown by Washa and Fluck (1950), where creep tests were performed for more than 10 years on concrete specimens with different cement types and the specimen which did not gain any strength during the study also exhibited the largest deformations due to creep.

The age at loading will also decrease the contribution from the drying creep on the total strains since some of the drying of the concrete already has occurred without affecting the creep behavior. This means that the age at loading also affects the prestress losses due to shrinkage since the shrinkage that occurred prior to the loading will not contribute to the total prestress losses.

The age at loading is an important parameter influencing the prestress losses in nuclear containments. The time between casting of the concrete and the tensioning of the tendons varied between 1 and 2 years for the different Swedish reactor containments, in contrast to other civil engineering structures where the tendons usually are tensioned as soon as possible.

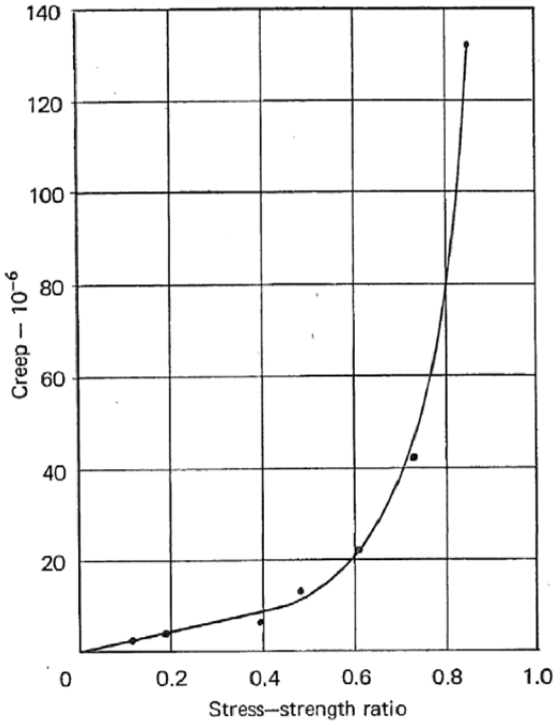

Figure 3.8. Influence of the stress-strength ratio on creep of concrete, Neville (1970).

Reinforcement ratio

As for shrinkage, the steel reinforcement in concrete has a restraining effect on the creep strains since some of the concrete stress will be transferred to the reinforcement as the long-term strains due to creep and shrinkage develop. It should be noted that the reinforcement will reduce the prestress losses in the tendons but not the loss of concrete stress, which is not beneficial for the performance of the structure. Oh et al. (1995) investigated the effect of different reinforcement ratios on creep of high-strength concrete and found that the reduction of creep strain in concrete with reinforcement ratios of 0.64 % and 1.78 % were 15 % and 33 % respectively, see figure 3.9.

The effect of reinforcement probably has a great influence on the prestress losses in nuclear reactor containments since these structures have relatively high reinforcement ratios, varying between 2 % and 3.3%. Anderson (2005) showed a simple model, which was based on modeling the concrete and steel as parallel springs, for calculating the effect of different reinforcement ratios on the deformations of concrete. Using this model with a reinforcement ratio similar to those in the Swedish containments would reduce the deformation of the concrete by 20 % to 25 %.

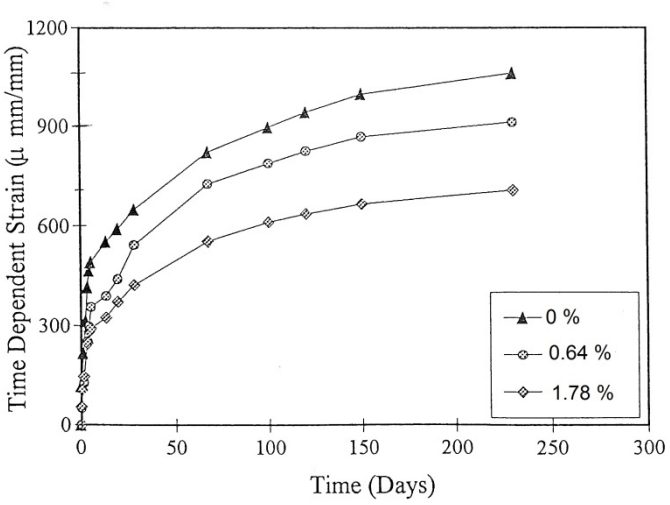

Figure 3.9. Effect of different reinforcement ratios on the creep of concrete, Oh et.al (1995).

Multi-axial stress

Reactor containments are prestressed both horizontally and vertically with concrete stresses of approximately 6 MPa in the vertical direction and 10 MPa in

the horizontal direction. A multi axial stress state will reduce the creep of concrete to some extent, Neville (1970). However, several studies have shown that the influence is relatively small, e.g. creep tests performed by Furr (1967) showed that creep in one-way and two-way prestressed concrete slabs were the same. Tests performed on sealed concrete specimen, Jordaan et al. (1969) showed little difference in creep strain between uni-axial and bi-axial loaded concrete. Finally, in a study by Lanig et al. (1991) a great number of multi-axial creep tests have been performed, which indicated that the difference in creep between uni-axially and bi-axially loaded concrete are negligible.

Temperature

Several studies have shown that the ambient temperature has a great influence on the creep of concrete and especially that the increase from standard conditions, i.e. 20°C, to approximately 40°C, has a much greater impact on the creep strains than subsequent increases up to approximately 150°C. This effect can clearly be seen in figure 3.10, which presents results from tests performed by Gross (1975), where a significant difference in creep was found between concrete specimens loaded at 20°C and at 40°C, respectively. Similar results were found by Hannant (1968), where it was observed that the creep strains increased approximately 2 times if the temperature was raised from 27°C to 52°C. In an investigation performed by Fahmi et al. (1972) concrete specimens were subjected to creep tests during sustained and cyclic temperature at 50 % and 100 % RH and the results showed that both the creep strains and the creep rate increased when the temperature was raised from 23°C to 60°C. Further, it was also found that cycling the temperature between 23°C and 60°C increases the creep of the concrete and that the first thermal cycle has the greatest influence on creep. According to a literature review performed by Schneider (1982), the creep of sealed concrete increases by approximately 50 %, when the temperature was raised from 20°C to 50°C. Another result of this review is that at temperatures below 100°C, the moisture transport inside the concrete affects creep to a higher extent than the increases in temperature.

Nasser and Neville (1965 and 1967) investigated the influence of different temperatures on the basic creep of concrete by submerging the specimens in water while under load. Interestingly, they found that the influence on creep decreases at higher temperatures, for example, the results showed that creep at 71°C were 3.5 times higher than the creep at 21°C, but creep at 84°C and 96°C were only 1.7 times higher (1965). They also performed tests on both old concrete, some 50 years old extracted from a pier structure, and on specimens prepared in the laboratory (1967). Similar results were obtained in this study, the increase in creep was highest for storage temperatures up to 71°C and at a temperature of 96°C creep was approximately equal to that at 21°C.

In paper V the influence of increased temperature on the prestress losses in prestressed concrete beams were investigated and the results showed that the prestress losses in beams stored in an ambient temperature of approximately 42°C was around 25 % greater than those for beams stored in a normal indoor climate, approximately 21°C.

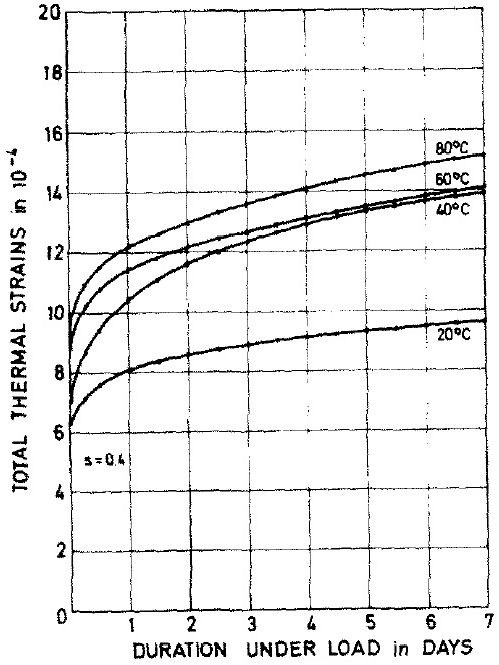

Figure 3.10. Influence of the ambient temperature on creep of sealed concrete specimens, (Gross 1975).

The measurements performed by Nilsson and Johansson (2006) and (2009) showed that the temperature varies between 25°C and 50°C for the BWR containment and is around 30°C for the PWR containment. This shows that the temperature is an important parameter affecting the magnitude of the creep strains in the concrete.

Size effects and moisture conditions

The size of the concrete structure only has a small influence on the basic creep, according to Neville (1970) the basic creep rate decreases with the size of the structure, however, this difference is only discernible during the first weeks after the application of the load.

However, the main influence of size is on the drying creep, since the size of the structure affects the drying rate and thus the drying creep rate and similarly as for

shrinkage it is the volume to surface ratio which is the governing parameter affecting the development of the drying creep strain. A number of studies have investigated the influence of the size of the specimen on the creep deformations in concrete see e.g. Hansen and Mattock (1966), Bryant and Vadhanavikkit (1987) and the review by Neville (1970). Hansen and Mattock (1966) performed creep tests on cylindrical and I-shaped concrete specimens of various sizes and the results showed that the creep decreased as the volume to surface ratio increased, see figure 3.11 The results also indicate that for large enough volume to surface ratios the creep is similar to that of a sealed structure. However, the duration of these tests were approximately 4 years and it is probable that for longer periods of loading the total deformations of the different sized specimens would be similar. Contradictory results were obtained in a study by Gamble and Parrott (1978), which indicated that the drying creep, i.e. the final value of the creep strain, is independent of the size of the specimen. A possible explanation for the size effect on creep is that since the drying is much slower for larger structures, the hydration in the inner parts of the structure will reach much higher levels and thus significantly higher concrete strength, which reduces creep, when the drying process initiates.

The ambient relative humidity mainly influences the drying creep and according to Neville (1995) the influence of the relative humidity on basic creep on concrete specimens in moisture equilibrium with the surrounding air is very small. However, the moisture content of the concrete specimen will influence creep, the lower the moisture content the lower the creep, Brown and Hope (1972). Results from several studies indicate that completely dry specimens exhibit significantly lower creep than those containing small amounts of moisture or even no creep at all, Brown and Hope (1972) and Neville (1970).

Similarly as for the development of shrinkage, the size of the containment walls is another important parameter affecting the drying creep. As mentioned previously, due to the steel liner the walls are subjected to one sided drying and since the walls are up to 1.2 m thick this will correspond to a drying of a 2.4 m thick wall. Furthermore, the low ambient RH, especially for the containment in a BWR, will also have a great influence on the drying creep.

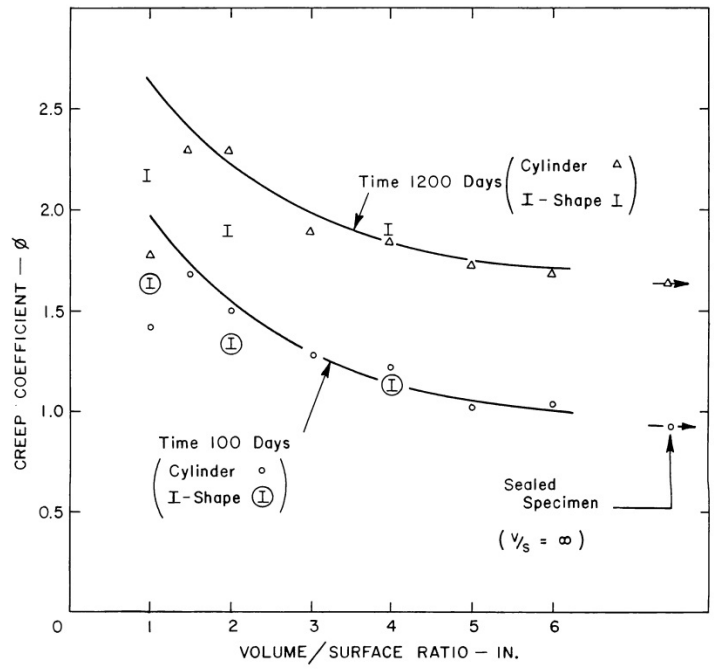

Figure 3.11. Influence of the volume to surface ratio of the structure on creep, Hansen and Mattock (1966).

Properties of the concrete

The properties of the concrete with the largest influence on creep are those which affect the strength development in the concrete e.g. water-cement ratio and type and fineness of the cement, i.e. factors which influence the stress-strength ratio. Considering the same age at loading and applied stress the use of different types of cement will influence creep, slow-hardening will exhibit the largest creep strains and rapid-hardening the lowest, Neville (1995). The development of strength while under load is also an important property of the cement, this means that rapid-hardening cement will experience less creep than concrete with slow-hardening cement. Another property worth mentioning is the fineness of the cement which also influence the development of concrete strength, the finer the cement, i.e. the higher the specific surface, the faster the strength development.

Similar as for shrinkage the aggregate content of the concrete will have a restraining effect on the creep deformations since the aggregate does not undergo creep. Since the most frequently used aggregate, such as granite and gneiss, has a significantly higher modulus of elasticity and thus higher restraining capacity than the cement paste the main influence on creep is that the higher aggregate content the lower the creep.

As described in section 3.3.1, the properties of the concrete used in reactor containments are standard properties for concrete used in large civil engineering structures and similar as for shrinkage, the properties will not have a major influence on the creep behavior of the containment walls.

3.3.3. Relaxation of tendons

Stress relaxation is defined as the time dependent loss of stress in the tendon at constant strain. The two main factors influencing relaxation are the stress-strength ratio and the ambient temperature. The loss due to relaxation increases with the stress-strength ratio, but is negligible at stress-strength ratios below 0.5, Ghali and Trevino (1985). Tests have shown that raising the ambient temperature significantly increases the relaxation loss in prestressing steel, see e.g. Cahill and Branch (1968), Roth (2004) and Leonhardt (1962). Cahill and Branch (1968) performed relaxation tests at different temperatures at stress levels of 70 % to 75 % of the ultimate tensile strength with durations up to 30 000 h. Their results are summarized in figure 3.12 and it can be seen that the temperature has a great impact on the relaxation behavior, e.g. the loss after 10 000 h at 20°C is approximately 1.5 % compared to losses at 40°C and 60°C, which were 3 % and 5 %, respectively. Similar results were obtained by Roth (2004), were it was found that the relaxation loss was doubled when increasing the temperature from 22°C to 55°C. Furthermore, in 1973 relaxation tests were performed at the nuclear power plant Forsmark on similar strands that were used in the containments, Roth (2004). These tests were performed at both 20°C and 50°C, respectively, with a duration of 1000 h. The tests were also performed at different stress levels in the steel. With a duration of 1000 h and at a stress level corresponding to 70 % of the ultimate tensile strength, the relaxation loss at a temperature of 20°C were 1.5 % and the loss for the strands subjected to 50°C were 2.4 %, see figure 3.13. These results were used in the calculation of the prestress losses in the Swedish nuclear containments in paper II.

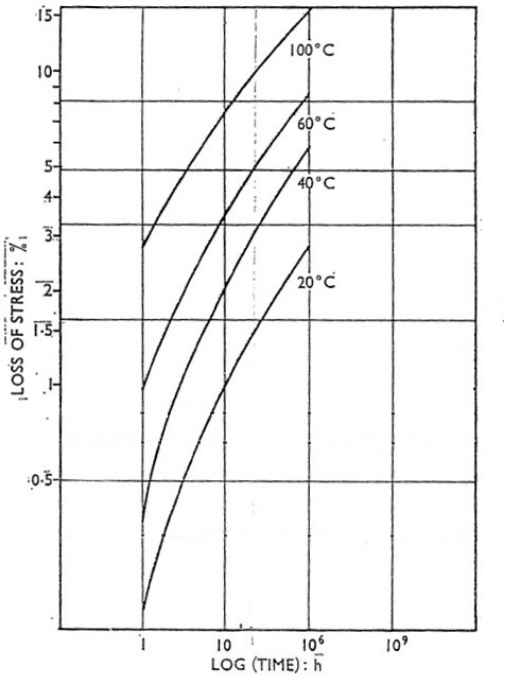

Figure 3.12. Loss due to relaxation at various ambient temperatures, Cahill and Branch (1968).

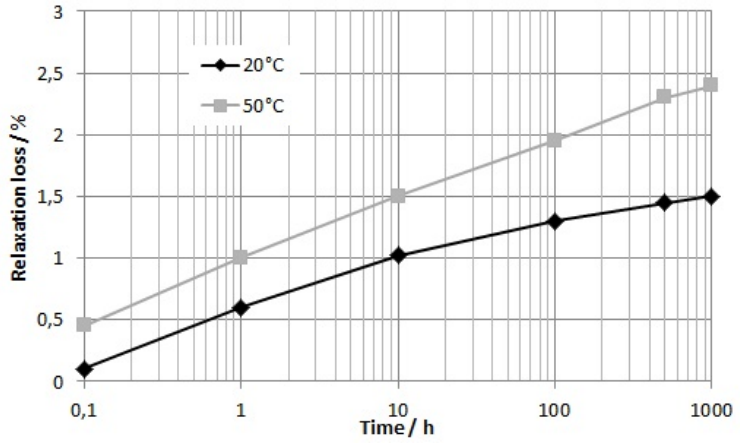

Figure 3.13. Results from the relaxation tests performed at Forsmark nuclear power plant in 1973, from Roth (2004).

Other factors which can influence the relaxation behavior to a minor extent are the diameter of the specimen and the number of wires in the strand, i.e. whether it is a multi- or single wire strand, Cahill and Branch (1967). The difference in relaxation behavior between single and multi-wire strands is due to that the outer wires can unwind around the core wire during loading and that there can be small variations in the material properties between the wires in the multi-wire strand.

3.4. Estimating prestress losses

3.4.1. Prediction models for creep and shrinkage of concrete

Several prediction models exist for estimating creep and shrinkage in concrete structures. The most commonly used in the literature are the PCI Committee on Prestress Losses (1975), the CEB/FIP MC90 and MC99 (1991 and 1999) (the same model used in Eurocode 2), the model B3 by Bazant and Murphy (1995), the model GL2000 by Gardner and Lockman (2001) and the ACI 209R-92 (1992). Common for all these models is that they are based on empirical relations from a large number of creep and shrinkage data. One exception is model B3, which claims to be semi-empirical, i.e. it is partly based on tests and partly on the observed physical behavior behind e.g. the basic creep and it is also the most complex with the highest number of input parameters and most complex equations. The input parameters which the models take into account are summarized in table 3.1. As can be seen, there is a relatively wide variation in number of input variables, however, some variables are common for all models, e.g. the properties of the concrete, either as compressive strength or as mix proportions (ACI 209), the ambient RH and the size and shape of the structure. According to an ACI report on modeling of creep and shrinkage, ACI 209.2R-08 (2008), the following parameters should be considered in a model; properties of the concrete, either as mix proportions or mechanical properties, ambient RH, age at loading, duration of drying, duration of loading and the size of the specimen.

Table 3.1. Input parameters considered in different prediction models.

Parameter	PCI	ACI 209	B3	CEB/FIB	GL2000
Age at onset of drying				■	■
Age at loading	■	■	■	■	■
Age of concrete	■	■	■	■	■
Aggregate content			■		
Air content		■			
Ambient RH	■	■	■	■	■
Cement content		■	■		
Cement type			■	■	■
Compressive strength	■		■	■	■
Compressive stress		■	■	■	
Curing method	■	■	■		
Curing time	■		■		
Fineness of aggregate		■			
Modulus of elasticity	■			■	■
Size and shape effects	■	■	■	■	■
Slump		■			
Type of aggregate	■				
Water content			■		

The approach for estimating creep strains is similar in all the models, i.e. expressing creep as a final creep coefficient. The exception is model B3 which expresses the creep strains as one part of the compliance function, i.e. the total deformations due to elastic shortening and creep per unit stress. In the calculations the final creep coefficient or compliance for the structure is based on e.g. the concrete properties, ambient RH and volume to surface ratio. The development of the creep strains during the chosen time frame is described by a time function based on the different age parameters and the size and shape effects. Except for model B3 basic and drying creep are not predicted separately but included in the total creep deformations.

The approach for calculating shrinkage is similar to that for estimating creep, a final value of the shrinkage strain is calculated, i.e. when the concrete has reached moisture equilibrium with the ambient climate, generally based on the properties of the concrete and the ambient RH. The development of the shrinkage is described by a time function based on the age parameters and the size and shape of the structure. For a period of 20 000 days, the time function from GL2000 is plotted in figure 3.14 for a typical reactor containment wall, as can be seen the development of shrinkage is slow, after 20 000 days only 40 % of the final shrinkage strains have developed. Furthermore, the CEB/FIP 1999 Model Code is the only of the models that separates the calculation of shrinkage into the autogenous and drying shrinkage, respectively.

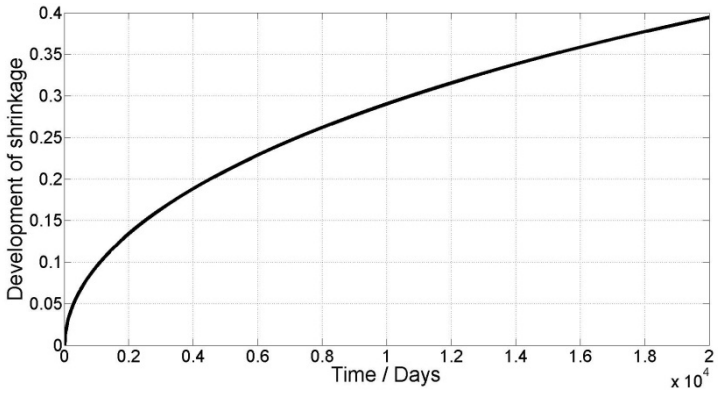

Figure 3.14. Time function describing the development of concrete shrinkage as percent of the final value, from GL2000 applied for a typical reactor containment wall.

Several studies have been conducted in which the accuracy of the different models has been evaluated showing varying results, however, the model GL2000 is generally found to be the most accurate closely followed by model B3. Brooks (2005) evaluated five different models, CEB-FIP, GL2000, B3, ACI 209 and the British standards as the residuals from creep and shrinkage tests with a duration of 30 years. For predicting the total strain for dry-stored specimens, it was found that GL2000 was the most accurate of these models and it was also the most accurate for estimating shrinkage and total creep. However, it was concluded that all the models significantly underestimate the total creep strains. In a similar study Al-Manaseer and Lam (2005) performed a statistical evaluation of the models B3, ACI 209, GL2000 and CEB-FIP. The results showed that B3 and GL2000 were the best models for estimating shrinkage and for the prediction of creep CEB-FIP, B3 and GL2000 were the most accurate, showing very similar results. Similarly to the results in Brooks (2005), all the models underestimate the creep strains. A comparative study including the same four models, Bazant and Li (2008), showed the model B3 to be the most accurate for predicting both shrinkage and creep, followed by GL2000. Furthermore, in a comparison performed by Gardner (2004), it was found that GL2000 and model B3 were the most accurate for predicting shrinkage and that GL2000 was the most accurate for predicting creep in drying concrete specimens. In addition, the results also showed that the accuracy of all models was increased when modified with measured values of the modulus of elasticity. Finally, Goel et.al (2007), compared the accuracy of several prediction models to both the results from field measurements of deformations and strains on a tall reinforced concrete building, Russell and Larson (1989) and reported experimental results. They reached similar conclusions as the previous studies, i.e. GL2000 was the most accurate of the models followed by model B3.

A large database known as the RILEM data bank containing the results from several hundred creep and shrinkage tests reported in the literature was created in 1978 and has been updated regularly ever since, the latest version is from 2008, Bazant and Li (2008). All prediction models have been calibrated against different versions of the data bank, except for ACI 209 which is based on some research studies mainly performed during the 1960s. It should be noted that except for the study performed by Brooks (2005) all evaluations of the models in the presented studies have been against this data bank.

In paper II, the prestress losses for the Swedish containments with unbonded tendons were modeled using the models B3, CEB-FIP MC 90 and 99, GL2000 and ACI 209, replacing the time function for the development of shrinkage with the actual drying development. The predicted losses were compared to the measured prestress losses in these structures. The results actually showed that the CEB-FIP MC 99 and ACI 209 were the most accurate of the models and that the difference between the models mainly depended on the prediction of creep. In contrast to all the other comparative studies it was found that the models overestimate the prestress losses for nearly all the considered cases. In addition, some possible explanations to the difference between the results from the prediction models and the measured values were proposed. The major drawbacks of the models are:

- The models are based on tests on small specimens, generally with a cubic or cylindrical shape. It is not certain that the results from these specimens reflect the behavior of large concrete structures, e.g. regarding the rate of drying and the development of the mechanical properties.
- Most creep and shrinkage tests are performed with relatively short duration, which makes it difficult to predict the behavior of concrete structures over large time spans.
- None of the models consider the influence of reinforcement on neither creep nor shrinkage which has a big influence on the long-term mechanisms, see section 3.3.1 and 3.3.2.
- The influence of temperature is not considered in any of the models, probably because most concrete structures are subjected to normal climatic conditions, i.e. below or around 20°C. The model B3 has an extension which deals with the temperature effect on creep, however, this was not used in paper II since it would further decrease the accuracy of model B3.
- Normally, concrete structures are subjected to varying ambient conditions, e.g. varying loads, temperature and moisture conditions, which means that the models do not represent the real conditions since the specimens are

usually subjected to static conditions during the tests and in those cases where e.g. the climate is varied it is done in a controlled fashion.

3.4.2. Prediction of relaxation

The prediction of relaxation in steel is a lot less cumbersome than the prediction of creep and shrinkage in concrete, usually only a few parameters need to be considered, e.g. in the PCI committee on prestress losses (1975) the only input parameters for low relaxation steel are the stress levels and duration of the load. In Eurocode 2 a slightly more complex equation is given which is based on the results from a standard relaxation test, i.e. the loss due to relaxation for a stress level of 70 % of the ultimate tensile strength at a mean temperature of 20°C, the duration of the standard test is 1000 h. Thus providing a possibility of increasing the accuracy of the predictions by using the result of tests on the prestressing steel used in the considered structure.

$$\Delta\sigma_{pr} = \sigma_{pi} \cdot \left(0.66 \cdot \rho_{1000} \cdot e^{9.1\mu} \left(\frac{t}{1000} \right)^{0.75(1-\mu)} \right) \cdot 10^{-3} \qquad (3.4)$$

where:

$\Delta\sigma_{pr}$ = loss of prestress due to relaxation, MPa
σ_{pi} = stress in tendon directly after tensioning, MPa
t = time after tensioning, h
ρ_{1000} = the relaxation loss from a standard relaxation test, %.
$\mu = \sigma_{pi} / f_{pk}$, where f_{pk} is the characteristic value of the tensile strength of the steel

3.4.3. Predicting the total prestress losses in a structure

When using the prediction models described above to predict the total prestress losses in a prestressed concrete structure it is important to consider that the stresses in the concrete will decrease with time and that using the initial concrete stress tends to overestimate the prestress losses. In other words, due to the long-term effects themselves the stress in the concrete will decrease with time and thus the force in the tendons causing them. According to Eurocode 2, this effect can be taken into account by using equation 3.5.

$$\Delta P_{c+s+r} = A_p \cdot \frac{\varepsilon_{cs} E_p + 0.8\Delta\sigma_{pr} + \frac{E_p}{E_{cm}} \varphi(t,t_0) \cdot \sigma_c}{1 + \frac{E_p}{E_{cm}} \frac{A_p}{A_c} \left(1 + \frac{A_c}{I_c} z_{cp}^2\right) \left[1 + 0.8\varphi(t,t_0)\right]} \qquad (3.5)$$

where:

ΔP_{c+s+r} = prestress loss in tendon, N
$\Delta\sigma_{pr}$ = loss due to relaxation, MPa
σ_c = initial concrete stress, MPa
ε_{cs} = shrinkage strain, -
$\varphi(t,t_0)$ = creep coefficient, -
E_c = modulus of elasticity of concrete, GPa
E_p = modulus of elasticity of tendon, GPa
A_c = cross section area of concrete, m^2
A_p = cross section area of tendons, m^2
I_p = moment of inertia of concrete section, m^4
z_p = distance between center of gravity of concrete section and tendons, m

3.4.4. Determining prestress losses in beams experimentally

Several studies have been reported in the literature where the remaining tendons forces have been determined in laboratory tests e.g. for old bridge beams, see e.g. Saiidi et al. (1997), Pessiski et al. (1996) and Eder et al. (2005) but also the appended papers I and V. The most common method for determining the remaining tendon forces is the so-called crack re-opening method, which was used in paper I and V. In this method the beam is normally subjected to a three or four point bending test in which the load is increased until flexural cracks appear in the bottom of the beam. In the following crack re-opening test the beam is unloaded, one or several of the cracks instrumented and loaded again in order to determine the crack re-opening load. Since the stress in the bottom fiber of the beam is zero at the crack re-opening load, therefore also called decompression load, the effective tendon force in the beam can be determined using Navier's equation, see equation 3.6. It should be noted that equation 3.6 is valid only for structures with straight centrically placed tendons.

$$\sigma_{cu} = -\frac{P}{A_c} + \frac{M_F}{W} + \frac{M_s}{W} \qquad (3.6)$$

where:

σ_{cu} = stress in the bottom fiber of the beam, in this case equal to zero, MPa.
P = remaining tendon force, N
A_c = cross-section area of beam, m^2
M_F = applied moment from the testing machine, Nm
M_S = moment due to self-weight of the beam, Nm
W = section modulus of the beam, m^3

Flexural crack re-opening loads can be determined using several different methods, most commonly the flexural cracks are instrumented with either strain or LVDT gauges. To determine the crack re-opening load, the displacement recorded by the gauge is plotted against the applied load, when the crack reopens, the slope of the curve changes drastically, see figure 3.15. The standard interpretation used in the literature of the crack re-opening load is the intersection point of the two slopes as in figure 3.15, see e.g. Saiidi et al.(1997), Eder et al. (2005), Halsey and Miller (1996) and the appended papers I and V. However, the findings in paper V showed that this interpretation overestimates the crack re-opening load and thus the tendon forces in the tested structure. A finite element model of the test procedure showed that the stress in the bottom fiber is zero at the point where the slope deviates from the initial non-linear behavior, the crack re-opening load in figure 3.15. The following method was proposed in paper V to determine the true crack re-opening load from the results of a crack re-opening test. From a finite element analysis of the testing procedure, the relation between the estimated intersection point and the crack re-opening load can be determined, e.g. in paper V, the intersection point was 42 % greater than the crack re-opening load. By plotting the applied load versus the relative displacement obtained from the test and estimating the intersection point, the crack re-opening load can be estimated by dividing the load at the intersection point with the relation obtained from the finite element analysis, see e.g. paper V, where the estimated intersection points were divided by 1.42.

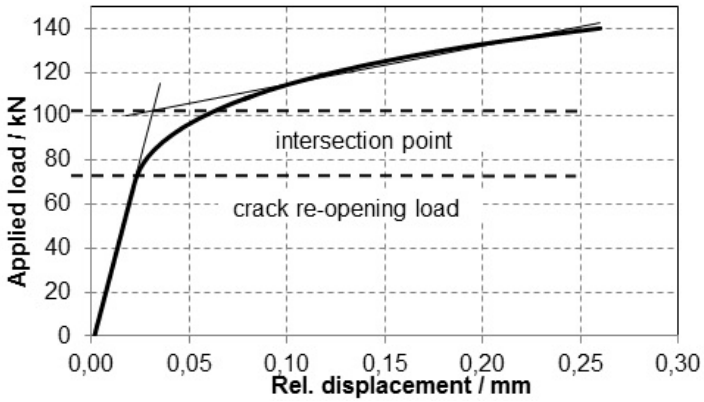

Figure 3.15. Principal of determining the crack re-opening load.

Other methods have also been used to estimate the crack re-opening load, for example, one method which was used by Shenoy and Frantz (1991), is to visually estimate when the crack reopens, however, the reliability of this method can be questioned since the crack re-opens before it is visible by the naked eye. Another uncertain method is to determine the tendon force from the cracking load of the first load cycle, the problem with this method is that the tensile strength of the concrete has to be known in order to calculate the tendon force using equation 3.6. Finally, a third method is to plot the vertical deflection versus the applied load, this curve will show a similar behavior as figure 3.15, i.e. the deflection rate increases after the crack has re-opened. However, the results from paper V showed that this method also overestimates the remaining tendon forces in the tested beam.

Two other methods completely different from those described previously have also been used in some studies, one is to expose a length of a prestressing strand, instrument it with e.g. strain gauges, cut the strand and from the change in strain the prestress force can be calculated. The drawbacks with this method are e.g. that the removal of the concrete can lead to shortening of the strand and that the prestress force is only obtained for the wire or strand that is cut and may not be representative for all the tendons in the structure. The other method is to embed vibrating wire strain gauges in the concrete during the fabrication of the beams, the change in concrete stress is then used to calculate the prestress losses. The drawback with this method is that the reliability of the gauges over long periods of time is uncertain since there is no possibility to calibrate or check the function of the gauges. In table 3.2, the methods used in previous studies for determining the remaining tendon forces are presented. As can be seen the most commonly used is the crack re-opening method, followed by cutting one or several of the strands.

Baran et al. (2005) performed a comparative study, both through a literature review and testing of several pre-tensioned concrete beams, of three different

methods for determining remaining tendon forces, embedded vibrating wire gauges, crack initiation and re-opening loads and cutting strands. It was concluded that the two most effective ways of determining prestress losses were by using embedded vibrating wire strain gauges and cutting strands. It was also found that the crack re-opening method overestimates the prestress losses when compared to those obtained from vibrating wires and cutting strands. However, the vibrating wire gauges were the only way of monitoring the prestress losses with time, since the beams were pre-tensioned no direct measurements of the tendon forces were performed during the study, which for some of the beams lasted for up to 526 days. This means that the true tendon forces and thus the true prestress losses were unknown. In addition, another method for determining the crack re-opening load was used; two LVDT gauges were monitored on the bottom surface, one across the first crack and the other adjacent to the crack. The readings from both these gauges were plotted against the applied load and showed a bilinear behavior after the crack re-opened, see figure 3.16, the crack re-opening load was then taken as the load where this bilinear behavior initiates.

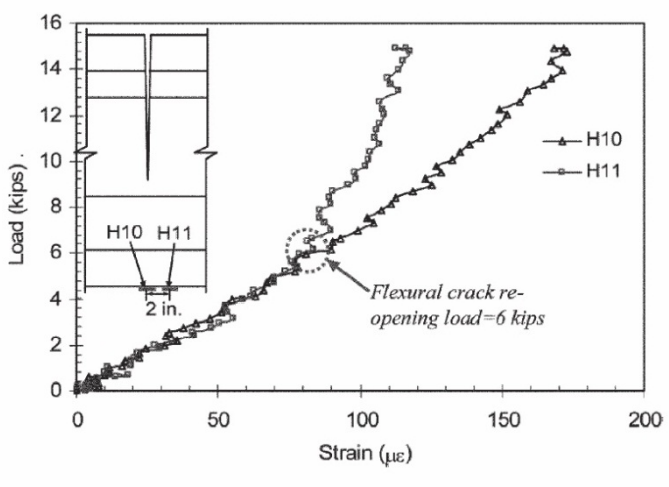

Figure 3.16. Interpretation of the crack re-opening load using two strain gauges, Baran et.al. (2005).

Two of the studies presented in table 3.2 used a different approach for estimating the crack re-opening load, Tabatabai and Dickson (1993) and Naito et.al. (2008). Tabatabai and Dickson estimated the crack re-opening load as the load which caused the change in slope in the applied moment versus crack gauge output, i.e. similarly to the interpretation in paper V. In addition, they also estimated the crack re-opening load as the change in slope in the load versus vertical deflection diagram and found that this load was equal to that obtained from the moment

versus crack gauge output diagram. It should be noted that the crack re-opening loads were estimated visually from the diagrams and the results from paper V indicated that the crack re-opens at loads lower than what is visible in the diagrams, which can be seen in figure 3.15. Naito et al. estimated the crack re-opening load by placing strain gauges adjacent to the first visible crack. The output from the strain gauges becomes more or less constant after the crack has re-opened and this was taken as the crack re-opening load.

Table 3.2. Methods used for determining tendon forces in previous studies.

Study	Methods
Saiidi et al. (1997)	Crack re-opening, intersection method Cutting strand
Pessiski et al. (1996)	Crack re-opening, intersection method
Eder et al (2005)	Crack re-opening, intersection method
Halsey and Miller (1996)	Crack re-opening, intersection method
Tabatabai and Dickson (1993)	Crack re-opening, cracking moment Load deflection plot
Baran et al (2005)	Embedded vibrating wire gauges Crack re-opening Cracking load Cutting strand
Czaderski and Motavalli (2006)	Cutting strand
Shenoy and Frantz (1991)	Crack re-opening, visual estimation
Rabbat (1984)	Crack re-opening, intersection method
Naito et al. (2008)	Crack re-opening based on strain gauge data
Paper I	Crack re-opening, intersection method
Paper V	Crack re-opening, intersection method with FEM

3.4.5. Correction of prestress losses in paper I

In paper I, the prestress losses of five 30 year old prestressed concrete beams were determined by using the intersection method to estimate the crack re-opening loads. Since the findings in paper V showed that this method overestimates the remaining tendon forces, the results from the tests in paper I was determined once more using the same procedure described in paper V, i.e. modeling the test procedure with a finite element model and correcting the results from the estimated intersection loads. The results from the finite element modeling are shown in figure 3.17 and 3.18 where the applied load is plotted both against the stress in the bottom fiber at midspan, figure 3.17, and the relative displacement, figure 3.18. From figure 3.17 it can be seen that the load at which the stress in the

bottom fiber of the beams is around 150 kN, which is approximately 48 % lower than the estimated intersection point in figure 3.18. The corrected prestress losses were calculated using equation 3.6, the self weight of the beams was also included in the calculations assuming a density of 24 kN/m3, the results are presented in table 3.3.

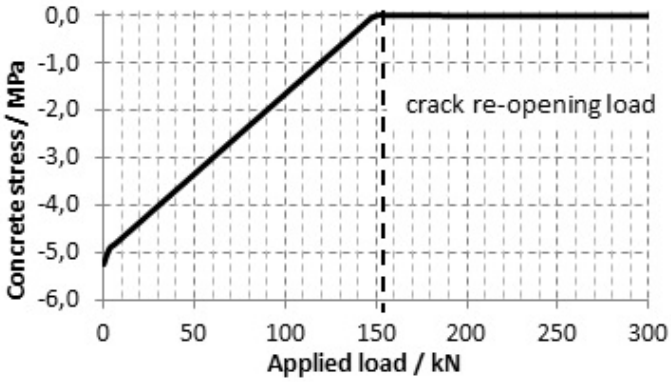

Figure 3.17. Stress in the bottom fiber plotted against the applied vertical load, from the FEM.

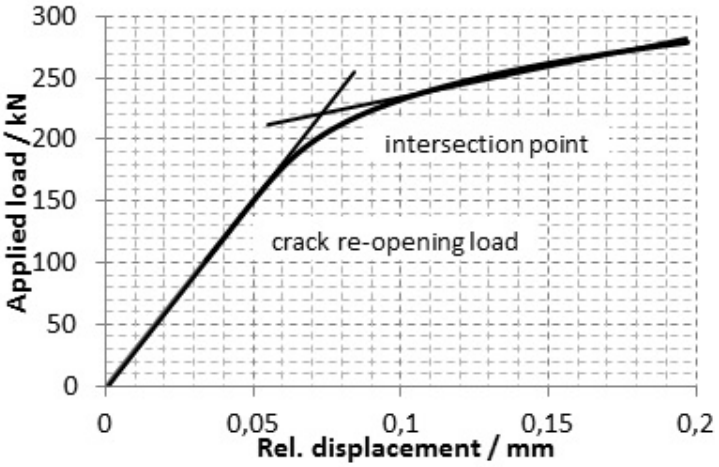

Figure 3.18. Applied vertical load plotted against the relative displacement from the FEM.

From the results in table 3.3 and the results from the prediction models in paper I, it can be seen that all of the models significantly underestimates the measured prestress losses, which also have been found in several similar studies where the accuracy of various prediction models have been evaluated against laboratory tests, see section 3.4.1.

Table 3.3. Corrected and original results from paper I.

Beam #	Initial tendon force / kN	Remaining tendon force / kN	Prestress losses / %	Prestress losses (Paper I) / %
1	2 520	1 119	56	38
2	2 520	1 128	55	38
3	2 520	722	71	61
4	2 440	1 118	54	37
5	2 440	906	63	48

3.4.6. Prestress losses in nuclear containments

In the Swedish containments with unbonded tendons the remaining tendons forces have been measured continuously at the in-service inspections, see section 2.5.2., the results from some of these measurements are presented in paper II and a more extensive evaluation is presented in Anderson (2005). In figure 3.19, some of the results from the in-service inspections are presented for the containments with unbonded tendons. Generally, the mean prestress losses for the Swedish containments vary between 5 and 10 %, the exception is Ringhals unit 2 where the losses are approximately 15 to 17 %. In addition, it has also been seen that the losses are greater for the horizontal tendons.

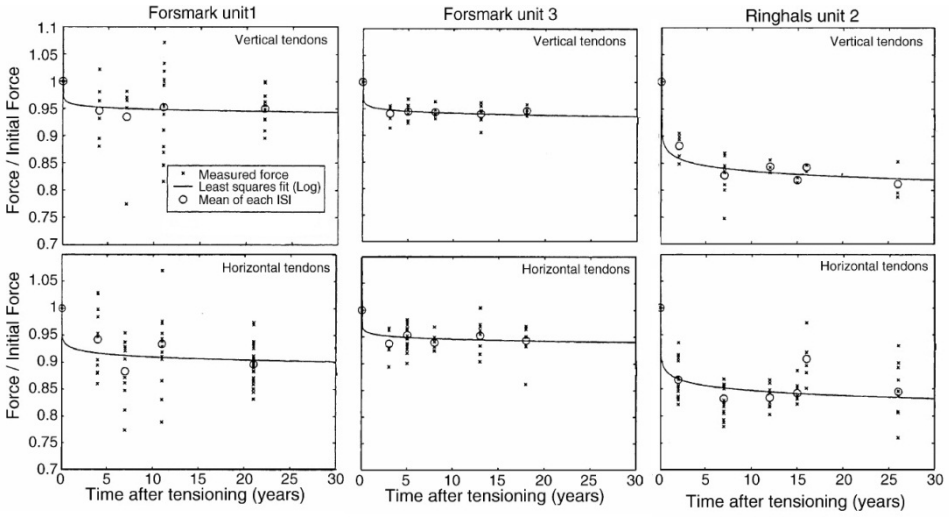

Figure 3.19. Prestress losses measured at in-service inspections for some of the Swedish containments, Anderson (2005).

During the design of the Swedish containments, the prestress losses were determined based on the research presented at the Conference on Prestressed

Concrete Pressure Vessels in London, 1968. For example, during the design phase for the containment at Forsmark unit 3 the prestress losses for the horizontal and vertical tendons were estimated to 34 % and 23 %, respectively, i.e. significantly higher than the actual measured losses which were around 6 % in the vertical and around 5 % in the horizontal tendons after 20 years.

4. Resonance frequencies

4.1. Resonance frequency

A mechanical system or an elastic body vibrates with higher amplitude at some frequencies, called the resonance or natural frequencies, where even relatively small excitation forces can cause large movements. The resonance frequency is usually expressed in Hertz (Hz), i.e. how many times per second the vibratory motion is repeated. The inverse of the frequency gives the period of the motion, i.e. the time required for one complete cycle of the motion. Most mechanical systems or bodies have an infinite number of resonance frequencies, the lowest frequency is called the fundamental frequency and the following are called the higher frequencies.

When a mechanical system is set in motion by an initial excitation, e.g. a hammer strike, and not subjected to any other load or disturbances it will vibrate freely, so called free vibrations, at all its excited resonance frequencies simultaneously. However, depending on the application of the load, some will be more accentuated than others. A system vibrates in different modes, depending on the excitation e.g. a simply supported beam can for example, vibrate in flexion, torsion or in its longitudinal direction. In figure 4.1 the fundamental and first higher modes of vibration for the flexural, torsional and longitudinal modes are shown for a beam with free ends. These are the modes of vibration that were investigated for the prestressed concrete beams in the appended papers III and IV.

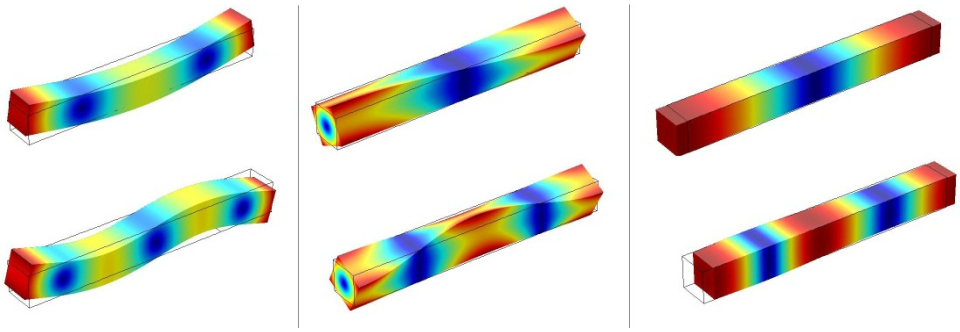

Figure 4.1. Different modes of vibration for the beams in the appended papers III and IV, flexural mode (left), torsional mode (middle) and longitudinal mode (right). The top figures show the fundamental modes and the bottom figures show the first higher modes.

The resonance frequencies of a body of a homogenous, elastic material are a function of several parameters:

- Mass of the solid, increasing the mass will reduce the resonance frequencies.
- Geometry of the solid, i.e. both the geometry of the cross-section, e.g. moment of inertia and the dimensions of the solid, i.e. the length.
- Elastic parameters of the material, e.g. modulus of elasticity, shear modulus and Poisson's ratio.
- Boundary conditions of the solid, e.g. support conditions, if the beam in figure 4.1 was supported as a cantilever beam, the modes of vibrations and resonance frequencies would be completely different.

The resonance frequencies for a beam are obtained by solving the equation of motion for the system. Considering only transverse vibrations, i.e. flexural modes, of a prismatic beam the equation for flexural vibrations will be:

$$EI\frac{\partial^4 v}{\partial x^4} = -\rho A\frac{\partial^2 v}{\partial t^2} \tag{4.1}$$

where:
E = modulus of elasticity, GPa
I = moment of inertia, m^4
ρ = density, kg/m^3
A = cross-section area, m^2

v = displacement in y direction, m
t = time, s

Figure 4.2a shows the fundamental flexural mode for a beam that vibrates freely. Solution for the equation of motion for this case gives the resonance frequencies, see Timoshenko et al. (1974):

$$f_i = \frac{k_i^2}{2\pi}\sqrt{\frac{EI}{\rho A}} \tag{4.2}$$

where k_i can be approximated as:

$$k_i \approx \frac{(i+0.5)\pi}{L} \tag{4.3}$$

where:
L = length of the beam, m
f_i = resonance frequency for mode number i, Hz
i = mode number, for the fundamental mode i is equal to 1

In order to measure the fundamental flexural mode of a beam that vibrates freely the supports can be placed as in figure 4.2b, which is the test setup of the resonance frequency measurements which are presented in the appended papers III and IV. This arrangement of the supports corresponds to the nodal points of the fundamental flexural mode.

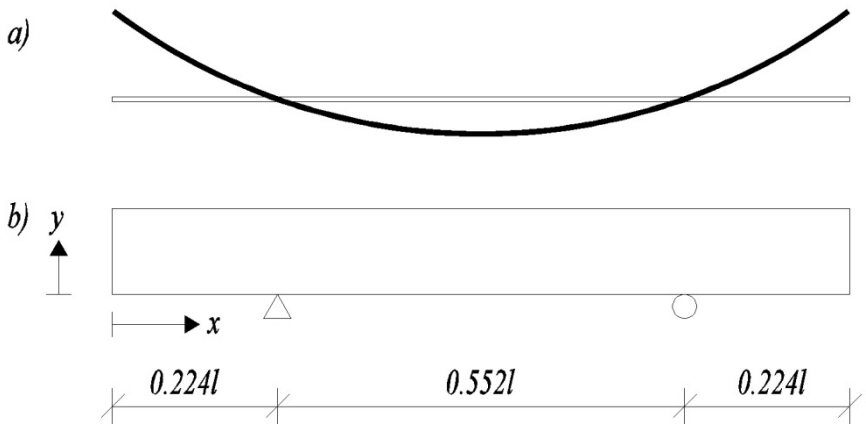

Figure 4.2. a) Example of beam that vibrates freely, for which the resonance frequencies are obtained by equation 4.2. b) Placement of supports to obtain the fundamental flexural mode for a beam that vibrates freely.

Inserting the values of the properties of the concrete test beams from the appended papers III and IV, presented in table 4.1, into equation 4.2 the fundamental and first higher flexural mode are calculated to 161.6 and 449.1 Hz, respectively. These values agree quite well with those obtained from the finite element analysis on the beams in the unstressed state, which were 158.6 Hz and 428.7 Hz, respectively and correspond to the mode shapes to the left in figure 4.1. It should be noted that in the finite element analysis the hole for the passage of the wires was included which can explain some of the difference between the two calculations.

Table 4.1. Properties of the test beams in papers III and IV.

Property	Value
Length, *L*	3 m
Modulus of elasticity, *E*	39.0 GPa
Moment of inertia, *I*	$12.51 \cdot 10^{-4}$ m^4
Density, ρ	2350 kg/m^3
Cross-section area, *A*	0.1225 m^2

In equation 4.1, the torsional stiffness and shear deformations of the beam are neglected, which will cause some errors in the calculations and according to Timoshenko et al (1974) the accuracy of the calculations for a rectangular beam increases by approximately 1.7 % when taking these effects into account. This means that the influence of the rotational stiffness and shear deformations is

greater for the higher resonance frequencies and thus the error in the calculations will increase with the mode number.

4.2. Influence of applied prestress force on resonance frequencies

The influence of an applied axial stress on the resonance frequencies of concrete beams have been investigated experimentally in several studies, see e.g. Saiidi et al. (1994), Lu and Law (2006), Zhang et al. (2012), Hop (1991) and the appended papers III and IV. The results from these studies show that the resonance frequencies of prestressed concrete beams increase with an applied compressive force, see figure 4.3. Somewhat conflicting results were obtained by Miyamoto et al. (2000) who performed dynamic tests on externally prestressed composite girders consisting of a concrete slab on top of two steel I-beams. It was found that the eccentricity of the tendons affects the influence of the tendon force, the resonance frequencies decreased with the applied force with a small eccentricity, i.e. 10 % of the height of the I-beams, and increased for a large eccentricity equal to the height of the I-beams. None of the previous studies have been able to explain the observed stress dependency through the use of linear elastic beam theory. When solving the equation of motion for a simply supported prestressed beam (supported at the ends) taking into account second order effects of a compressive axial force, P, Timoshenko et al. (1974), the resonance frequencies are given by equation 4.4. According to this expression the resonance frequencies of a prestressed concrete beam will decrease with an applied compressive force. The effect that the resonance frequencies decrease with the applied compressive stress, will be the same for a beam that vibrates freely, when considering second order effects.

$$f_i = \frac{i}{2L}\sqrt{\frac{1}{\rho A}\left(EI\left(\frac{i\pi}{L}\right)^2 - P\right)} \tag{4.4}$$

where:
f_i = resonance frequency for mode number i, Hz
i = mode number, for the fundamental mode i is equal to 1
E = modulus of elasticity, GPa
I = moment of inertia, m^4
ρ = density, kg/m^3

A = cross-section area, m^2
L= length of the beam, m
P = axial compressive force, N

It is therefore obvious that second order effects cannot explain the experimental observations that resonance frequencies increase when a compressive force is present. For a negative value of the applied compressive force P, i.e. a tension force and by stating that the stiffness of the beam is zero, i.e. $EI = 0$, equation 4.4 becomes the well known equation for calculating the resonance frequencies of a vibrating string.

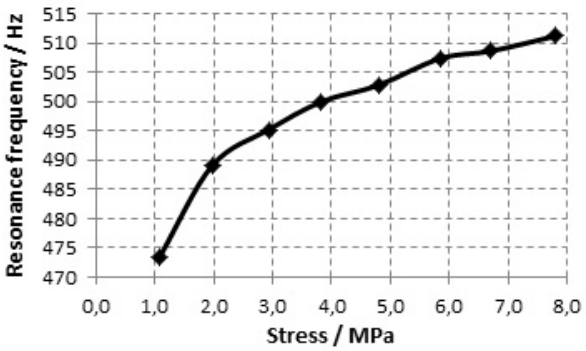

Figure 4.3. Stress dependency of the resonance frequency for the fundamental torsional mode of a prestressed concrete beam. From the measurements performed in the appended paper III.

Several studies with the purpose of explaining both the influence of prestressing force on the resonance frequencies and the inconsistency between string theory and laboratory tests have been performed. Saiidi et al. (1994) performed dynamic measurements on a prestressed concrete beam at different levels of the tendon force, they found that the fundamental flexural mode increased by 32 % when the tendon force was increased from 0 to 131 kN. In contrast, using the expression in equation 4.4 the corresponding shift in frequency due to the applied force would be a decrease of the fundamental flexural mode by 40 %. It was claimed that the conflict between measurements and theory was due to the presence of micro cracks in the concrete caused by the drying shrinkage. In the unloaded state these micro cracks affect the stiffness, i.e. EI, of the concrete beam negatively and by applying the prestressing force the micro cracks close and thus the stiffness of the beam is increased. Dynamic measurements in combination with strain measurements on the tendons were also performed on a post-tensioned concrete bridge over a period of 455 days. The results showed that the fundamental flexural mode decreased with the loss of tendon force. In addition, an empirical model taking the effect of the applied load on the resonance frequencies into account was

derived from a linear regression analysis of the laboratory measurements. These obtained results were discussed by Dall'Asta and Dezi (1996), Deàk (1996) and Jain and Goel (1996). Dall'Asta and Dezi (1996) derived an expression for the effect of the tendon force on the resonance frequency where both the bending stiffness of the beam and the prestressing cable was taken into account. From this expression, it was concluded that the influence of the applied force on the resonance frequencies is negligible. According to Deàk (1996), the application of an external load will reduce the resonance frequencies since if large enough it will cause buckling of the beam. However, it was claimed that a prestressing force will not have the same effect since it is unavoidable that the tendon at some point will come in contact with the duct. The prestressing force can therefore not be considered as an external force and thus the prestressing force does not affect the resonance frequencies of a linear elastic prestressed concrete beam. Jain and Goel (1996) had the same approach to the problem i.e. they considered the prestressing force as an internal force and from expressions derived for this case it was concluded that the prestress force will not influence the resonance frequencies.

A similar approach for determining the stress dependency was proposed by Kim et al. (2004), i.e. that they proposed a model where the bending stiffness, *EI*, is stress dependent. The model was verified against the results from the measurements by Saiidi et al. (1994) and the analytical results were in relatively good agreement with the measurements. Zhang et al. (2012) further developed the empirical expression of the stress dependent bending stiffness by Saiidi et al. (1994) and compared to measurements on prestressed concrete beams. It was found that their expression captured the force effect on the fundamental flexural mode, but was unable to describe the influence on the higher modes.

Hamed and Frostig (2006) approached the problem by considering a prestressed beam as a combination of two different substructures, the compressed concrete beam and the tensioned cable. They derived expressions for the influence of a prestressing force on the resonance frequencies both for prestressed beams with bonded and unbonded tendons. It was concluded that it was mathematically proven that an applied compressive force does not influence the resonance frequencies of prestressed concrete beams, assuming a linear elastic material.

Contrary to all other previous studies Kerr (1976), who derived an expression for the influence of an axial force on the resonance frequencies of a cantilever beam and performed dynamic measurements on a prestressed cantilever beam, found that neither the analytical expression nor the test showed any influence of the axial force on the resonance frequencies.

It should be noted that the studies mentioned above only examines the effect of prestressing force on the flexural modes of prestressed beams and since the torsional stiffness and shear deformations are neglected the developed models are

unable to capture the influence of compressive stress on e.g. torsional and longitudinal vibrations which also are stress dependent according to the results from the appended papers III and IV. However, by taking both the torsional stiffness and shear deformations into account in equation 4.6 and 4.7 will not change the predictions of the equations, i.e. they will still predict a decrease of the resonance frequencies with the applied prestressing force, Raju and Rao (1986).

In the appended papers III and IV, dynamic measurements were performed on three prestressed concrete beams, it was shown that the resonance frequencies for the flexural, torsional and longitudinal modes increased with the tendon force. The results also showed that stress dependency of the resonance frequencies for all the investigated modes can be adequately described by the acoustoelastic theory, see section 5.

4.3. Measuring resonance frequencies

The measurements of resonance frequencies of a structure, usually referred to as resonant ultrasound spectroscopy, RUS, or resonant acoustic spectroscopy, RAS, are used for a wide variety of applications in different fields of engineering, Migliori and Sarrao (1997). RUS are e.g. used in structural health monitoring to detect cracks and other damages in civil engineering structures, Carden and Fanning (2004). RUS is also used to measure the dynamic modulus of elasticity of e.g. concrete samples. Under constant ambient conditions and for a known geometry of the specimen and density of the material, the modulus of elasticity can easily be calculated if the resonance frequency is measured, e.g. for a beam vibrating in flexure the modulus of elasticity can be calculated from equation 4.4.

Two different methods exist for the excitation of the specimen, operational modal analysis and experimental modal analysis, respectively. In operational modal analysis, the structure is equipped with sensors and the excitation is the natural actions on the structure, e.g. traffic loads on a bridge. Since experimental modal analysis is the method used in the appended papers III and IV, operational modal analysis will not be further discussed. In experimental modal analysis the structure is excited manually, e.g. by an impact hammer or a shaker. The impact hammer is usually equipped with a force sensor measuring the force of the impact as a function of time. The vibrations can e.g. be recorded using an accelerometer and to record the signal from both the accelerometer and the impact hammer they are connected to a signal conditioner which in turn is connected to a data acquisition system, e.g. a laptop computer. The positioning of the accelerometer and impact points are crucial for the results and should be in the points of maximum displacement for the studied modes of vibration, e.g. for the first flexural modes of

the beam in figure 4.2 the maximum displacements are at the ends of the beam, see figure 4.1.

One of the most frequently used sensors to record the vibrations of a test specimen is a piezoelectric accelerometer. It consists of a piezoelectric material, usually a quartz crystal, mounted by a seismic mass. As the accelerometer vibrates the seismic mass exerts a force on the crystal which generates a voltage proportional to the force exerted on the crystal. The output from the accelerometer is thus a variation in voltage over the time period during which the specimen vibrates. This is the time domain representation of the signal i.e. how the signal varies over time and is usually expressed as the variation of the amplitude of the vibrations with time. In figure 4.4a, the results from one of the measurements for the flexural mode for one of the prestressed beams studied in papers III and IV is shown. In order to further analyze the signal the time domain representation can be transformed into the frequency domain using a Fourier transform. The frequency domain plot shows how much of the energy in the vibrations which lies within each frequency, see figure 4.4b which shows the signal from figure 4.4a in the frequency domain, the two lowest resonance frequencies can easily be identified as the two peaks in the plot.

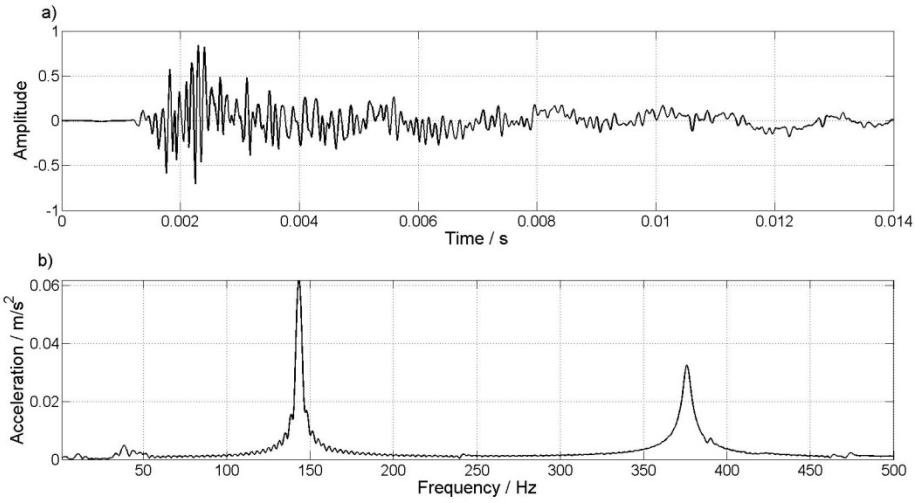

Figure 4.4 a) Signal from measurements of the flexural mode of a prestressed concrete beam in the time domain. b) Same signal as in figure a in the frequency domain.

The accuracy of resonance frequency measurements is generally very good, e.g. for the measurements performed in the appended paper IV differences in the resonance frequencies of the order 0.04 Hz was measured. The precision of the measurements is also very high, coefficients of variation as low as 0.004 % was

obtained in the measurements in paper IV. It should be noted that a longer time signal, of 1 s, was recorded during the measurements in the appended papers III and IV and that only a part of the time signal is displayed in figure 4.4a.

5. Acoustoelasticity

5.1. Theory of acoustoelasticity

The theory of acoustoelasticity regards the influence of mechanical stress on the acoustic waves in non-linear elastic materials, usually it is the increase in wave velocity due to an applied compressive stress that is of interest. The theory is based on Murnaghan's (1951) nonlinear elastic theory of isotropic solids, which is a hyper elastic material model, i.e. the stress-strain relationship for the material is derived from the energy of deformation. It was developed by Hughes and Kelly (1953) who derived expressions for the influence of a hydrostatic stress state on the elastic wave velocities in solids. The influence of stress is described by Lame's second-order, i.e. λ and μ, and Murnaghan's third-order elastic constants, i.e. l, m and n.

Consider the body in figure 5.1 which is subjected to a uniaxial stress in the x-direction, the expressions for the wave velocities in different directions derived by Hughes and Kelly (1953) can for a uniaxial stress state be written as equations 5.1 – 5.2, using second- and third-order elastic constants, Egle and Bray (1976). The wave V_{XX} refers to the wave travelling in the x-direction which is polarized in the x-direction, i.e. a compressional wave in the direction of loading, Similarly, V_{XZ} refers to a shear wave travelling in the direction of loading and polarized in the z-direction. Similar expressions can be derived for the three other wave velocities in figure 5.1 as well.

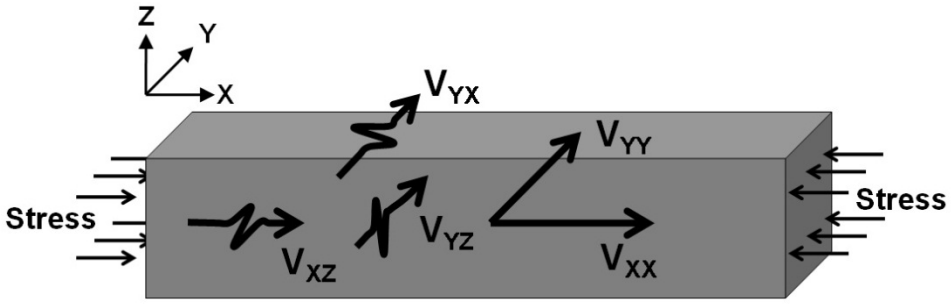

Figure 5.1. Definition of the directions of wave propagation.

$$V_{xx}^{\ 2} = \frac{1}{\rho_0}\left(\lambda + 2\mu + \left[4(\lambda + 2\mu) + 2(\mu + 2m) + \upsilon\mu\left(1 + \frac{2l}{\lambda}\right)\right]\varepsilon\right) \tag{5.1}$$

$$V_{xz}^{2} = \frac{1}{\rho_0}\left(\mu + \left[4\mu + \upsilon\frac{n}{2} + m(1 - 2\upsilon)\right]\varepsilon\right) \tag{5.2}$$

where:
ρ_0 = density of the material in the unstressed state, kg/m^3
λ = Lame's first elastic constant, second order, GPa
μ = Lame's second elastic constant, second order (shear modulus), GPa
υ = Poisson's ratio, -
l, m, n = Murnaghan's third order elastic constants, GPa
ε = static strain, -

One common way to describe the acoustoelastic effect is through the acoustoelastic constant L_{ij} which describes the relative change in wave velocity due to the applied axial stress or strain, the subscript *i* refers to the direction of propagation of the wave and the subscript *j* to the direction of polarization, L_{ij} is defined as:

$$L_{ij} = \frac{1}{V_{ij}^{0}} \cdot \frac{dV_{ij}}{d\varepsilon} \tag{5.3}$$

where:

dV_{ij} = the change in wave velocity for a wave propagating in the *i* direction, polarized in the *j* direction.

V^0_{ij} = wave velocity in the unstressed state, m/s
$d\varepsilon$ = the change in static strain in the direction of loading, -

By measuring the wave velocities in at least three directions, thus obtaining L_{ij}, in a specimen it is possible to determine the Murnaghan constants for the material by inverting the equations for the acoustoelastic constant. However, it is advantageous to measure at least one or two additional wave velocities in order to check the accuracy of the measurements and the calculated values of *l, m* and *n*. For example in a uniaxially loaded specimen five of the different wave velocities that can be measured are shown in figure 5.1.

According to Hughes and Kelly (1953), the acoustoelastic effect can be described as a stress dependent bulk modulus which increases linearly with the applied pressure. It should be noted that the acoustoelastic theory is only valid as long as the moduli vary linearly with the applied stress, i.e. as long as the response from the material is within the elastic regime and below the plastic limit. For uniaxial stress state the following nonlinear stress-strain relationship where the nonlinearity parameter β describes the stress dependency of the modulus of elasticity is valid, Payan et al. (2009):

$$\sigma = E\varepsilon\left(1+\beta\varepsilon\right) \tag{5.4}$$

where:
σ = stress, MPa
E = modulus of elasticity, GPa
ε = strain, - and:

$$\beta = \frac{3}{2} + \frac{l+2m}{\lambda+2\mu} \tag{5.5}$$

From equation 5.5 it can be seen that the acoustoelastic effect depends on the relation between the second and third-order elastic constants and not on the absolute values of the Murnaghan constants.

Acoustoelasticity has been studied for several different materials, for example rocks and for various types of metals, see e.g. Hughes and Kelly (1953), Egle and Bray (1976), Huang et al. (2001) and Payan et al. (2009). Hughes and Kelly performed measurements of the wave velocities in bars made of iron, Pyrex glass and polystyrene subjected to uniaxial stress state. It was found that the bulk and shear moduli of iron and polystyrene increase monotonically with the applied

compressive stress and that the moduli for Pyrex glass decrease with the applied compressive stress. The second and third order elastic constants were also determined for the investigated materials.

Egle and Bray performed measurements of the ultrasonic wave velocities in specimens of rail steel subjected to both uniaxial tensile and compressive loading. The results are shown in figure 5.2, where the stress dependency of the ultrasonic velocities is obvious. What further can be seen is that the influence is greatest for compressional waves propagating in the direction of loading, i.e. V_{11} in the figure, and is smallest for shear waves which both propagate and are polarized in the directions perpendicular to the applied stress, i.e. V_{23}. This wave and the compressional wave propagating perpendicular to the direction of loading, i.e. V_{22}, showed an opposite behavior in that the velocities decreased with the applied compressive stress. This behavior is expected since the strain in the transverse direction will be positive, i.e. a tensile strain, which thus will cause a decrease in wave velocity.

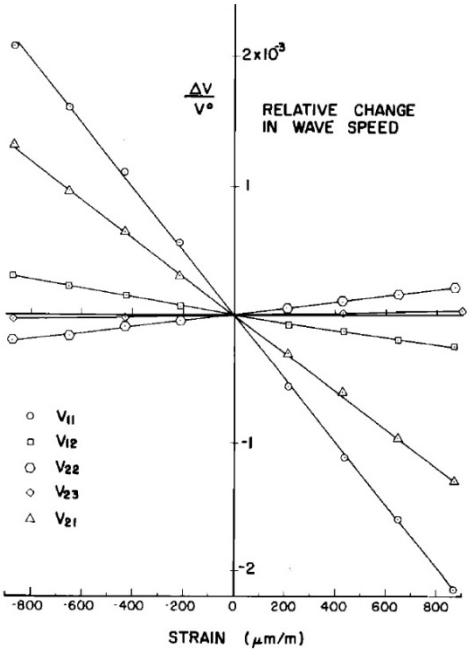

Figure 5.2. Influence of the applied stress on the ultrasonic wave velocity in rail steel, Egle and Bray (1976). Index *1* refers to the direction of loading, which e.g. means that V_{11} refers to the velocity of a compressional wave propagating in the direction of loading.

The influence of stresses on the elastic waves in different types of rock has been studied in order to e.g. estimate the in-situ stresses and has been studied both in the

context of acoustoelasticity, see e.g. Huang et al. (2001) and Johnson and Rasolofosaon (1996), and through the influence of micro cracks see e.g. Nur and Simmons (1969) and Sayers et al. (1990).

Nur and Simmons (1969) performed measurements of the velocities of elastic waves in cylindrical specimens of granite which was subjected to compressive stress. Both the velocities of compressional and shear waves were measured at angles varying between 0° and 90° to the direction of loading. It was found that the velocities increased with the applied stress for both types of waves and in all directions of propagation. Similarly as for steel, the influence was greatest for compressional waves propagating in the direction of loading. In figure 5.3, the results from some of the measurements are shown as the relative change in wave velocity plotted against the applied compressive stress for compressional waves, i.e. P-waves, and shear waves, i.e. S-waves. The degree sign refers to the direction of propagation with respect to the direction of loading, i.e. 0° is the direction of loading. Johnson and Rasolofsaon (1996) investigated the measurements performed by Nur and Simmons (1969) and other measurements in the literature performed on e.g. sandstone and marble in the context of acoustoelasticity and found that the wave velocities in the studied types of rocks increased with the applied compressive stress. They also calculated the acoustoelastic constants and Murnaghan's third order elastic constants for the studied types of rocks.

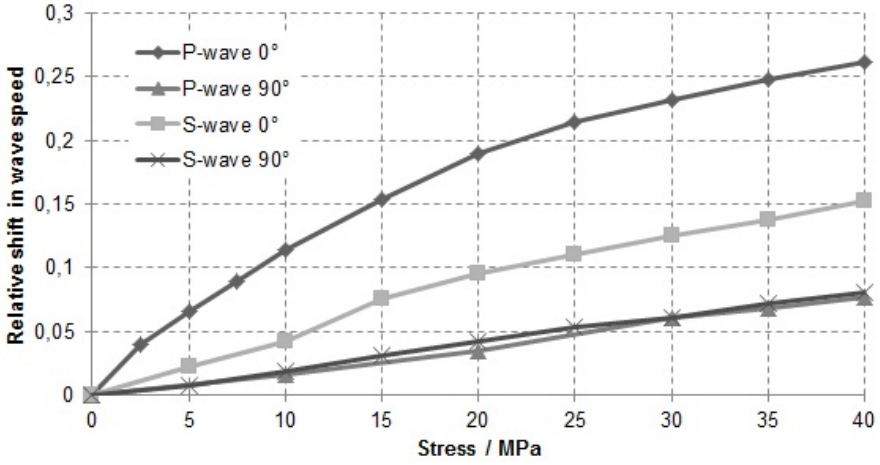

Figure 5.3. Influence of the direction of loading and compressive stress on compressional (P) and shear (S) waves in granite, Nur and Simmons (1969).

Sayers et al. (1990) explained the stress dependency of the elastic waves through the formation, growth and coalescence of micro cracks in the rock. In the theoretical model the cracks were assumed to be ellipsoidal voids which are

embedded in an isotropic medium and the orientation and distribution of these micro cracks was described using a micro crack density and distribution function. They measured the velocity of ultrasonic compressional and shear waves in a specimen of sandstone subjected to tri-axial stress state, the stress in the direction of propagation of the waves was varied and the stress in the directions perpendicular to this was kept constant at 4.1 MPa. Note that in this case the direction 3 is the direction of maximum stress. The load was increased up to failure of the specimens, which was around 120 MPa. The results showed that for stresses below 30 MPa, the wave velocities in all directions increased with the applied load, see figure 5.4. The compressional wave propagating in the direction of loading increased monotonically with the applied stress up to failure of the sandstone specimen, however the velocities of the compressional waves propagating perpendicular to the direction of loading decreased at stresses above 30 MPa. Similar behavior was found for the shear waves, the velocity of both the shear wave propagating in the direction of loading and the one polarized in the direction of loading but propagating perpendicular to loading increased with the applied stress but dropped somewhat prior to the maximum stress. The behavior at stresses below 30 MPa was attributed to the closing of existing micro cracks and grain boundaries and no additional cracking due to the applied load was expected at these stress levels. However, at stress levels above 30 MPa, new micro cracking was assumed to occur and the existing ones will grow. It seems reasonable to assume that this can explain the behavior of the compressional waves propagating perpendicular to the direction of loading since cracks in these two directions probably will increase with the applied load and thus cause the decrease in wave velocity, while the cracks in the direction of loading remain closed due to applied load.

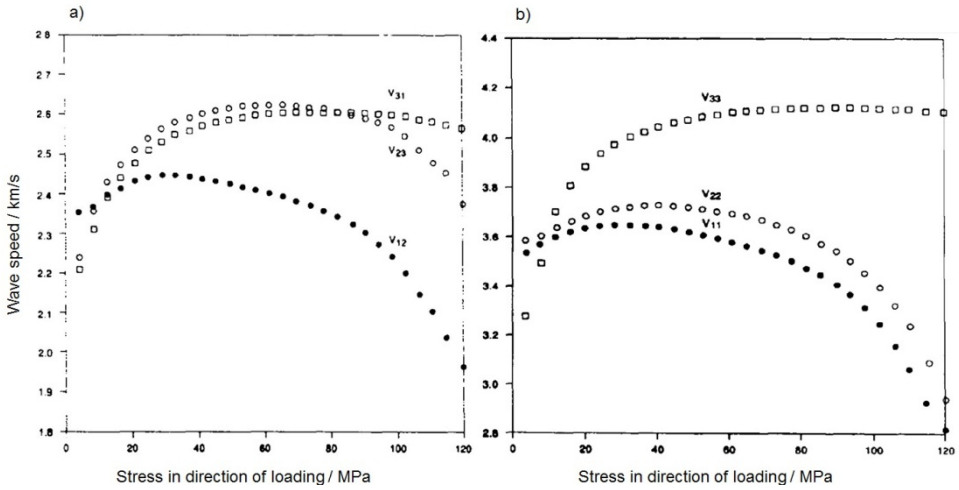

Figure 5.4. Influence of applied stress on the velocities of shear (a) and compressional (b) waves in Berea sandstone subjected to hydrostatic pressure, Sayers et al. (1990). The index 3 refers to the direction of maximum load.

Huang et al. (2001), compiled some of the studies on the influence of stress on the elastic wave velocities in rocks and compared the results from these measurements with calculations based on acoustoelasticity. The results showed that the change in elastic wave velocity estimated by the acoustoelastic theory were in good agreement with the measured values from the different studies. In addition, both the proposed micro crack model by Sayers et al. (1990) and the acoustoelastic theory was applied on the measurements performed by Nur and Simmons (1969), both theories were in good agreement with the results. It was concluded that the theory of acoustoelasticity is a macroscopic version of Sayers micro crack model and that the acoustoelastic theory is more suitable for estimating in-situ stress in rocks since it deals explicitly with the stress dependence of elastic waves.

5.2. Acoustoelastic effects in concrete

Only a few studies have been performed on the acoustoelastic effect in concrete, usually with the purpose of estimating the stress state in the concrete or the detection of damages, and all have focused on the influence of stress on the ultrasonic wave velocity, see e.g. Lillamand et al. (2010), Payan et al. (2009), Shokouhi et al. (2010) and Larose and Hall (2009).

In most studies coda wave interferometry has been used to study the influence of stress on the velocity of ultrasonic waves. Coda wave interferometry, CWI, is used to detect changes in a medium through the scattering of elastic waves. In concrete heterogeneities exist due to e.g. micro cracks, aggregate and reinforcement bars. These irregularities will cause scattering of a wave propagating through the concrete and parts of the wave will arrive later than the part first registered by the measurement equipment. These scattered waves are called coda waves and are very sensitive for changes in the material, such as development of new cracks or increased compressive stress. Since any change will alter the scattering behavior of the material CWI can thus be used to detect changes in a material over time.

Payan et al. (2009) performed measurements on the ultrasonic wave velocities in a cylindrical concrete specimen during the application of uniaxial loading and used CWI to investigate the influence of the applied stress. In order to obtain a fully elastic response the load was only increased up to 30 % of the ultimate compressive strength of the concrete. The results showed a strong acoustoelastic effect, see figure 5.5, where the acoustoelastic constants for the different measured waves also are given. As a part of the work within this thesis presented at the QNDE conference, see chapter 7, the relative change in velocities for different wave types were calculated using a nonlinear finite element model based on the values of the Murnaghan constants obtained by Payan et al. (2009). The results are shown in figure 5.6 along with the corresponding values of the acoustoelastic constants for the different waves. Similarly as for different types of rocks and steel the calculations showed that the compressional wave propagating in the direction of loading shows the greatest stress dependency and the shear wave propagating and polarized in the directions perpendicular to the load showed the lowest stress dependency. This was also found from ultrasonic measurements performed by Lillamand et al. (2010). In addition, Payan et al. (2009) also calculated Murnaghan's third order elastic constants, l, m and n and the nonlinear parameter β from equation 5.5 for the studied concrete sample, these values are given in table 5.1 along with other published values of β for concrete. As a comparison the values of l, m, and β for other materials found in the literature are also presented in table 5.1 and as can be seen the values for concrete are similar to those for granite and several times greater than those reported for steel and glass. There is a

variation in the values of β for concrete reported in the literature which seems reasonable since the concrete in the different studies had different mix proportions and mechanical properties. More interesting is that the measurements performed by Shokouhi et al. (2010) showed that the value of β is affected by earlier loading of the specimen. They performed measurements of the ultrasonic wave velocities in prismatic concrete specimens subjected to uniaxial compressive stress for a total of nine loading cycles. The values of β presented in table 5.1 are the highest and lowest of the obtained values, -75 was obtained for the second loading cycle and -143 for the eighth loading cycle, i.e. the absolute value of β increased with loading cycle. However, the applied compressive stress was increased for almost each loading cycle and in the fifth and sixth loading cycle the applied stress levels were 45 % and 60 % of the ultimate compressive strength, respectively, i.e. above the elastic regime which for these specimens was found to be below approximately 30 % to 35 % of the ultimate strength. These results indicate that the nonlinear parameter is affected by the damage induced by previous loading cycles, i.e. it depends on the stress history of the specimen. Similar results were obtained by Schurr et al. (2011), their measurements showed that the value of β were several times higher for damaged concrete specimens compared to that for undamaged specimens.

For a material with negative values of the Murnaghan's constants and β the velocity of elastic waves will increase with applied compressive stress, which is the case e.g. for concrete, steel and various types of rocks. Further, since the acoustoelastic effect according to equation 5.4 depends on the square of the strain, it can easily be seen from the values in table 5.1 that the acoustoelastic effect is very small in all of the studied materials.

Table 5.1. Murnaghan's constants and nonlinear parameter β for different materials.

Material	*l* / GPa	*m* / GPa	*n* / GPa	*β*
Steel [1]	-248	-623	-714	-9.8
Pyrex glass [2]	14	92	420	2.7
Polystyrene [2]	-348	-103	110	-97
Granite [3]	-3 371	-6 742	-6 600	-441
Sandstone [3]	-97 800	-99 400	-84 900	-9 600
Marble [3]	-40 300	-35 400	20 300	-1 900
Concrete [4]	-3 007	-2 283	- 1 813	-157
Concrete [5]	-	-	-	-143 to -75
Concrete [6]	-	-	-	-36
Concrete [7]	-	-	-	-40

[1] Egle and Bray (1976), [2] Hughes and Kelly (1953), [3] Johnson and Rasolofsaon (1996), [4] Payan et al. (2009), [5] Shokouhi et al. (2010), [6] Schurr et al. (2011), [7] Larose and Hall (2009)

In a study by Stähler et al. (2011), ultrasonic measurements were performed during the launching of a segment of a prestressed concrete bridge girder. According to the design calculations the stress in the structure changed from 0.5 MPa to 14 MPa during the launching. CWI was used to evaluate the effect of the varying stress on the velocities of the ultrasonic waves. Since the actual stress state in the structure was unknown, theoretical calculations of the changes in the stress state during the launching were performed. A 3D finite element model of the wave propagation in the structure based on the calculated stress state was performed and the results from the measurements was in good agreement with the calculations which shows that the acoustoelastic effect can be detected for measurements on real structures in the field.

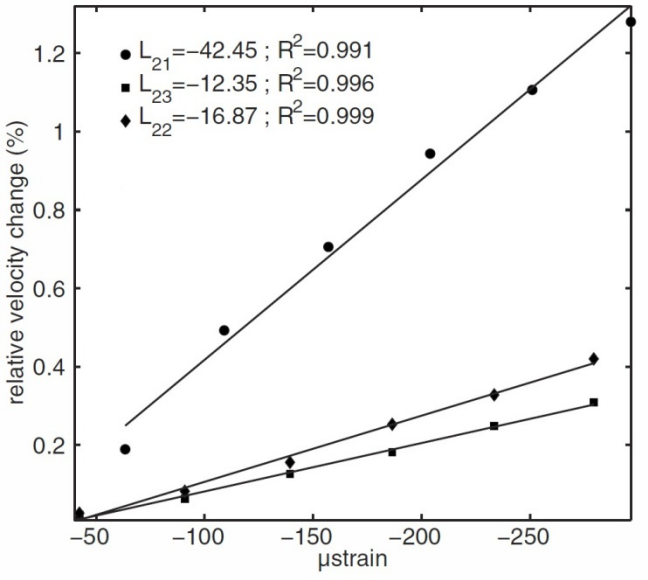

Figure 5.5. Influence of compressive stress on the ultrasonic wave speed in concrete, Payan et al. (2009). The first index refers to the direction of propagation and the second index to the direction of polarization, the load was applied in direction 1.

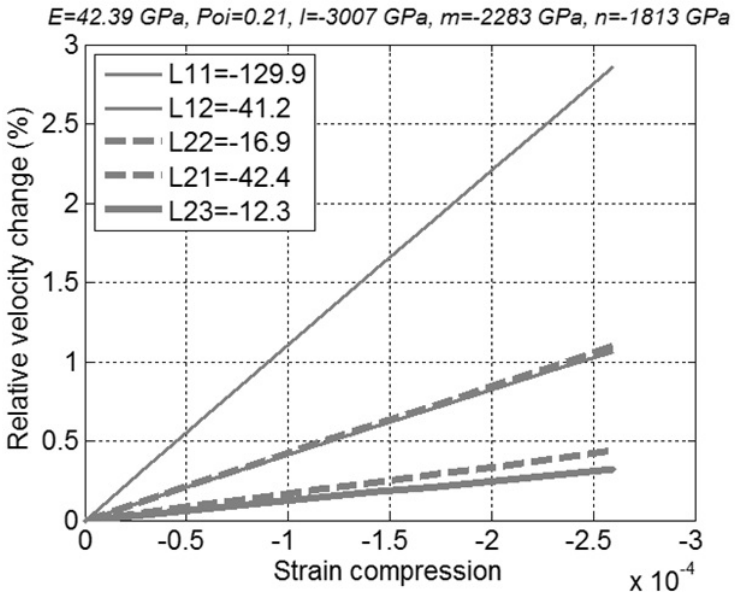

Figure 5.6. Calculated relative change in wave velocity and corresponding acoustoelastic constants, based on the values from Payan et al. (2009).

In the appended papers III and IV, the acoustoelastic effect on the resonance frequencies of prestressed concrete beams was investigated both for short- and long-term measurements. The investigated modes of vibration are those shown in figure 4.1. Since the acoustoelastic theory states that the elastic constants of concrete are stress dependent, this means that the resonance frequencies of concrete structures also should be stress dependent. In addition, the resonance frequencies are actually caused by the different wave types, when e.g. exciting the beams in the longitudinal mode a compressional wave will propagate through the beam and reflect at the free end of the beam. Those waves generated at the resonance frequencies of the beam will after the reflection at the free end be in phase with the incident waves and thus the amplitude of the reflected wave will, for each reflection, be amplified and cause the longitudinal vibrations of the beam. Similarly, the shear waves generated in one end of the beam will cause the torsional modes of vibration. The generation of the flexural mode of vibration is a bit more complicated and is due to Lamb waves propagating through the solid. Lamb waves have two different modes, the symmetric mode which generates longitudinal waves and the asymmetrical mode generating flexural waves. They are generated from surface waves in solids where the wavelength is equal or greater than the thickness of the solid, allowing the wave to penetrate to the other surface. For the asymmetrical mode this will cause the entire solid to vibrate in the flexural mode.

Moreover, several of the modes of vibration are proportional to the wave velocities in the solid. This can be seen by considering two different wave velocities for a bar, compressional and shear waves propagating in the longitudinal direction of the bar. The velocities for these waves can be calculated by equations 5.6 and 5.7, see e.g. Achenbach (1973) or Migliori and Sarrao (1997).

$$V_P = \sqrt{\frac{E}{\rho}} \tag{5.6}$$

$$V_S = \sqrt{\frac{G}{\rho}} \tag{5.7}$$

where:
V_p = compressional wave velocity, m/s
V_s = shear wave velocity, m/s
E = modulus of elasticity, GPa
G = shear modulus, GPa
ρ = density, kg/m^3

The resonance frequencies for the fundamental modes of vibration caused by these two wave types are determined from the following expressions, Migliori and Sarrao (1997):

$$f_{1P} = \frac{1}{2L} \cdot V_P \tag{5.8}$$

$$f_{1S} = \frac{1}{2L} \cdot V_S \tag{5.9}$$

where:
f_{1P} = resonance frequency for the fundamental longitudinal mode, Hz
f_{1S} = resonance frequency for the fundamental shear mode, Hz
V_P = compressional wave velocity, m/s
V_S = shear wave velocity, m/s
L = length of the beam, m

The mode shape for the fundamental modes corresponds to one half wavelength of the motion, i.e. the wavelength equals 2L and thus considering equations 5.8 and 5.9 the proportionality between wave velocity and resonance frequency is obvious. It should be noted that the equations 5.6 to 5.9 describe the wave velocity for a one-dimensional case of a bar and may be used with caution for accurate calculations of the resonance frequencies for a three-dimensional case, especially

for the higher modes of vibration. However, the expressions are relatively accurate for the fundamental modes. Considering the values for the beams in the appended papers III and IV in table 4.1 and that the shear modulus of the concrete is 16.1 GPa (calculated from the modulus of elasticity with a Poissons ratio of 0.21), equations 5.8 and 5.9 give a fundamental longitudinal and torsional mode of 678 Hz and 436 Hz, respectively. These values agree quite well with those obtained from the measurements on the beams, which were 659 Hz and 419 Hz, respectively.

The results from the short-term measurements showed that the resonance frequencies of the beams increased with the applied prestressing force, see figure 4.3, which also was predicted using a nonlinear finite element model based on the Murnaghan constants given in table 5.1. In figure 5.7 the results from the finite element calculations as the relative frequency shift versus the applied stress are shown including calculations for the flexural mode of vibration which was not included in paper III. As can be seen the resonance frequencies increase with the applied compressive stress and also show a similar behavior as for the different wave types, i.e. the longitudinal mode shows the greatest stress dependency which corresponds to the compressional wave propagating in the direction of loading.

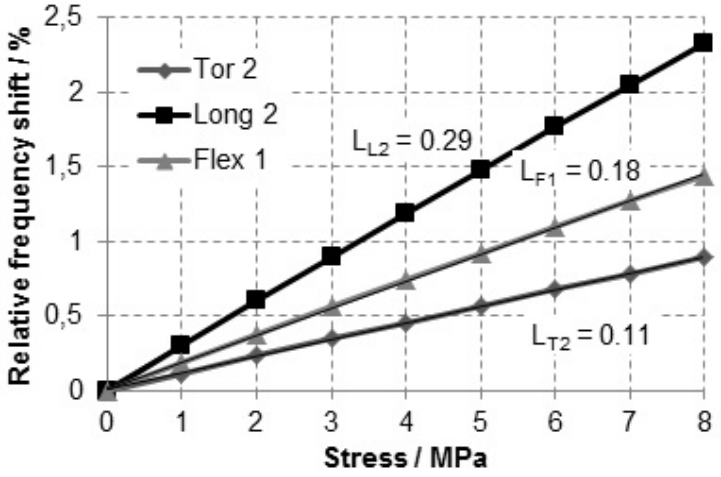

Figure 5.7. Predicted relative frequency shift of the resonance frequencies of prestressed concrete beams for the fundamental flexural mode and first higher torsional and longitudinal mode.

The first results from the long-term measurements showed that the resonance frequencies for all the beams, including the reference beam which was not prestressed, increased with time even though the tendon forces decreased. Theoretically they should decrease along with the prestress losses. This behavior

was attributed to the ongoing cement reactions in the concrete causing the mechanical properties of the concrete to increase with time and since the resonance frequencies depend on the modulus of elasticity this would explain the increase of the resonance frequencies. In figure 5.8 the increase of the resonance frequency for the fundamental flexural mode is calculated using equation 4.2, the development of the modulus of elasticity with time was modeled using the expression from Eurocode 2. Considering that the decrease in concrete stress due to the prestress losses was approximately 0.86 MPa, which from figure 5.7 would give a decrease in the resonance frequency of 0.2 % corresponding to 0.3 Hz, i.e. significantly less than the increase due to the cement reactions which was 5 % corresponding to 8 Hz. However, by subtracting the resonance frequencies of the reference beam from the prestressed beams, and thus removing the effect of the cement reactions, it was found that the resonance frequencies decreased with time in concordance with the loss of prestressing force, see figure 5.9. Furthermore, due to unexpected problems with the climate control system for the climate chamber in which the beams were stored indicated that the nonlinear behavior of the beams is affected by both the ambient temperature and the ambient relative humidity. The effects of the failures can be seen in figure 5.9 at the 15th February when the temperature dropped 5°C from 20°C to 15°C, number 1 in the figure and at the 7th April when the relative humidity decreased from 60 % to 45 %, number 2 in figure 5.9.

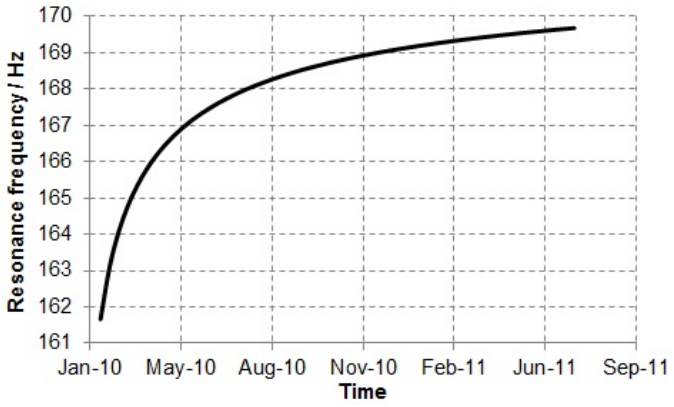

Figure 5.8. Theoretical increase of the resonance frequency with time due to the development of the modulus of elasticity predicted from Eurocode 2.

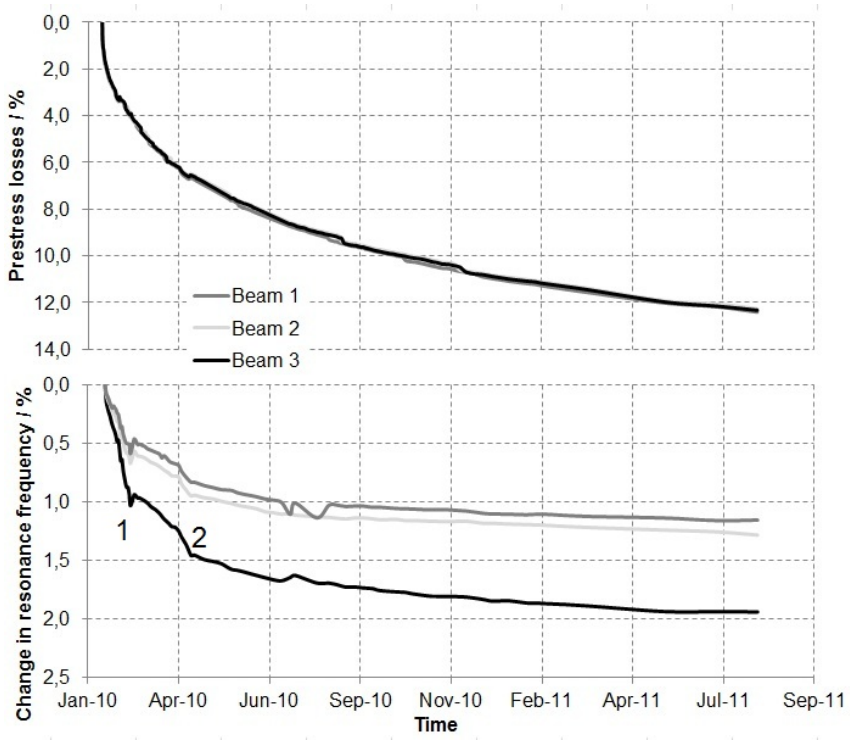

Figure 5.9. Prestress losses and decrease in resonance frequencies from the long-term measurements performed in the appended paper IV.

6. Summary of appended papers

Paper I and V regards the testing of several prestressed concrete beams in order to determine the prestress losses. In paper I, five 30 year old prestressed beams from the Finnish nuclear power plant Olkiluoto were tested and in paper V, eight prestressed beams subjected to an increased temperature were tested in order to investigate the influence of the temperature on prestress losses.

In paper II different prediction models for creep, shrinkage and relaxation were applied to calculate the prestress losses in the Swedish reactor containments with unbonded tendons. The results from the prediction models were compared to losses measured at the regular in-service inspections.

Paper III and IV deals with the influence of a prestress force on the dynamic behavior of prestressed concrete beams in the context of acoustoelasticity, in this case the increase in resonance frequency due to compressive stress.

Paper I

Lundqvist P., Rihiimäki J., 2010, Testing of five 30-year-old prestressed concrete beams, PCI Journal, Vol. 55, No. 4, pp. 50-58.

Several prestressed concrete beams were constructed simultaneously as the nuclear power plant Olkiluoto was built in Finland in the mid-seventies. The purpose was to monitor the development of the prestress losses in the containments, however, due to unrealistic results the testing program was cancelled and the remaining beams have been stored inside the containments ever since. Five of these beams were tested in order to determine the prestress losses, which were also calculated using different models for predicting creep and shrinkage of the concrete and the relaxation in the tendons. The measured prestress losses were quite high, ranging between 37 % and 61 %. Depending on the age at loading, the accuracy of the models varied, for the beams prestressed at a quite early age, 135 days, the models B3 and CEB/ FIP MC90 were the most accurate. When the time between casting and prestressing increased, approximately 2 years, the model GL2000 was in good agreement with the measured results. The scatter in the measured results was

attributed to cracking in the anchor zone, causing movements in the anchors. The difference between the results obtained from the prediction models and the tests was attributed to the ambient climate in which the beams were stored.

Paper II

Lundqvist P., Nilsson L-O., 2011, Evaluation of prestress losses in nuclear reactor containments, Nuclear Engineering and Design 241, pp. 168-176.

The tendon forces in Swedish containments with unbonded tendons are measured at regular in-service inspections. In this paper, the prestress losses obtained from these in-service inspections are compared to losses estimated using several prediction models for creep, shrinkage and relaxation. In an attempt to increase the accuracy of these models, modifications of the expressions for the development of shrinkage were made based on previous measurements of the humidity and temperature inside two Swedish containments. CEB-FIP Model Codes 1990 and 1999, ACI 209, Model B3 and GL2000 were the models used for predicting creep and shrinkage and the expressions in Eurocode 2 was used for the prediction of relaxation. The most accurate of the models were CEB/FIP MC 99 and ACI 209 and the accuracy of the prediction models was increased by 0.5 to 1.2 percentage units of prestress losses when using the modified development of shrinkage. Possible explanations for the deviation between the calculated and measured losses can be the restraining effect of mild reinforcement on creep and shrinkage and the influence of friction on the horizontal tendons.

Paper III

Lundqvist P., Rydén N., 2012, Acoustoelastic effects on the resonance frequencies of prestressed concrete beams – short-term measurements, NDT&E International, Vol. 50, September, pp.36-41.

In the work presented in this paper, the influence of a compressive force on the dynamic behavior of three prestressed concrete beams was investigated in the context of acoustoelasticity by applying resonant acoustic spectroscopy during static loading and unloading. The results showed that the measured resonance frequencies increased with increasing compressive stress which also could be predicted using a non-linear finite element model based on Murnaghan's third order elastic theory. In addition, previous studies on the dynamic behavior of prestressed concrete structures have shown the same behavior, however, these results have been difficult to explain theoretically and the results from this study can possibly provide a new theoretical basis for the observed stress dependency of the resonance frequencies of concrete structures. Furthermore, the results indicate that by measuring one or several resonance frequencies a change in the state of stress in a concrete structure can be detected.

Paper IV

Lundqvist P., Rydén N., 2012, Acoustoelastic effects on the resonance frequencies of prestressed concrete beams – long-term measurements, submitted to NDT&E International.

In this paper, resonance frequency measurements were performed on the same beams as in paper III for a period of approximately 17 months, in an attempt to monitor the prestress losses. The results showed that it is possible to measure the resonance frequencies continuously over a longer period of time with good accuracy and reliability and also that after a correction for the development of the modulus of elasticity with time, the change in resonance frequencies correlates with changes in tendon forces. Further, it was also found that resonance frequencies are affected by the ambient temperature and relative humidity.

Paper V

Lundqvist P., 2012, Thermal effects on long-term loss in prestressed concrete, submitted to Construction and Building Materials.

The influence of the high temperature, similar to that inside the Swedish reactor containments, on the prestress losses was investigated in this paper by constructing eight prestressed concrete beams of which six were subjected to similar climatic conditions as those inside reactor containments during a period of almost 3 years. The two remaining beams were subjected to a normal climate of the order 20°C. Five of the beams were grouted and in the remaining three load cells were used to monitor the decrease of tendon forces with time. The so-called crack re-opening method was used at the end of the study to determine the remaining tendon forces in all of the beams. It was found that the prestress losses in the beams subjected to the elevated temperature were approximately 25 % greater than those subjected to normal temperature. In addition, it was also found that the results from the crack re-opening tests, when interpreted according to previously used methods described in the literature, tend to underestimate the tendon forces. However, by modifying the results using a simple finite element model of the testing procedure improved the accuracy in determining the remaining tendon forces.

7. Other publications

Some parts of the work presented in this thesis have been presented at the following conferences and workshops.

Lundqvist P., 2008, Bonded tendons in nuclear reactor containments XX Nordic Concrete Research Symposium, Bålsta, Sweden, 8 - 11 June

Lundqvist P., Anderson P., 2008, Measured loss of prestress in 30 year old concrete structures, CSNI Workshop, Prague, Czech Republic, 1 - 3 October

Lundqvist P., 2010, Nuclear reactor containments – Evaluation of prestress losses and prediction models, The third International fib Congress and Exhibition, Washington, USA, 29 May – 2 June

Rydén N., Lundqvist P., Thelandersson S., 2010, Acoustoelastic effects on the natural frequencies of pre-stressed concrete beams, Quantitative Nondestructive Evaluation (QNDE) 2010, San Diego, USA, AIP Conference Proceedings, v 1335, p 1379-85.

Lundqvist P., Rydén N., 2010, Measurements of resonance frequencies on prestressed concrete beams, Fontrevaud 7, Avignon, France, 26 -30 September

Lundqvist P., Rydén N., 2011, Short- and long-term measurements of resonance frequencies on prestressed concrete beams, XXI Nordic Concrete Research Symposium, Hämeenlinna, Finland, 30 May – 1 June

8. Conclusions and further research

8.1. Conclusions

Estimating the remaining tendon forces in prestressed concrete structures with bonded tendons is associated with great difficulties since no direct measurements of the tendon forces are possible. The work presented in this thesis has been aimed at evaluating different methods for assessing prestress losses in these types of structures and the conclusions drawn from this work are summarized below.

For theoretical estimation of prestress losses in a prestressed concrete structure several empirically based prediction models for estimating creep and shrinkage of concrete exist. Prestress losses in nuclear reactor containments calculated using these models were in relatively good agreement with the losses obtained from the in-service inspections, but showed a tendency to overestimate the losses somewhat. On the contrary, when applied on test beams with high prestress losses the models significantly underestimate the measured prestress losses. In addition, the accuracy of the models can be increased if the actual drying conditions of the structure are taken into account. Creep was found to be the phenomenon which had the greatest contribution to the total prestress losses, it was also the difference in the prediction of creep which mainly separated the results between the different models. Some drawbacks of the models affecting the accuracy are that they do not consider the influence of reinforcement and increased ambient temperature. Furthermore, for estimating the prestress losses in the Swedish nuclear reactor containments the models CEB/FIP MC 1999 and ACI 209 were found to be the most accurate models when modified by taking the actual drying conditions into account.

A few semi-destructive and destructive methods are used for determining the remaining tendon forces in prestressed beams and slabs, the most common applied in the literature is the so-called crack re-opening method in which the specimen is subjected to a bending test in order to determine the vertical load required to reopen an existing crack in the bottom fiber of the specimen. At this load the stress in the bottom of the specimen is equal to zero and the effective tendon force can

thus be calculated. The results from crack re-opening tests presented in this thesis showed that the normal procedure for determining the crack re-opening load from the experimental data, i.e. interpreting the crack re-opening load as the intersection points of the two slopes in the crack width versus the applied load diagram, is erroneous. The true crack re-opening load is found at the point when the slope in the crack width versus applied load diagram deviates from its initially linear behavior and can be found by using a simple two-dimensional finite element model of the test procedure.

The climatic conditions inside nuclear reactor containments, i.e. relatively high temperature ranging between 25°C and 50°C and low relative humidity, affect the prestress losses in the containment walls. Prestress losses in old prestressed concrete beams stored inside a nuclear reactor containment showed significantly higher losses than those obtained from numerous studies on bridge beams in the literature. The effect is mainly due to the increase of concrete creep and relaxation of the tendons due to the increased temperature but also due to the effect from the low ambient relative humidity on both the final shrinkage and drying creep values. In addition, results from tests performed on prestressed beams stored in a climate closely resembling that of nuclear reactor containments showed that the prestress losses in these beams were approximately 25 % greater than those in beams stored in a normal indoor climate. These results also showed no significant difference between the prestress losses in beams with bonded and unbonded tendons.

Several previous studies have shown that the dynamic behavior of prestressed concrete structures is stress dependent, i.e. the resonance frequencies increase with the applied prestress force and from a linear elastic approach this behavior has been difficult to explain theoretically. In the work presented in this thesis the stress dependency of the resonance frequencies of prestressed concrete beams were verified during short-term measurements and it was shown that the stress dependency can be described by a nonlinear finite element model based on the theory of acoustoelasticity. In some recent studies the acoustoelastic effect, i.e. the increase in velocities of elastic waves due to applied compressive stress, has shown to be strong and easily measureable in concrete. The acoustoelastic effect can be described by stress dependent elastic constants, which thus would explain the stress dependency of the resonance frequencies. Furthermore, the results from long-term measurements showed that the resonance frequencies of prestressed concrete beams can be measured continuously over longer period of time with good accuracy and reliability. It was also found that after correcting for the development of the modulus of elasticity with time, the change in resonance frequencies correlates with the loss of tendon forces. These results indicate that the stress state in a simple concrete structure can be monitored nondestructively by measuring the resonance frequencies of the structure.

8.2. Further research needs

From the work conducted on the assessment of prestress losses in prestressed concrete structures with an emphasis on those in nuclear containments, the following needs of future research in this field are suggested below.

Clearly, the lack of knowledge regarding the mechanisms causing prestress losses is a major problem and some important research topics are:

- The influence of elevated temperatures, i.e. around 30°C to 60°C, on creep of concrete, but also on the relaxation of prestressing steel.
- The influence of ordinary reinforcement in the concrete on both shrinkage and creep of concrete.
- The age of the concrete at the time of loading is one important parameter affecting the prestress losses and very few studies have been performed for high ages at loading, i.e. after one year or more, which is the case for reactor containments.
- Some contradictory results on the size effect on the drying creep of concrete have been reported in the literature, see section 3.3.2, and this effect should be investigated more thoroughly.

The development of more accurate prediction models for creep and shrinkage of concrete with a strong emphasis on those particular conditions in a reactor containment is necessary for estimating the remaining tendon forces in reactor containments with bonded tendons. It is also important for reliable and more accurate predictions during the design stage of new nuclear power plants. This model must take the influence of elevated temperature and the influence of reinforcement into account and also be adapted to high ages at loading.

Another potential problem identified in this thesis requiring further investigation is the method used for measuring the remaining tendon forces in the containments with unbonded tendons. As described in section 2.5.2, the remaining tendon force is interpreted similarly as the crack re-opening load for a prestressed beam, i.e. as the intersection point in the displacement versus force diagram, see figure 2.8. Considering that the results from the appended paper V showed that the true crack re-opening load was approximately 40 % lower than the intersection point indicates that the tendon forces measured in-situ may be overestimated.

Studies on the nonlinear dynamic behavior of prestressed concrete structures described by the acoustoelastic theory have shown promising and interesting results for monitoring prestress losses. However, extensive research is needed for the development of a method which can be used for monitoring changes in the

stress state of real structures in the field. To achieve this goal some examples of topics which need to be investigated further are:

- More measurements of the third order elastic constants on different concretes and how they are related to e.g. water/cement ratio or mix proportions. Finding the relation between the third order constants and other mechanical properties of concrete may possibly provide a method of determining the third order constants from e.g. the compressive strength, similar to the expressions for estimating the modulus of elasticity from the compressive strength.
- A method which deals with the influence of the cement hydration on long-term measurements of the resonance frequencies.
- Since all other mechanical properties of concrete change with time due to the cement hydration it is reasonable to assume that this also is the case for the third order elastic constants and this should also be investigated.
- The influence of the ambient temperature and relative humidity on both the resonance frequencies and the nonlinear behavior of concrete structures.

In addition, further measurements on both laboratory specimens and real structures in the field are important and would give valuable information on other effects not identified in this thesis which need further investigation.

9. References

ACI Committee 209, 1992, Prediction of creep, shrinkage and temperature effects in concrete structures, ACI 209R-92., American Concrete Institute: Detroit, Michigan, USA.

ACI Technical document 209.2R-08, 2008, Guide for modeling and calculating shrinkage and creep in hardened concrete, ACI Committee 209, American Concrete Institute: Detroit, Michigan, USA.

Achenbach J.D., 1973, Wave propagation in elastic solids, North-Holland Publishing Company, Amsterdam, Holland.

Al-Manaseer A., Lam J-P., 2005, Statistical evaluation of shrinkage and creep models, ACI Materials Journal, Vol. 102, No. 3, pp. 170-176.

Anderson P., Berglund L-E., Gustavsson J., 2005, Average force along unbonded tendons: a field study at nuclear reactor containments in Sweden, Nuclear Engineering and Design 235, pp. 91-100.

Anderson P., 2005, 30 years of measured prestress at Swedish nuclear reactor containments, Nuclear Engineering and Design 235, pp. 2323-2336.

Baran E., Shield C.K., French C.E., 2005, A comparison of methods for experimentally determining prestress losses in pretensioned prestressed concrete girders, Ned H. Burns Symposium, American Concrete Institute Special Publication SP-231-10, pp. 161-180.

Barslivo G., Österberg E., Aghili B., 2003, Utredning kring reaktorinneslutningar – konstruktion, skador samt kontroller och provningar, SKI Rapport 2002:58. (in Swedish)

Bazant Z.P., Murphy W.P., 1995, Creep and shrinkage prediction model for analysis and design of concrete structures – Model B3. Materials and Structures, V. 28. No. 180, pp. 357-365.

Bazant Z.P., Li G-H., 2008, Comprehensive database on concrete creep and shrinkage, Structural Engineering report No. 08-3/AC210c, Northwestern University, Evanston, Illinois, USA.

Bazant Z.P., Li G-H., 2008, Unbiased statistical comparison of creep and shrinkage prediction models, ACI Materials Journal, Vol. 105, No. 6, pp. 610-621.

Brooks J.J., 1989, Influence of mix proportions, plasticizer and superplasticizers on creep and drying shrinkage of concrete, Magazine of Concrete Research, Vol. 41, No 148, pp. 145-153.

Brooks J. J., 2005, 30-year creep and shrinkage of concrete, Magazine of Concrete Research, Vol. 57, No. 9, pp. 545-556.

Brown N.H., Hope B.B., 1972, Theories of creep of concrete, Civil Engineering Research Report No. 72, Queen´s University at Kingston, Ontario, Canada.

Bryant A.H., Vadhanavikkit C., 1987, Creep, shrinkage-size and age at loading effects, ACI Materials Journal, Vol. 82, No. 2, pp. 117-123.

Burström P-G., 2001, Byggnadsmaterial, Uppbyggnad, tillverkning och egenskaper. Studentlitteratur, Lund, Sweden. (in Swedish)

Cahill T., Branch G.D., 1968, Long-term relaxation behavior of stabilized prestressing wires and strands, Proceedings: Conference on prestressed concrete pressure vessels, Institution of civil engineers, London, Great Britain.

Campbell-Allen D., Rogers D.F., 1975, Shrinkage of concrete as affected by size, Materials and Structures, Vol. 8, No. 45, pp. 193-202.

Carden P.E., Fanning P., 2004, Vibration based condition monitoring: a review, Structural Health Monitoring, Vol. 3, pp. 355-377.

CEB Bulletin d`Ínformation no. 199, 1991, Evaluation of the time dependent properties of concrete, Comite European du Beton/Federation Internationale de la Precontrainte: Lausanne, Switzerland.

CEB-FIP Bulletin 1, Structural Concrete, Textbook on behavior, design and performance-updated knowledge on the CEB/FIP Model code 1990. 1999, The International Federation for Structural Concrete: Lausanne, Switzerland.

CEB-FIP Bulletin 13, 2001, Nuclear Containments, State-of-art report, The International Federation for Structural Concrete: Lausanne, Switzerland.

Czaderski C., Motavalli M., 2006, Determining the remaining tendon force of a large-scale, 38-year-old prestressed concrete bridge girder, PCI Journal, Vol. 51, No. 4, pp. 56-68.

Collins M. P., Mitchell D., 1991, Prestressed concrete structures, Prentice Hall, New Jersey, USA.

Dall'Asta A., Dezi L., 1996, Discussion: Prestress force effect on vibration frequency of concrete bridges, Journal of Structural Engineering, Vol. 122, No. 4, pp. 458-458.

Deàk G., 1996, Discussion: Prestress force effect on vibration frequency of concrete bridges, Journal of Structural Engineering, Vol. 122, No. 4, pp. 458-459.

Eder R. W., Miller R. A., Baseheart M. T., Swanson J. A., 2005, Testing of two 50-year-old precast post-tensioned concrete bridge girders, PCI Journal, Vol. 50, No. 3, pp. 90-95.

Egle D.M., Bray D.E., 1976, Measurements of acoustoelastic and third-order elastic constants for rail steel, Journal of the Acoustical Society of America, Vol. 60, No. 3, pp. 741-744.

Eurocode 2: Design of concrete structures, 2005, European standard, prEN 1992-1-1. European Committee for Standardization.

Fahmi H. M., Polivka M., Bresler B., 1972, Effect of sustained and cyclic elevated temperature on creep of concrete, Cement and Concrete Research, Vol. 2, No 5, pp. 591-606.

Furr H. L., 1967, Creep tests of two-way prestressed concrete, ACI Journal, No 64-29, pp. 288-294.

Gamble B.R., Parrott L.J., 1978, Creep of concrete in compression during drying and wetting, Magazine of Concrete Research, Vol. 30, No. 104, pp. 129-138.

Gardner N.J., Lockman M.J., 2001, Design provisions for drying shrinkage and creep of normal strength concrete. ACI Materials Journal, V. 98, No. 2, pp.159-167

Gardner N.J. 2004, Comparison of prediction provisions for drying shrinkage and creep of normal-strength concretes. Canadian Journal for Civil Engineering. V. 31, No. 5, pp.767-775.

Ghali A., Treviño J., 1985, Relaxation of Steel in Prestressed Concrete, PCI Journal, Sept-Oct 1985, pp. 83-94.

Goel R., Kumar R., Paul D.K., 2007, Comparative study of various creep and shrinkage prediction models for concrete, Journal of Materials in Civil Engineering, Vol. 19, No. 3, pp. 249-260

Gross H., 1975, High temperature creep of concrete, Nuclear Engineering and Design 32, pp. 129-174.

Halsey J. T., Miller R., 1996, Destructive testing of two forty-year-old prestressed concrete bridge beams, PCI Journal, Vol. 41, No. 5, pp. 85-93.

Hamed E., Frostig Y., 2006, Natural frequencies of bonded and un bonded prestressed beams-prestress force effect, Journal of Sound and Vibration 295, pp. 28-39.

Hannant D.J., 1968, Strain behaviour of concrete up to 95°C under compressive stresses, Proceedings: Conference on prestressed concrete pressure vessels, Institution of civil engineers, London, Great Britain.

Hansen T.C, Mattock A.H., 1966, Influence of size and shape of member on the shrinkage and creep of concrete, ACI Journal, Vol. 63, No. 2, pp. 267-290.

Hop T., 1991, The effect of degree of prestressing and age of concrete beams on frequency and damping of their free vibration, Materials and Structures, Vol. 24, pp. 210-220.

Huang X., Burns D.R., Toksöz M.N., 2001, The effect of stresses on the sound velocity in rocks: Theory of acoustoelasticity and experimental measurements. Consortium Report, Earth resources laboratory, Massachusetts Institute of Technology, Cambridge, MA, USA.

Hughes D.S., Kelly J.L., 1953, Second-order elastic deformations of solids, Physical Review, Vol. 92, No. 5, pp. 1145-1149.

IAEA, 1996, Defense in depth in nuclear safety, INSAG-10, International Atomic Energy Agency, Vienna.

IAEA, 2004, Design of reactor containment systems for nuclear power plants, Safety guide NS-G-1.10, International Atomic Energy Agency, Vienna.

IAEA, 2006, Fundamental safety principles, Safety fundamentals SF-1, International Atomic Energy Agency, Vienna.

Institution of Civil Engineers, 1968, Conference on prestressed concrete pressure vessels at Church House, Westminister, London, Great Britain.

Jain S.K., Goel C., 1996, Discussion: Prestress force effect on vibration frequency of concrete bridges, Journal of Structural Engineering, Vol. 122, No. 4, pp. 459-460.

Johnson P.A., Rasolofsaon P.N.J., 1996, Nonlinear elasticity and stress-induced anisotropy in rock, Journal of Geophysical research, Vol. 101, No. B2, pp. 3113-3124.

Jordaan I. J., Illston J. M., 1969, The creep of sealed concrete under multiaxial compressive stresses, Magazine of Concrete Research, Vol. 21, No 69, pp. 195-203.

Kerr A.D., 1976, On the dynamic response of a prestressed beam, Journal of Sound and Vibration, Vol. 49, No. 4, pp. 569-573.

Kim J-T., Yun C-B., Ryu Y-S., Cho H-M., 2004, Structural Engineering and Mechanics, vol. 17, No. 3-4, pp. 467-482.

Kockal N. U., Turker F., 2007, Effect of environmental conditions on the properties of concretes with different cement types, Construction and Building Materials 21, pp. 634-645.

Kovler K., Zhutovsky S., 2006, Overview and future trends of shrinkage research, Materials and Structures, Vol. 39, pp. 827-847.

Lanig N., Stöckl S., Kupfer H., 1991, Versuche zum kriechen und zur restfestigkeit von beton bei mehrachsiger beanspruchung, Beuth Verlag Berlin.

Larose E., Hall S., 2009, Monitoring stress related velocity variations in concrete with a 2x10-5 relative resolution using diffuse ultrasound (L), Journal of the Acoustical Society of America, Vol. 125, No. 4, pp.1853-1856.

Leonhardt F., 1962, Spannbeton für die praxis, Wilhelm Ernst & Sohn, Berlin, Germany.

Lillamand I., Chaix J.F., Ploix M.A., Garnier V., 2010, Acoustoelastic effect in concrete material under uniaxial compressive loading. NDT&E International Vol. 43, pp.655-660.

Lu Z.R., Law S.S., 2006, Identification of prestress force from measured structural responses, Mechanical Systems and Signal Processing 20, pp. 2186-2199.

Migliori A., Sarrao J.L., 1997, Resonant ultrasound spectroscopy – applications to physics, materials measurements and nondestructive evaluation, John Wiley & Sons, New York, USA.

Miyamoto A., Tei K., Nakamura H., Bull J.W., 2000, Behavior of prestressed beams strengthened with external tendons, Journal of Structural Engineering, Vol. 126, No. 9, pp. 1033-1044.

Murnaghan F.D., 1951, Finite deformation of an elastic solid, John Wiley & Sons, New York, USA.

Naito C., Sause R., Thompson B., 2008, Investigation of damaged 12-year old prestressed concrete box beams, Journal of Bridge Engineering, Vol. 13, no. 2, pp. 139-148.

Nasser K.W, Neville A.M., 1965, Creep of concrete at elevated temperatures, ACI Journal, Vol. 62, No. 12, pp. 1567-1580.

Nasser K.W, Neville A.M., 1967, Creep of old concrete at normal and elevated temperatures, ACI Journal, Vol. 64, No. 2, pp. 97-103.

Nasvik J., 2006, Controlling shrinkage, Concrete Construction - World of Concrete, Vol. 51, No. 7, July, pp. 44-50.

Neville A.M., 1970, Creep of concrete, plain, reinforced and prestressed, North-Holland publishing company – Amsterdam, Netherlands

Neville A.M., 1995, Properties of concrete, Fourth edition, Longman Group Limited, Essex, England.

Nilsson L-O., Johansson P., 2006, Climatic conditions at the surfaces of concrete containments – examples for two BWR and PWR reactors, NUCPERF 2006 – EFC Event no 284: Workshop on: Corrosion and Long Term Performance of Concrete in NPP and Waste Facilities, 27- 360 march 2006, Cadarache, France.

Nilsson L-O, Johansson P., 2007, Climatic conditions at the surfaces of concrete containments – examples for two BWR and PWR reactors. The 19th International Conference on Structural Mechanics in Reactor Technology (SMiRT 19), August 12-17, Toronto, Canada

Niyogi A.K., Hsu P., Meyers B.L., 1973, the influence of age at time of loading on basic and drying creep, Cement and Concrete Research, vol. 3, pp. 633-644.

Nur A., Simmons G., 1969, Stress-induced velocity anisotropy in rock: an experimental study, Journal of Geophysical Research, Vol. 74, No. 27, pp. 6667-6674.

Oh B. H., Cha S. W., Um J. Y., Lim D. H., 1995, Effects of reinforcement and humidity on the creep and shrinkage behaviour of high-strength concrete members, Creep and Shrinkage of Concrete, Proceedings of the Fifth International RILEM Symposium, pp. 517-522.

Pandey M.D., 1997, Reliability-based assessment of integrity of bonded prestressed concrete containment structures, Nuclear Engineering and Design 176, pp. 247-260.

Parrott L. J., 1973, An examination of the effects of age at loading upon the creep of hardened cement paste, Magazine of Concrete Research, Vol. 25, No 85, pp. 197-200.

Payan C., Garnier V., Moysan J., Johnson P.A., 2009, Determination of third order elastic constants in a complex solid applying coda wave interferometry, Applied Physics Letters, Vol. 94, pp. 011904-1: 011904-3.

PCI Committee of Prestress Losses, 1975, Recommendations for estimating prestress losses. PCI Journal, V. 20, No. 4, pp. 45-70.

Pessiki S., Kaczinski M., Wescott H. H., 1996, Evaluation of effective prestress force in 28-year-old prestressed concrete bridge beams, PCI Journal, Vol. 41, No. 6, pp. 78-89.

Pickett G., 1942, Creep of concrete under a sustained load, Journal of the American Concrete Institute, Vol. 38, No. 4, pp. 333-355.

Pickett G., 1956, Effect of aggregate on shrinkage of concrete and a hypothesis concerning shrinkage, ACI Journal, Vol. 27, No., 5, pp. 581-590.

Rabbat B. G., 1984, 25-year-old prestressed concrete bridge girders tested, PCI Journal, Vol. 29, No. 1, pp. 177-179.

Raju K.K., Rao G.V., 1986, Free vibrations of prestressed beams, Journal of Structural Engineering, Vol. 112, No. 2, pp. 433-437.

Regulatory Guide 1.35, 1990. In-service inspection of ungrouted tendons in prestressed concrete containments, U.S. Nuclear Regulatory Commission (NRC).

Regulatory Guide 1.90, 1977. Inservice inspection of prestressed concrete containment structures with grouted tendons, U.S. Nuclear Regulatory Commission (NRC).

Ross A.D., 1944, Shape, Size and Shrinkage, Concrete and Constructional Engineering, pp. August, 1944, London, 193-199.

Roth T., Silfwerbrand J., Sundquist H., 2002, Betonginneslutningar i svenska kärnkraftsverk, SKI Rapport 2002:59. (in Swedish)

Roth T., 2004, Lifetime issues concerning prestressing steel in concrete structures, Licentiate thesis, Royal Institute of Technology, Stockholm, Sweden.

Russell H.G., Larson S.C., 1989, Thirteen years of deformations in water Tower Place, ACI Materials Journal, Vol. 86, no. 2, pp.182-191.

Saiidi M. S., Labia Y., Douglas B., 1997, Full-scale testing and analysis of 20-year-old pretensioned concrete box girders, ACI Structural Journal, Vol. 94, No. 5, pp. 471-482.

Saiidi M. S., Douglas B., Feng F., 1994, Prestress force effect on vibration frequency of concrete bridges, Journal of Structural Engineering, Vol. 120, No. 7, pp. 2233-2241.

Sayers C.M., Van Munster J.G., King M.S., 1990, Stress-induced ultrasonic anisotropy in Berea sandstone, International Journal of Rock Mechanics and Mining Science & Geomechanics, vol. 27, No. 5, pp. 429-436.

Schneider U., 1982, Behavior of concrete at high temperatures, Deutscher Ausschuss für Stahlbeton Heft 337, Wilhelm Ernst & Sohn, Berlin, Germany.

Shenoy C. V., Frantz G. C., 1991, Structural tests of 27-year-old prestressed concrete bridge beams, PCI Journal, Vol. 36, No. 5, pp. 80-90.

Shokouhi P., Zoëga A., Wiggenhauser H., 2010, Nondestructive evaluation of stress-induced damage in concrete, Advances in Civil Engineering, Vol. 2010, article ID 740189, 9 pages.

Schurr D.P., Kim J-Y., Sabra K.G., Jacobs L.J., 2011, Damage detection in concrete using coda wave interferometry, NDT&E International, Vol. 44, No. 8, pp. 728-735.

Song H-W., Kim S-H., Byun K-J., Song Y-C., 2002, Creep prediction of concrete for reactor containment structures, Nuclear Engineering & Design 217, pp. 225-236.

Stähler S.C., Sens-Schönfelder C., Niederleithinger E., 2011, Monitoring stress changes in a concrete bridge with coda wave interferometry, Journal of the Acoustical Society of America, Vol. 129, No. 4, pp. 1945-1952.

Tabatabai H., Dickson T. J., 1993, Structural evaluation of a 34-year-old precast post-tensioned concrete girder, PCI Journal, Vol. 38 No. 5, pp. 50-63.

Timoshenko S., Young D.H., Weaver W., 1974, Vibration problems in engineering, John Wiley & Sons, New York, USA.

Washa G., Fluck P., 1950, Effect of sustained loading on compressive strength and modulus of elasticity of concrete, ACI Journal, Vol. 46, No 5, pp. 693-700.

www.vattenfall.se, visited 2011-11-05.

Zhang Y., Zheng Y., Li H., 2012, A dynamic test of fully prestressed concrete beams, Advanced Materials Research, Vols. 368-373, pp. 2483-2490.

Paper I

Testing of five 30-year-old prestressed concrete beams

Peter Lundqvist
and Juha Riihimäki

The most common way to contain a nuclear reactor is by using a concrete structure that is prestressed both horizontally and vertically. The main function of the containment is to prevent any radioactive discharge to the environment in case of a severe internal accident in the reactor. In addition, the containment is expected to protect the reactor from external actions, such as airplane crashes and explosions. The most severe type of accident in a nuclear power plant is a loss of coolant accident (LOCA), which can be initiated by a pipe rupture in the cooling system, increasing both the pressure and the temperature inside of the containment.

The increased internal pressure at a LOCA is called the design pressure. The prestressing system is designed to counterbalance the tensile stresses in the concrete that occur at the design pressure, thus maintaining the structural integrity of the containment. However, creep and shrinkage of the concrete and relaxation of the prestressing steel cause the effective prestress forces in the containment to decrease with time.

Two primary methods are used to protect the prestressing tendons from corrosion: cement grouting (bonded tendons) or grease injection (unbonded tendons). One major disadvantage of using bonded tendons is the difficulty of performing assessments of the status of the tendons, such as measuring the remaining tendon forces or detecting corrosion damages.

When the nuclear power plant Olkiluoto was built in Finland in the mid-1970s, several prestressed concrete beams were fabricated. The prestress-loss monitoring consisted of testing one beam about every three years. However, the test results were deemed unreliable and the entire testing program was cancelled. The remaining beams have been stored inside of the reactor containment building ever since. The remaining tendon forces in five of these beams were tested, and the prestress losses obtained from the tests

Editor's quick points

- The remaining tendon forces in five beams used for nuclear reactors were tested, and the prestress losses obtained from the tests were compared with several different models for predicting creep and shrinkage of the concrete and relaxation of the prestressing steel.
- Most of the prediction models underestimate the measured prestress losses.
- One possible explanation for the deviation between prediction models and measured prestress losses is the influence of the ambient climate.

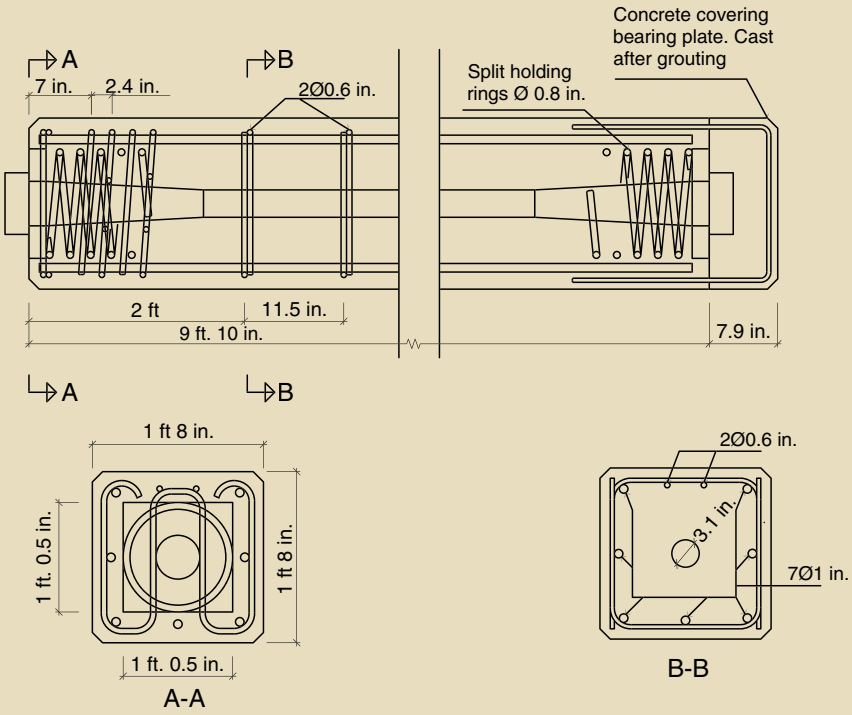

Figure 1. Details are shown for the beams with the VSL post-tensioning system. The arrangement of reinforcement and tendons is the same for all beams. The only differences between the beams with the two post-tensioning systems are the dimensions of bearing plates and ducts. Note: 1 ft = 0.3048 m; 1 in. = 25.4 mm.

were compared with several different models for predicting creep and shrinkage of the concrete and relaxation of the prestressing steel.

Research significance

In many countries, including Sweden and the United States, nuclear reactors are licensed for an operating period of 40 years. Within 10 years, the first of the Swedish reactors, built in the 1970s, will reach the end of its operating license, and the license holders wish to extend the service life of the reactors by some 20 years. One requirement for the renewal of the licenses is that the safety of the reactor be verified and guaranteed during the prolonged operating period.

Safety verification requires that the effective prestressing forces in the prestressed concrete reactor containment structure will still be sufficient to maintain the integrity of the structure when subjected to the design pressure. Therefore, it is of utmost importance to monitor, or at least estimate with high accuracy, the prestress losses in the containment. Furthermore, it is also of great importance to be able to estimate prestress losses, which significantly affect structural capacity, in other prestressed concrete structures with bonded tendons, such as bridges and hydropower dams.

Description of the beams

A total of five beams were tested, two from Olkiluoto reactor 1 (OL1) and three from reactor 2 (OL2). **Figure 1** shows the beam details. The beams were manufactured in 1975 (OL1) and 1977 (OL2) at the same time that the containment walls were cast. The beams are 9 ft 10 in. (3 m) long and have a square cross section of 19.7 in. × 19.7 in. (0.5 m × 0.5 m).

Two different post-tensioning systems have been used. For the beams from reactor 1, VSL type 19, 0.5-in.-diameter (13 mm) strand was used. In the beams from reactor 2, BBRV type R 238, seventy-two 0.24-in.-diameter (6 mm)

Figure 2. Shown is the arrangement of the beams in the testing machine.

strands were used. The tendon in the VSL system consists of a number of strands, each of which consists of seven wires. The tensioning is performed by pulling directly on the strands that are fixed by inserting wedges in the anchor head. The tendon in the BBRV system consists of a number of individual wires fixed directly to the anchor head. The tensioning is performed by lifting the anchor head and placing shims between the anchor head and the anchor plate. In each beam, one tendon is placed in the center of the cross section.

The anchorage system consists, in both cases, of a square bearing plate with split holding rings and a circular anchor head with openings for the passage of the wires. The initial tensioning forces in the beams from reactors 1 and 2 were 550 kip (2.4 MN) and 567 kip (2.5 MN), respectively. After the initial tensioning, the anchor set losses were eliminated by lifting the anchor head and placing shims between the anchor head and the anchor plate. After tensioning, the ducts were injected with cement grout.

The water–cement ratio of the concrete ranged from 0.49 to 0.54. Slow-hardening cement that conformed to ASTM C150 type IV was used.[1] The beams were cast with the same concrete that was used for the containment walls. Unfortunately, information regarding the curing method and curing time was not available.

The beams have been stored inside of the containment building at about 90 °F (32 °C) and 21% relative humidity (*RH*).

Testing procedure

The beams were arranged as simply supported in the testing machine and subjected to a single point load at midspan (**Fig. 2**). The beams were loaded in deflection control with increments of 3.9×10^{-4} in. (0.01 mm) per second until flexural cracks appeared at the bottom of the beam. The initial crack was marked and the beam unloaded and reloaded again until the crack reopened. In order to determine this so-called decompression load, one linear variable displacement transducer (LVDT) gauge was mounted across the crack (**Fig. 3**). The beams were loaded and unloaded three times in order to monitor the accuracy of the measurements.

The decompression load was determined from the load–versus–crack width diagram, in which a significant change in the displacement, recorded by the LVDT gauge, occurred after the crack reopened. The decompression load was determined by intersecting the tangents of the two slopes. **Figure 4** shows the crack width–versus–load diagram for one of the loading cycles for beam number 1. The final decompression load was calculated as the mean value of the three loading cycles. The intersection point was found using the following procedure: the intersection point δ was estimated visually (that is, by hand).

Two regression lines were adapted to the upper and lower slopes of the curve, respectively. For the lower slope, the regression line was adapted from the point at which the displacement was 4×10^{-4} in. (0.01 mm) (avoiding the irregularities in the region 0 to 4×10^{-4} in.) to the point on the slope corresponding to the deflection δ of -2×10^{-4} in. (0.005 mm). For the upper slope, the regression line was adapted between the point corresponding to the deflection δ of $+2 \times 10^{-4}$ in. (0.005 mm) to the endpoint of the slope, 7.3×10^{-4} in. (0.02 mm). This procedure (that is, adding/subtracting 2×10^{-4} in. (0.005 mm) to/from the intersection point) was used in order to avoid the irregularities when the change in slope occurs, which is clearly seen in Fig. 4. The final intersection point was found by intersecting the upper and lower regression lines.

Figure 3. The linear variable displacement transducer gauge is mounted across the crack.

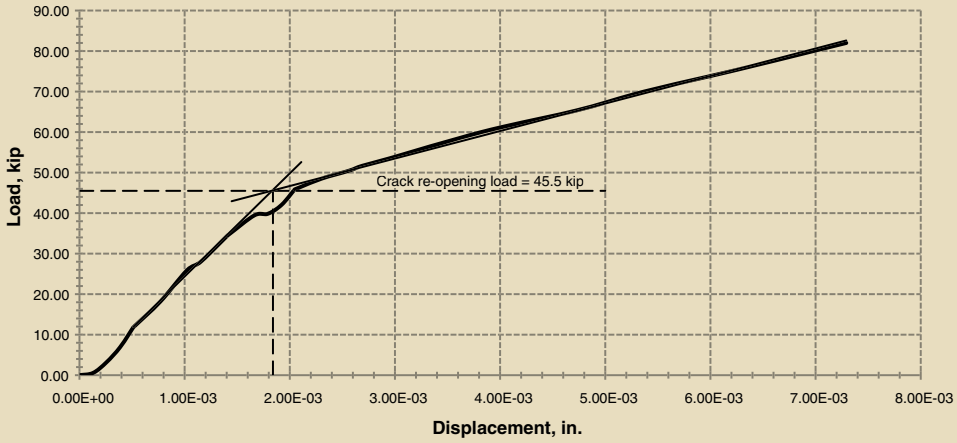

Figure 4. The graph shows the crack width–vertical load diagram for one of the loading cycles for beam number 1. The decompression load is determined by intersecting the two slopes. Note: 1 in. = 25.4 mm; 1 kip = 4.448 kN.

Table 1. Measured prestress forces and prestress losses

Beam no.	Initial prestress force, kip	Measured prestress force, kip		Prestress losses, %
		Average	Range	
1	567	349	343 to 358	38
2	567	351	346 to 356	38
3	567	215	211 to 226	61
4	550	346	343 to 353	37
5	550	281	276 to 284	48

Note: Beams 1 through 3 are from OL2 with the BBRV system. Beams 4 and 5 are from OL1 with the VSL system. 1 kip = 4.448 kN.

Because the stress at the bottom of the beam is zero at the decompression load, the remaining tendon force can be calculated using Navier's formula, which gives the following equation:

$$0 = \frac{P_{eff}}{A_c} - \frac{M}{S}$$

where

P_{eff} = remaining tendon force

A_c = cross-sectional area of beam

M = bending moment applied from testing machine

S = section modulus of the beam

The cross-section area of the beams is 2.7 ft^2 (0.25 m^2), and the section modulus is 0.74 ft^3 (0.021 m^3).

Testing results

Table 1 presents the measured and initial prestressing forces and prestress losses for each beam.

The variation in the results can be explained by the fact that during the testing of beams 3 and 5, splitting cracks occurred and propagated at both ends and did not close after unloading. In addition, extensive cracking was observed in the zones surrounding the bearing plates in these two beams. This indicates that the anchors moved inward during the testing, which causes a shortening of the tendon, thus increasing the prestress losses. Due to the short length of the tendons, a movement of 0.04 in. (1 mm) will result in prestress losses of about 5%.

Furthermore, for beam 3 the time between casting and tensioning was 63 days, while for the others it was more than 135 days. In all of the beams, slow-hardening cement (that is, ASTM C150 Type IV) was used, which means that the strength development of the concrete is slow.

The age at loading is an important parameter influencing creep, in particular if the loading occurs before the concrete is fully hardened. The creep will increase the earlier the load is applied, and this will significantly affect the prestress losses in the beam. The early loading and the movement of the bearing plates are the most probable explanations for the greater losses in beam 3 and for the greater prestress losses in beam 5. The movement of the bearing plates is the most probable explanation.

The prestress losses in the beams are relatively greater compared with results from tests of old bridge beams in the literature,[2–4] where the measured prestress losses ranged from 17% to 20%. This is probably because the beams were stored indoors at about 90 °F (32 °C) and 21% *RH* and were subjected to any variations in climate. Since both drying creep and shrinkage are due to the drying of the concrete, the ambient climate (that is, *RH* and to some extent the temperature) strongly affects these phenomena, thus increasing the prestress losses in the beams. In addition, both the relaxation of the tendons and the basic creep of the concrete are strongly affected by the temperature. Thus the high ambient temperature is another factor increasing the prestress losses in the beams.

Prediction models

The prestress losses in the beams have been calculated using various models for creep and shrinkage of concrete and one model for relaxation of the tendons. The models that were used for calculating creep and shrinkage are the European Committee for Concrete (CEB)/ International Federation for Prestressing (FIP) model code 1990[5] and 1999,[6] ACI 209,[7] Model B3,[8] GL2000,[9] and the PCI Committee on Prestress Losses.[10] The PCI model was also used for calculating the relaxation in the tendons. The method in the CEB/FIP model code has been used, even though it is stated that the creep and shrinkage model is only valid for concrete subjected to a mean *RH* between 40% and 100%.

Table 2. Input parameters for prediction models

Parameter	Beam number			
	1, 2	3	4	5
Curing method	Membrane	Membrane	Membrane	Membrane
Curing time, days	135	63	647	687
Age of concrete, days	11,063	11,056	11,922	11,961
Age at loading, days	135	63	647	687
Age at onset of drying, days	135	63	647	687
Compressive strength at 28 days, ksi	4.5	4.5	4.5	4.5
Elastic modulus at 28 days, ksi	2815	2815	2815	2815
Elastic modulus at loading, ksi	3118	3000	3278	3278
Cement type	Slow hardening			
Cement content, lb/ft^3	25	23.4	24.6	23.5
Water content, lb/ft^3	12.5	12.8	12.8	11.6
Aggregate content, lb/ft^3	108	108	109	120
Air content, %	1.3	1.5	0.9	1.6
Fine aggregate, %	53	55	52	50
Aggregate type	Normalweight			
Slump, ft	0.39	0.39	0.31	0.28
Ambient *RH*, %	20.9	20.9	20.7	20.7
Ambient temperature, °F	90	90	88	88
Type of prestressing steel	Low relaxation			

Note: *RH* = relative humidity. 1 in. = 25.4 mm; 1 ft = 0.3048 m; 1 ksi = 6.895 MPa; 1 lb = 0.453 kg.

The tendon forces, and thus the concrete stress, will decrease with time due to creep, shrinkage, and relaxation. Because creep is proportional to the stresses in the concrete, the creep rate will decrease with time. In addition, the change in tendon force will also affect the relaxation rate. These effects are taken into account by using the procedure in Eurocode 2[11] in which a mean value over time of the concrete stress is used when calculating the prestress losses. The effects on relaxation are also taken into account.

The creep and shrinkage models are empirical, and each model is based on a huge amount of data from shrinkage and creep tests. The procedure for estimating the strains is similar for both creep and shrinkage: a final creep coefficient/shrinkage strain is calculated from different parameters (for example, compressive strength, water–cement ratio, and ambient *RH*). The development of strains over a certain period of time is described by a time function calculated from concrete age, age at loading, and the volume-to-surface ratio of the structure.

Table 2 lists the input parameters for the models. Most of the data regarding the beams were available; however, some of the most important information, such as the modulus of elasticity and the compressive strength of the concrete, was missing. Therefore, the following assumptions had to be made:

- On two different occasions, in 1980 and 1983, tests were performed on concrete cylinders that were cast simultaneously with some of the beams from reactor 1. The age of the concrete at the time of testing was 3 years and 3 months and 6 years and 2 months, respectively. The 28-day compressive strength and the modulus of elasticity at 28 days and at loading were estimated from the test values by calculating backwards using the equations regarding the development of strength and modulus of elasticity over time according to CEB/FIP[6] (Table 2).

Table 3. Prestress losses calculated with the various prediction models

Beam no.	Testing, %	MC 90,* %	MC 99,† %	ACI,‡ %	PCI,** %	B3,†† %	GL2000,‡‡ %
1	38	23	25	17	24	37	31
2	38	23	25	17	24	37	31
3	61***	26	27	18	24	38	31
4	37	19	20	15	22	36	29
5	48***	21	20	14	22	36	29

* Source: CEB 1991.

† Source: *fib* 1999.

‡ Source: ACI Committee 209 1992.

** Source: PCI Committee of Prestress Losses 1975.

†† Source: Bazant and Murphy 1995.

‡‡ Source: Gardner and Lockman 2001.

*** Test result may be misleading due to slip in anchors during tests.

- It is assumed that the beams were cured using membrane curing, the same method that was used for the containment structures.

- The removal of the curing membrane (that is, the onset of drying) is assumed to have occurred simultaneously with the tensioning of the tendons.

Three cores were extracted from beam number 3 to determine the compressive strength of the concrete. The results from the different cores were scattered and the strength, 3.26 ksi (22.5 MPa), was lower than that measured on cylinders in 1980 and 1983. A closer examination of the cores revealed numerous air voids in the concrete, which indicates a poor quality when casting the concrete. Due to the unrealistic results, the measured strength was not used in the prediction models.

A comparison between the results from the prediction models and the measured prestress losses (**Table 3**) shows that model B3 was the most accurate of the prediction models and that most of the prediction models underestimate the measured prestress losses in the beams (disregarding the results for beams 3 and 5). Possible explanations for the accuracy of model B3 are that it is the most complex of the models with the highest number of input parameters and that the approach for predicting creep is only semi-empirical and partly based on theoretical knowledge of the phenomena affecting creep. In addition, it is the only model that separates basic and drying creep.

Explanations for the difference between the predicted and measured losses can be found by considering different parameters. The models are developed to be applicable to a wide variety of structures under more or less normal climatic conditions (that is, normally about 70 °F ([20 °C]). Because none of the models takes into account the effect of temperature on prestress losses, the ambient climate is probably the parameter that has the biggest influence on the deviation between predicted and measured prestress losses. The models are developed from creep and shrinkage test data, and normally the duration of these tests is only a couple of years. This is probably also a parameter that affects the accuracy of the models because the prestress losses in the beams have been developing for more than 30 years.

The fact that the prestress losses obtained from the tests are greater than those from the prediction models indicates that the assumption that the onset of drying occurs simultaneously with the tensioning is correct. Otherwise, due to the longer period of drying prior to the tensioning (in particular for beams 4 and 5), both the shrinkage contributing to the prestress losses and the drying-creep strains of the concrete would decrease.

Conclusion

- The prestress losses in the beams are relatively high compared with results from similar tests found in the literature, which is probably due to the ambient climate in which the beams were stored. An almost constant temperature of 90 °F (32 °C) and low *RH* increases both the creep and shrinkage strains in the concrete.

- Model B3 was the most accurate of the prediction models and was in good agreement with the prestress losses obtained from the tests.

- Most of the prediction models underestimate the measured prestress losses. One possible explanation for

the deviation between prediction models and measured prestress losses is the influence of the ambient climate.

Acknowledgments

The work presented in this paper is a part of the PhD project "Status of Bonded Tendons in Nuclear Reactor Containments," conducted at the Division of Structural Engineering at Lund University in Sweden. The authors gratefully acknowledge the support and the assistance from several individuals employed at Teollisuuden Voima Oyj, the electricity-generating public company that owns and operates the two nuclear power plant units in Olkiluoto, Finland. The financial support from Elforsk, the Swedish Electrical Utilities R&D Co., with contributions from Vattenfall and Eon, the power-producing companies that operate the Swedish nuclear power plants, and the Swedish nuclear inspectorate is also gratefully acknowledged.

References

1. ASTM C150.

2. Pessiki, S., M. Kaczinski, and H. H. Wescott. 1996. Evaluation of Effective Prestress Force in 28-Year-Old Prestressed Concrete Bridge Beams. *PCI Journal*, V. 41, No. 6 (November–December): pp. 78–89.

3. Czaderski, C., and M. Motavalli. 2006. Determining the Remaining Tendon Force of a Large-Scale, 38-Year-Old Prestressed Concrete Bridge Girder. *PCI Journal*, V. 51, No. 4 (July–August): pp. 56–68.

4. Shenoy, C. V., and G. C. Frantz. 1991. Structural Tests of 27-Year-Old Prestressed Concrete Bridge Beams. *PCI Journal*. V. 36, No. 5 (September–October): pp. 80–90.

5. Comite Euro-International du Beton (CEB). 1991. *Evaluation of the Time Dependent Properties of Concrete*. Bulletin d`Ínformation no. 199. Thomas Telford Services Ltd.: Lausanne, Switzerland.

6. Federation for Structural Concrete (*fib*). 1999. *Structural Concrete, Textbook on Behaviour, Design and Performance: Updated Knowledge on the CEB/FIP Model Code 1990*. *fib* Bulletin 1. *fib*: Lausanne, Switzerland.

7. American Concrete Institute (ACI) Committee 209. 1992. *Prediction of Creep, Shrinkage and Temperature Effects in Concrete Structures*. ACI 209R-92. ACI: Detroit, MI.

8. Bazant, Z. P., and W. P. Murphy. 1995. Creep and Shrinkage Prediction Model for Analysis and Design of Concrete Structures — Model B3. *Materials and Structures*, V. 28, No. 180: pp. 357–365.

9. Gardner, N. J., and M. J. Lockman. 2001. Design Provisions for Drying Shrinkage and Creep of Normal Strength Concrete. *Canadian Journal for Civil Engineering*, V. 98, No. 2 (March–April): pp. 159–167.

10. PCI Committee of Prestress Losses. 1975. Recommendations for Estimating Prestress Losses. *PCI Journal*, V. 20, No. 4 (July–August): pp. 45–70.

11. European Committee for Standardization. 2002. *Eurocode 2: Design of Concrete Structures*. European standard prEN 1992-1-1. Brussels, Belgium: European Committee for Standardization.

Notation

A_c = cross-sectional area of beam

M = bending moment applied from testing machine

P_{eff} = remaining tendon force

RH = relative humidity

S = section modulus of the beam

δ = deflection, estimated visually by the intersection point in load-crack-width diagram

About the authors

Peter Lundqvist, MSc, is a PhD student at the Division of Structural Engineering at Lund University in Sweden.

Juha Riihimäki, MSc, is the manager at Teollisuuden Voima Oyj in Olkiluoto, Finland.

Synopsis

The Swedish nuclear reactors are enclosed by a prestressed concrete containment. To prevent corrosion, the ducts in several containments have been grouted. When using this system, problems arise in monitoring the prestress losses. When the nuclear power plant Olkiluoto was built in Finland in the mid-1970s, several prestressed concrete beams were constructed. Five of these beams were recently tested in order to determine the prestress losses. The prestress losses have also been calculated using different models for predicting creep and shrinkage of the concrete and the relaxation in the tendons. This paper presents the results from both the tests and the models.

The measured prestress losses were quite high, ranging from 37% to 61%. The most accurate of the prediction models was model B3, which was in good agreement with the measured prestress losses. Explanations for the scatter in the measured results and the difference between the results obtained from the prediction models and the tests are proposed in this paper.

Keywords

Beam, bonded tendon, creep, prestress loss, relaxation, shrinkage.

Review policy

This paper was reviewed in accordance with the Precast/Prestressed Concrete Institute's peer-review process.

Reader comments

Please address any reader comments to journal@pci.org or Precast/Prestressed Concrete Institute, c/o *PCI Journal*, 200 W. Adams St., Suite 2100, Chicago, IL 60606.

Paper II

Author's personal copy

Nuclear Engineering and Design 241 (2011) 168–176

Contents lists available at ScienceDirect

Nuclear Engineering and Design

journal homepage: www.elsevier.com/locate/nucengdes

Evaluation of prestress losses in nuclear reactor containments

Peter Lundqvist[a,*], Lars-Olof Nilsson[b]

[a] Div. of Structural Engineering, Lund University, Lund, Sweden
[b] Div. of Building Materials, Lund University, Lund, Sweden

ARTICLE INFO

Article history:
Received 11 March 2010
Received in revised form 23 August 2010
Accepted 5 November 2010

ABSTRACT

The most critical safety barrier in a nuclear power plant, the concrete containment, is prestressed by hundreds of tendons, both horizontally and vertically. The main purpose of the containment is to prevent radioactive discharge to the environment in the case of a serious internal accident. Due to creep and shrinkage of concrete and relaxation of the prestressing steel, tendon forces decrease with time. These forces are thus measured in Swedish containments with unbonded tendons at regular in-service inspections. In this paper, the prestress losses obtained from these in-service inspections are compared to losses estimated using several prediction models for creep, shrinkage and relaxation. In an attempt to increase the accuracy of these models, existing expressions for the development of shrinkage were modified using previous findings on the humidity and temperature inside two Swedish containments. The models which were used and modified for predicting creep and shrinkage were CEB-FIP Model Codes 1990 and 1999, ACI 209, Model B3 and GL2000. Eurocode 2 was used for the prediction of relaxation. The results show that the most accurate of the models were CEB/FIP MC 99 and ACI 209. Depending on the model, the accuracy of the prediction models was increased by 0.5–1.2 percentage points of prestress losses when using the modified development of shrinkage. Furthermore, it was found that the differences between the different models depend mainly on the prediction of creep. Possible explanations for the deviation between the calculated and measured models can be the influence of reinforcement on creep and shrinkage of concrete and the influence of friction on horizontal tendons.

© 2010 Elsevier B.V. All rights reserved.

1. Introduction

The containment enclosing the reactor vessel is an essential safety barrier in a nuclear power plant. Its main purpose is to prevent radioactive discharge to the environment in the case of a severe internal accident. The most common type of containment is a concrete structure which is prestressed by both horizontal and vertical tendons. In Sweden, the corrosion protection of the tendons is accomplished either by cement grouting (bonded tendons) or by injection of, for example, grease (unbonded tendons).

The main accident scenario which the containment is designed to withstand is the so-called loss of coolant accident (LOCA). A LOCA can be initiated by for example a pipe rupture in the cooling system causing a discharge of steam into the containment. The release of steam increases both the temperature and pressure inside the containment, which induces tensile stresses in the concrete walls. The containment is prestressed in order to counterbalance these tensile forces, i.e. maintain the concrete in a compressive state. Other functions of the containment are to protect the reactor vessel against external actions, such as aircraft crashes, explosions and earthquakes.

Due to creep and shrinkage of the concrete and the relaxation of the prestressing steel, tendon forces decrease with time. Since the safety of the structure depends on these forces, being able to monitor or at least to estimate the prestress losses is of utmost importance. For containments with unbonded tendons, the forces in randomly selected tendons are typically measured at regular intervals during in-service inspections. This is not possible, however, in containments with bonded tendons, where no reliable means of monitoring the tendon forces are available.

In this paper, measurements of unbonded tendons are compared with results from predictions of prestress losses calculated using different prediction models for concrete creep and shrinkage and relaxation of the prestressing steel. The models which were used for predicting creep and shrinkage were CEB-FIP Model Codes 1990 and 1999, ACI 209, Model B3 and GL2000. Eurocode 2 was used for the prediction of relaxation. In some of the containments, temperature and relative humidity were measured both in the concrete and in the ambient climate. Using these measurements it was possible to modify the drying equations in the prediction models and thereby increase the accuracy of the prediction models. The prediction

* Corresponding author. Tel.: +46 46 222 9882; fax: +46 46 222 4212.
E-mail address: peter.lundqvist@kstr.lth.se (P. Lundqvist).

0029-5493/$ – see front matter © 2010 Elsevier B.V. All rights reserved.
doi:10.1016/j.nucengdes.2010.11.007

Author's personal copy

Nomenclature

A_c	cross-section area of concrete (m^2)
A_p	cross-section area of tendons (m^2)
E_c	modulus of elasticity of concrete (GPa)
E_p	modulus of elasticity of tendon (GPa)
L	the depth of the containment wall
N	number of tendons
n	the order in which the tendon was tensioned (for the initially tensioned tendon n is equal to 1)
t	time after tensioning (h)
$U(x, t)$	dimensionless water content
w_i	initial moisture content (kg/m^3)
$w(x, t)$	moisture content at x m from drying surface, t is the time between initial tensioning and measurement of tendon forces (kg/m^3)
w_∞	equilibrium moisture content (kg/m^3)
$\Delta\sigma_{pr}$	loss of prestress (MPa)
$\Delta\sigma_{pr}$	loss due to relaxation (MPa)
ΔP_{c+s+r}	prestress loss in tendon (N)
ε_{cs}	shrinkage strain
ε_{el}	strain due to elastic shortening
$\bar{\varepsilon}_{sh}(t)$	mean shrinkage strain over the cross-section
$\varepsilon_{sh}(x, t)$	shrinkage strain for an arbitrary point, x, in the wall at time t
$\varepsilon_{sh,\infty}$	the final shrinkage strain predicted by the models
μ	σ_{pi}/f_{py}, where f_{py} is the yield strength of the steel
ρ_{1000}	the relaxation loss 1000 h after tensioning to 70% of the ultimate strength at a mean temperature of 20 °C (%)
σ_c	concrete stress (MPa)
σ_c	initial concrete stress (MPa)
σ_{pi}	stress in tendon directly after tensioning (MPa)
$\varphi(t, t_0)$	creep coefficient

of relaxation was improved using results from the relaxation tests.

2. The reactor containment

In this study, the prestress losses in Swedish containments with unbonded tendons were evaluated, i.e. the containments for three pressurized water reactors (PWR) and three boiling water reactors (BWR). The main features of the containments for the two different reactor types are virtually the same, e.g. the shape is that of a concrete cylinder. The thickness of the cylinder walls varies between 0.76 and 1.2 m. Both the BWR and the PWR containments are resting on thick reinforced concrete slabs. The PWR containment is topped with a prestressed concrete dome and the BWR containment is topped with a prestressed concrete slab with a steel lid for accessing the reactor vessel. On the inner surface of the containments a steel liner, between 5 and 10 mm thick, secures the leak tightness. The inside of the liner is protected by a non load-bearing reinforced concrete shell, with thickness varying between 0.26 and 0.33 m.

Some differences exist between the two types of containments, e.g. the dimensions of the containment, the PWR containment has an inner diameter of approximately 35 m, compared to the diameter of the BWR containments which is approximately 24 m. The height of the PWR containments varies between 61 and 63 m, while the height of the BWR containments is approximately 40 m. The major difference is that the BWR containments are enclosed by a reactor building and are therefore not subjected to environmental exposure. The PWR containment is also the reactor building and encloses not only the reactor vessel but also other parts of the system such as the steam generators and pressurizer.

The outer cylinder wall of the containments is prestressed both horizontally and vertically and two different prestressing systems have been used for the containments. The system used in a majority of the reactors is the BBR (Birkenmaier, Brandestini and Ros) system with tendons consisting of 139 wires, each with a diameter of 6 mm. The other is the VSL (Vorspann System Losinger) system with tendons consisting of 19 strands, each with a diameter of 13 mm; each strand consists of 7 wires. The cylinder walls are heavily reinforced, with reinforcement ratios varying between 2 and 3.3%. Fig. 1 shows the main features of the two types of reactor containments, Anderson (2005).

3. Measurements

3.1. Prestress losses

All measurements used in this study to determine prestress losses were from two nuclear power plants in Sweden: Forsmark, which has three BWR reactors and is located on the east coast, and Ringhals, which has three PWR reactors and is located in western Sweden. The measurement data used were from inspections of unbonded tendons in Swedish nuclear power plants performed according to the American guidelines, Regulatory Guide 1.35 (1990). In accordance with this guide, the inspections had been performed every 5th year and at each in-service inspection the forces were measured in 4% of the tendons. The tendon force was measured by lifting the anchor head using a hydraulic jack and registering when the anchor head started to move, a so-called lift-off test. Measurements were performed on both horizontal and vertical tendons. At each inspection some tendons were also dismantled and inspected for corrosion and other material defects.

3.2. Humidity and temperature

In previous studies, Nilsson and Johansson (2006) and Nilsson and Johansson (2009), measurements of humidity and temperature were performed during service at two reactor containments, one of the PWR at Ringhals and at one of the BWR, unit 2, at Barsebäck nuclear power plant, located in the south of Sweden. The relative humidity (RH) and the temperature were measured both in the concrete and the ambient air. No measurements were conducted on the inside of the containment since the containments of both reactor types is equipped with a steel liner which prevents any moisture exchange with the climate. The containment wall is thus subjected to one-sided drying.

At the BWR containment at Barsebäck, measurements in the concrete were performed during a 3-month period at three levels in the wall, see Fig. 2. At the bottom and the top of the containment, the RH distribution through the wall were measured both in-situ with RH probes and on cores extracted from the wall, see Fig. 3. The results from the climatic measurements show that both ambient RH and temperature at the external surface varies along the height of the containment, approximately 5–10% RH and 50 °C in the upper parts and some 15–35% RH and 25 °C in the lower parts. Since the containment is enclosed by the containment building there is no temperature gradient in the wall and the concrete is subjected to a relatively constant climate. From the RH distribution it is obvious that the wall is still drying and that the drying is faster for the upper and warmer parts of the wall. Further, it was also found that the difference in vapor content between the indoor and outdoor air, the so-called moisture supply, was approximately 0.5 g/m^3. Thus the RH of the indoor air can be estimated by using weather data and by adding a moisture supply of 0.5 g/m^3.

Author's personal copy

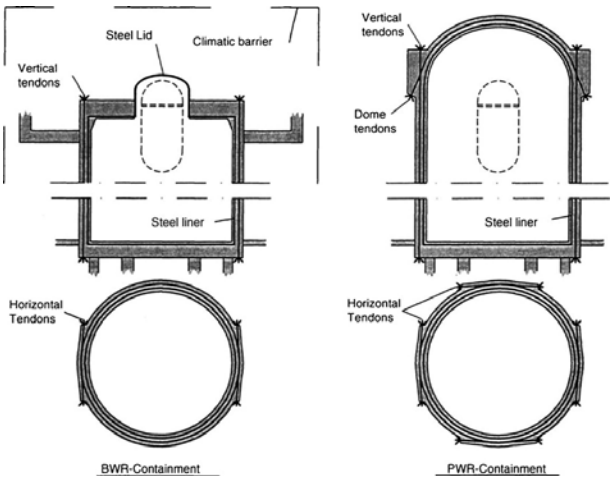

Fig. 1. Main features of two types of reactor containments, Anderson (2005).

At the PWR containment, Ringhals unit 3, the measurements of RH were performed for 1 year at various heights in the wall, see Fig. 4. The measurements in the concrete have been performed with RH probes at a depth of 30 mm from the outer surface. The results from the measurements show that the mean relative humidity in the concrete is approximately 75% during a year. The mean relative humidity outdoors is approximately 74% during a year, i.e. almost identical to the RH in the concrete. The drying is, however, ongoing due to the temperature gradient over the wall.

A model for calculating the moisture distribution in the containment wall and thus the drying of the wall using climatic data of the outdoor air has been developed and verified against the measurements performed at Barsebäck, Nilsson and Johansson (2009). The model was also used to calculate the moisture distribution in the wall of Ringhals unit 3 for a period of 30 years.

4. Prediction models

Different prediction models for creep and shrinkage of concrete and relaxation of the tendons have been used to calculate the prestress losses in the containments. The models that were used for calculating creep and shrinkage are the CEB/FIP Model Code 1990,

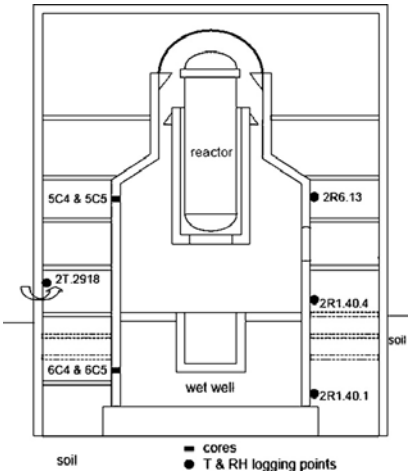

Fig. 2. Measuring points in the BWR containment, Nilsson and Johansson (2006).

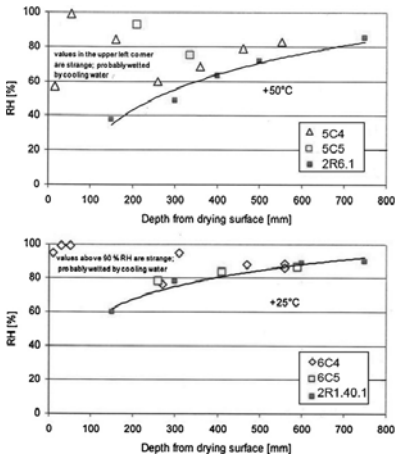

Fig. 3. The RH distribution in the upper and the lower parts of the wall of the BWR containment, Nilsson and Johansson (2009).

Author's personal copy

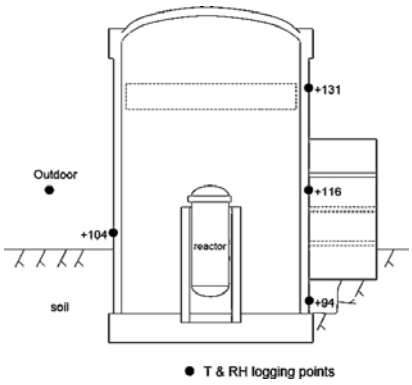

Fig. 4. Measuring points in the PWR containment, Nilsson and Johansson (2006).

CEB-FIP (1991) and 1999, CEB-FIP (1999) ACI 209, ACI Committee (1992), Model B3, Bazant and Murphy (1995), and GL2000, Gardner and Lockman (2001). The calculations of the relaxation in the tendons were performed according to the method in the Eurocode 2, European Committee for Standardization (2005). The method in the CEB/FIP model codes has been used, even though it is stated that the model is only applicable for concrete subjected to an external mean relative humidity ranging between 40 and 100%. The models for predicting creep and shrinkage are empirical and based on a large number of creep and shrinkage data. There is a wide variation both in the complexity of the models and in their approach to estimating creep and shrinkage. Several different parameters such as mix proportions, ambient climate, age of concrete and 28-day strength, are required as input to these models.

The approach for estimating creep is similar in the different models. A final creep coefficient is calculated based on different input parameters, such as ambient RH and volume to surface ratio. The development of creep during a certain time period is described by a time function with input parameters such as concrete age and age at loading. Model B3 differs somewhat from the other models and is, in comparison the most complex, having the highest number of input parameters and the most complex equations. Unlike the other models, it expresses creep as one part of the compliance function (the other part being elastic deformations), i.e. creep per unit stress. The creep compliance can be transformed to a creep coefficient by multiplying with the modulus of elasticity of the concrete. Furthermore, B3 is the only one of the models that calculates basic creep and drying creep separately. Drying creep is the additional creep due to drying of the concrete.

The approach for calculating shrinkage is similar for all models. A final shrinkage strain is calculated, e.g. based on the 28-day strength and ambient RH. The development of shrinkage up to a certain age is calculated by a time function based on e.g. volume to surface ratio and concrete age. The time function from model B3 applied for the containments up to 20,000 days is shown in Fig. 5. The CEB/FIP 1999 Model Code is the only of the models that separates the calculation of shrinkage into two parts, namely autogenous and drying. Autogenous shrinkage is the part of shrinkage which is due to the self desiccation of the concrete. The approach for calculating shrinkage is similar to that of calculating creep, i.e. a final creep coefficient is calculated and a time function describes the development.

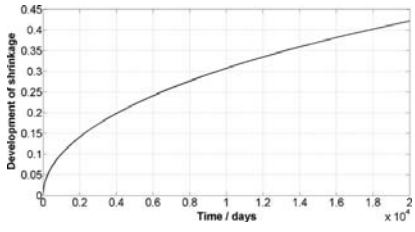

Fig. 5. The time function for development of shrinkage from model B3.

For calculation of the relaxation of the tendons the method in the Eurocode 2 was used, see Eq. (1).

$$\Delta\sigma_{pr} = \sigma_{pi}\left(0.66\rho_{1000}\, e^{9.1\mu}\left(\frac{t}{1000}\right)^{0.75(1-\mu)}\right) \times 10^{-3} \quad (1)$$

where $\Delta\sigma_{pr}$ = loss of prestress due to relaxation, MPa; σ_{pi} = stress in tendon directly after tensioning, MPa; t = time after tensioning, h; ρ_{1000} = the relaxation loss 1000 h after tensioning to 70% of the ultimate strength at a mean temperature of 20 °C, %. $\mu = \sigma_{pi}/f_{pk}$, where f_{pk} is the characteristic value of the tensile strength of the steel.

At the time of construction, relaxation tests (1000 h at 70% of ultimate strength) were performed at Forsmark, both at 20 °C and 50 °C, Roth (2004). The mean value of the results from these tests were 1.4% and 2.7% relaxation, respectively, which clearly show the influence of increased temperature on the relaxation of prestressing steel.

5. Calculation of prestress losses

The prestress losses for six containments with unbonded tendons have been calculated using the prediction models described above. The containments investigated are Ringhals unit 2 to 4 and Forsmark unit 1 to 3, at which measurements of tendon forces have been performed. Both horizontal and vertical losses have been calculated. In addition to calculating the mean losses for horizontal tendons in the containments at Forsmark, the losses in the upper and lower parts were also calculated. This was performed due to the variation in temperature and RH along the height in the BWR containments, which at least theoretically, will influence both creep and shrinkage at the different levels.

Since no climatic measurements have been performed at Forsmark, it was assumed that the temperature distribution in the walls at Forsmark is equal to that at Barsebäck. This is a reasonable assumption because of the similarities in design. The results from the climatic measurements in the BWR containment at Barsebäck show that the temperature varies over the height of the containment, approximately 50 °C in the upper and 25 °C in the lower parts. The mean temperature for the entire containment is estimated to 37.5 °C.

The monthly mean vapor content of the outdoor air at Forsmark, averaged over 30 years from 1969 to1990, was determined using weather data for the city of Söderhamn, located approximately 100 km north of Forsmark. By adding 0.5 g/m^3 to the vapor content of the outdoor air, the corresponding values of the RH of the air inside the reactor building were calculated, see Fig. 6. From the representative RH data in Fig. 6 and the time between the initial tensioning and latest measurement, see Table 1, the moisture distribution in the walls was calculated using the model developed by Nilsson and Johansson (2009). In Fig. 7 the mean change in moisture content over the cross-section for a period of 30 years is shown for Forsmark unit 1.

Author's personal copy

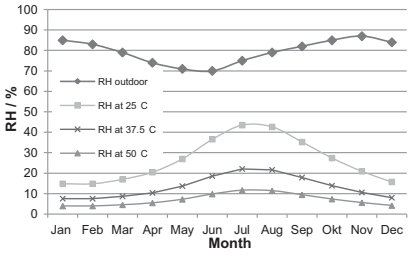

Fig. 6. The monthly averages of the RH distribution for a representative year in the indoor and outdoor air at Forsmark.

Table 1
Time between tensioning and measurement.

Unit	Time/years
Forsmark 1	23
Forsmark 2	18
Forsmark 3	22
Ringhals 2	27
Ringhals 3	26
Ringhals 4	25

One of the input parameters for the prediction models is the mean RH in the ambient air for which the structure is subjected to during its lifetime. The mean RH governs the equilibrium moisture level after long time for the concrete. From the data in Fig. 6, the mean RH for the containments at Forsmark was calculated for the three different temperatures. The mean RH for the entire containment, corresponding to 37.5 °C, was calculated to 15% RH. The mean RH for the lower and upper parts of the containment was calculated to 26.3% and 7.0%, respectively. The corresponding equilibrium moisture contents in the concrete, w_∞ in Eq. (2), were estimated from desorption isotherms developed by Nilsson and Johansson (2009).

In order to estimate the development of shrinkage it was assumed that the time development of shrinkage is synchronized with the drying process. From the temperature measurements and the calculations of the moisture distribution in the walls at different ages the degree of drying of the concrete was estimated. In order to improve the accuracy of the different prediction models, the time function describing the development of shrinkage was replaced by the simulated time development of drying. The shrinkage that occurred prior to prestressing was accounted for by subtracting those strains from the final value. The time between the initial tensioning and the latest measurement of tendon forces

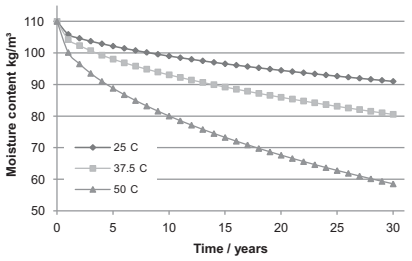

Fig. 7. The calculated mean change in moisture content in the containment wall at the different levels at Forsmark unit 1.

varies between the different containments, see Table 1. This means that the time during which the different containments have been subjected to drying varies and thus the development of shrinkage strains.

The drying of the concrete varies over the cross-section of the wall, see Fig. 3. The development of drying over the cross-section was determined using the dimensionless water content $U(x, t)$, see Eq. (2), which is equal to 1 when drying begins and equal to 0 when drying is completed.

$$U(x,t) = \frac{w(x,t) - w_\infty}{-w_i - w_\infty} \tag{2}$$

where $w(x, t)$ = moisture content at x m from drying surface, t is the time between initial tensioning and measurement, see Table 1, kg/m^3; w_∞ = equilibrium moisture content, kg/m^3; w_i = initial moisture content, kg/m^3.

The shrinkage strain for an arbitrary point in the wall at a certain time can be expressed as:

$$\varepsilon_{sh}(x,t) = \varepsilon_{sh,\infty}(1 - U(x,t)) \tag{3}$$

where $\varepsilon_{sh}(x, t)$ = shrinkage strain for an arbitrary point, x in the wall at time t; $\varepsilon_{sh,\infty}$ = the final shrinkage strain predicted by the models; $U(x, t)$ = dimensionless water content, see Eq. (2).

Since the drying of the concrete and therefore also the shrinkage vary over the cross-section of the wall, the shrinkage contributing to the prestress losses was determined by integrating the shrinkage strains over the cross-section according to Eq. (4).

$$\bar{\varepsilon}_{sh} = \frac{1}{L}\int_0^L \varepsilon_{sh}(x,t)\,dx \tag{4}$$

where $\bar{\varepsilon}_{sh}(t)$ = mean shrinkage strain over the cross-section; L = the depth of the wall, varying between 0.8 and 1.2 m for the different containments; $\varepsilon_{sh}(x, t)$ = shrinkage strain at x m from the drying surface of the wall, t is the time between initial tensioning and measurement, see Table 1.

Due to the prestressing procedure the elastic shortening of the concrete will contribute to the prestress losses. The initially tensioned tendon will experience the highest losses and the tendon which was tensioned last will not be affected by elastic shortening. From the order in which the tendons initially were tensioned, the contribution from the elastic shortening on the prestress losses was estimated. The elastic shortening was calculated by the following expression:

$$\varepsilon_{el} = \frac{(N-n)}{N-1}\frac{\sigma_c}{E_c} \tag{5}$$

where ε_{el} = strain due to elastic shortening; σ_c = concrete stress, MPa; E_c = modulus of elasticity of concrete, GPa; N = number of tendons; n = the order in which the tendon was tensioned (for the initially tensioned tendon n is equal to 1).

In the vertical direction, the mean value of the initial tendon forces and the entire cross section were used when calculating the concrete stress. The dead load of the containment was added to the vertical concrete stress, only when calculating creep. The dead load acting on the containments at Ringhals gives a compressive stress of 0.8 MPa. For Forsmark unit 1 and 2 the corresponding stress is 0.7 MPa and for unit 3 it is 0.6 MPa. For the containments at Forsmark, the initial concrete stress in the horizontal direction was calculated at two different levels, in the upper and lower parts, respectively. The stresses were calculated using the mean value of initial tendon forces and the distance between centers of the tendons for one meter in the vertical direction of the cross section. The concrete stress for the entire containment was calculated as the mean value of the stresses in the upper and lower parts. For the containments at Ringhals the concrete stresses in the horizontal direction were calculated for one meter in the vertical direction of

Author's personal copy

Table 2
Input parameters for prediction models.

Parameter	Unit		
	Forsmark 1, 2	Forsmark 3	Ringhals 2, 3, 4
Curing time, days	20	20	20
Age at loading, years	~2	~2	~1–2
Compressive strength, MPa	44.4	44.4	44.4
Elastic modulus, GPa	35.3	35.3	35.3
Volume/surface ratio, mm	850	1200	760
Cement type	Slow hardening	Slow hardening	Slow hardening[a]
Cement content, kg/m^3	370	400	375
Water content, kg/m^3	170	190	160
Aggregate content, kg/m^3	1880	1810	1910
Air content, %	<8	<8	<8
Fine aggregate, %	40–60	40–60	40–60
Slump, mm.	<130	<130	<130
Type of prestressing steel	LR[b]	LR[b]	LR[b]
Tensile strength of steel, MPa	1830	1800	1800

[a] In Ringhals unit 2, normal hardening cement has been used.
[b] LR = low relaxation steel.

the cross section using the distance between centers of the tendons and the mean value of the initial tendon forces. Due to the design of the containment, only the outer wall is assumed to be load-bearing in the vertical direction, whereas, in the horizontal direction both the outer and inner walls are assumed to carry load.

No direct measurements regarding the compressive strength of the concrete was available. However, the concrete quality was known, K50, which corresponds to a mean compressive strength of 44.4 MPa. The modulus of elasticity was estimated to 35.3 GPa from the compressive strength according to CEB/FIP MC 1999, CEB-FIP (1999). In Anderson (2005), the additional data required as input to the models were found and are shown in Table 2.

Using the procedure in Eurocode 2, where a mean value over time of the concrete stress is used when calculating the prestress losses, the prestress losses due to shrinkage, creep and relaxation were calculated, see Eq. (6). This procedure was used because the effective tendon forces, and thus the concrete stress, will decrease with time due to creep, shrinkage and relaxation and since creep is proportional to the stress the creep rate will decrease with time.

$$\Delta P_{c+s+r} = A_p \frac{\varepsilon_{cs} E_p + 0.8\Delta\sigma_{pr} + (E_p/E_c)\varphi(t, t_0)\sigma_c}{1 + (E_p/E_c)[1 + 0.8\varphi(t, t_0)]} \quad (6)$$

where ΔP_{c+s+r} = prestress loss in tendon, N; $\Delta\sigma_{pr}$ = loss due to relaxation, MPa; σ_c = initial concrete stress, MPa; ε_{cs} = shrinkage strain; $\varphi(t, t_0)$ = creep coefficient; E_c = modulus of elasticity of concrete, GPa; E_p = modulus of elasticity of tendon, GPa; A_c = cross section area of concrete, m^2; A_p = cross section area of tendons, m^2.

The relative prestress losses in percent were calculated by adding the losses due to elastic shortening to the results from Eq. (6) and dividing this sum with the initial tensioning force in the tendons.

6. Results and discussion

The results in Tables 3–5 show that the prediction models studied overestimate the measured prestress losses in most cases. This overestimation is illustrated by the broad variation of predictions seen in Figs. 8 and 9, where the straight line represents perfect agreement between calculated and measured losses. An exception is the results from Ringhals unit 2, which is further discussed below. Generally, there is a better agreement between measured and calculated losses in the vertical direction, which probably, as discussed below, is due to the influence of friction on the horizontal tendons. Furthermore, a comparison of the results from the prediction models and the measured prestress losses shows that the predictions by ACI 209 and CEB/FIP MC 99 were, in most cases, closest to the measured value.

Table 3
Measured and calculated horizontal and vertical losses in Forsmark NPP.

Models	Forsmark unit 1		Forsmark unit 2		Forsmark unit 3	
	Vertical	Horizontal	Vertical	Horizontal	Vertical	Horizontal
ACI	6.4%	6.3%	6.6%	5.0%	6.2%	6.3%
B3	9.0%	9.1%	8.6%	7.0%	7.2%	7.1%
CEB-FIP 90	8.7%	8.8%	8.5%	7.1%	8.4%	7.8%
CEB-FIP 99	7.6%	7.6%	7.5%	6.0%	6.5%	6.5%
GL2000	9.5%	9.7%	9.2%	7.7%	8.1%	8.1%
Measured	5.6%	8.8%	7.4%	14.5%	6.4%	3.7%

Table 4
Measured and calculated horizontal losses in Forsmark NPP.

Models	Forsmark unit 1		Forsmark unit 2		Forsmark unit 3	
	Upper	Lower	Upper	Lower	Upper	Lower
ACI	6.9%	5.9%	5.7%	4.6%	7.0%	5.6%
B3	13.1%	7.8%	9.9%	6.0%	9.0%	6.2%
CEB-FIP 90	10.5%	7.9%	8.7%	6.3%	9.1%	7.0%
CEB-FIP 99	8.9%	6.9%	7.4%	5.4%	7.6%	5.7%
GL2000	11.4%	8.8%	9.3%	6.9%	9.3%	7.4%
Measured	9.1%	8.4%	12.9%	16.1%	3.1%	4.3%

Author's personal copy

Table 5
Measured and calculated horizontal and vertical losses in Ringhals NPP.

Models	Ringhals unit 2		Ringhals unit 3		Ringhals unit 4	
	Vertical	Horizontal	Vertical	Horizontal	Vertical	Horizontal
ACI	7.1%	8.2%	7.5%	8.4%	7.5%	8.4%
B3	10.8%	12.3%	9.8%	11.1%	9.7%	11.1%
CEB-FIP 90	9.5%	10.7%	9.4%	10.5%	9.3%	10.5%
CEB-FIP 99	8.8%	9.9%	8.3%	9.3%	8.2%	9.2%
GL2000	11.4%	12.9%	11.0%	12.4%	10.9%	12.3%
Measured	17.2%	15.5%	8.2%	6.7%	7.6%	5.1%

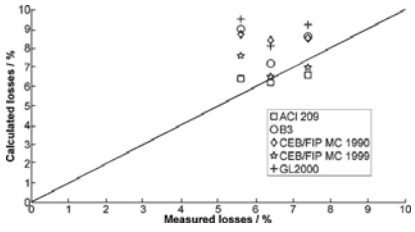

Fig. 8. Comparison between the predictions of the models and the measured losses for the vertical direction at the three units in Forsmark. The straight line represents the perfect agreement between measured and calculated losses.

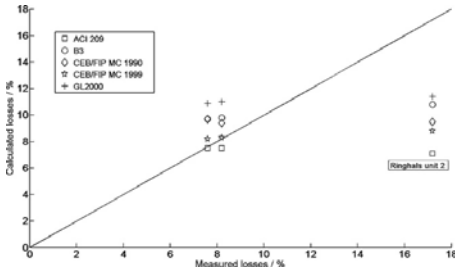

Fig. 9. Comparison between the predictions of the models and the measured losses for the vertical direction at the three units in Ringhals.

The shrinkage strains calculated by the models correspond quite well to each other: typically ACI 209 renders the lowest and GL2000 the highest shrinkage values. The greatest difference between two models was found for the vertical losses in Forsmark unit 1, where the losses due to shrinkage were predicted to 0.8 and 2.3% for ACI 209 and GL2000, respectively.

The results from this study show that differences between the models mainly depend on the prediction of creep. This difference is clearly seen in Fig. 10, which shows the predictions for the vertical tendons at Forsmark unit 2 The greatest difference in predictions of vertical losses due to creep was found for Forsmark unit 1, where CEB/FIP MC 1999 predicted losses of 2.5%, compared to those obtained from GL2000, which were 4.5%. Furthermore, it was found that CEB/FIP MC 1999 predicts the lowest losses due to creep, i.e. the lowest creep coefficient.

Table 6 presents the results for the development of shrinkage calculated with the time functions incorporated in the different models together with the development of shrinkage estimated from drying data, see Section 5. The same time function is used in both of the CEB/FIP model codes. As is apparent, all of the models underestimate the time development of shrinkage, except for

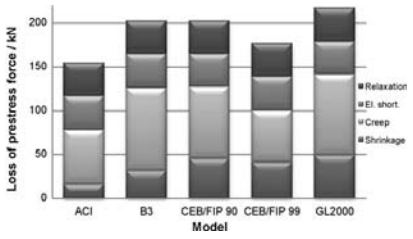

Fig. 10. Comparison between the predictions of the different models in the vertical direction at Forsmark unit 2. The measured loss of prestress force was 175 kN, i.e. equal to the predictions by CEB/FIP MC 1999.

ACI 209. Furthermore, except for ACI 209, there are no major differences in the predicted development of shrinkage between the models. Depending on the model, the accuracy of the prediction models increased by 0.5–1.2 percentage points of prestress losses when the estimated development of shrinkage was used.

The deviation between the calculated and measured prestress losses can be explained by considering variations in several parameters. First of all, the high reinforcement ratios in the containments studied, varying between 2 and 3.3%, probably influenced both the creep and shrinkage of the concrete. In a previous study, Oh et al. (1995), the effect of different reinforcement ratios was investigated for creep and shrinkage of high-strength concrete. It was found that a reinforcement ratio of 1.78% correlated with a reduction of approximately 30% in both the creep and shrinkage strains in concrete, compared to concrete without any reinforcement. This can explain the lower losses predicted for the containments investigated, since none of the models takes into account the amount of reinforcement in the structure.

A second parameter affecting accuracy relates to the procedures for developing the models, which are based on using a huge amount of data from creep and shrinkage tests. Normally, the test specimens are relatively small to ensure that they are easy to handle. When applying these models to a nuclear containment, i.e. large structures with large volume to surface ratios, the size difference could be a source of error. For example, the rate of drying depends on the size of the structure and the development of shrinkage and drying creep is faster for small specimens. Thus, even though the

Table 6
Shrinkage development in the vertical direction.

Unit	Shrinkage development (percent of final shrinkage)				
	ACI 209	B3	CEB/FIP	GL2000	Estimated
Forsmark 1	99.6	28.5	28.7	26.6	35.3
Forsmark 2	99.5	25.3	25.5	23.7	31.2
Forsmark 3	99.6	20.1	20.3	18.9	24.1
Ringhals 2	99.6	34.2	33.5	31.9	53.4
Ringhals 3	99.6	33.4	32.7	31.1	52.3
Ringhals 4	99.6	33.1	32.4	30.8	51.1

Author's personal copy

models take the volume to surface ratio into account, there are probably uncertainties when transferring the results from small specimens to large structures. Furthermore, the duration of the tests is limited, usually only a couple of years, since they would otherwise be very time-consuming. This parameter is probably also a source of error since the prestress losses in the containments have been developing for more than 20 years.

Uncertainties in the procedure of measuring the tendon forces is another parameter which affects the accuracy of the results. For example, the tendon force is determined as the force applied by the hydraulic jack at the instant when the anchor head starts to move and thus difficulties arise in determining when the movement of the anchor head begins. Further, only a small number of all the tendons are tested at each in-service inspection and it is difficult to determine if the losses in these tendons represents the losses for the entire containment. Finally, as described below, the influence of friction on the horizontal tendons can affect the results from the measurements.

Finally, the concrete in the containments is subjected to biaxial loading, which influences the creep to some extent. However, according to multi-axial creep tests found in the literature, Furr (1967), Jordaan and Illston (1969) and Lanig et al. (1991), this effect is negligible.

As for the scatter in the measured prestress losses indicated in Tables 3–5, several factors can explain this, at least theoretically: the influence of friction and the redistribution of forces along the length of the tendons. Since the horizontal tendons are curved, some with an accumulated bending angle of more than 360°, the friction between duct and tendon will influence the prestress losses, Anderson (2005). For instance tendons with an accumulated bending angle of 360° will experience approximately 40% prestress losses due to friction. Friction between tendon and duct can also influence the accuracy of the measurements. When using the lift-off technique it is only the force at the end of the tendon which is measured. According to Anderson (2005), the average prestress losses along a tendon influenced by friction are smaller than the losses at the end of the tendon. This behavior is due to force redistribution along the length of the tendon which is caused by discontinuities along the tendon, for example non-uniformly distributed deformations due to creep and shrinkage or temperature changes in the concrete. The magnitude of the force redistribution varies between different tendons due to differences in, for example, duct, bending angle and outline of the structure, i.e. some tendons will experience greater losses at the ends. Results from measurements of the average force along tendons at Forsmark unit 2 indicate that the loss of force along the tendon was less than the loss at the end, Anderson (2005). Therefore, it was concluded that the high losses in the horizontal tendons in Forsmark unit 2 were due to force redistribution along the tendons and that it is thus possible that the actual average losses are similar to those in Forsmark unit 1. The fact that the horizontal losses predicted for Forsmark unit 1 are in good agreement with the measured values supports this conclusion, i.e. that these measurements are more reliable and that there is a limited influence of friction on these tendons.

The influence of friction and redistribution of forces along the tendons can explain the strange results from the measurements of the losses in the upper and lower parts of the containments 2 and 3 at Forsmark. Theoretically, the losses in the upper parts should be greater than those in the lower parts of the containment which the results from the models confirm. However, the results from the measurements show the opposite, which probably is because of the uncertainties attached to the measuring procedure, i.e. due to the influence of friction. Thus, calculating the losses in upper and lower parts did not increase the accuracy of the predictions.

The results in Table 5 show that the prestress losses for Ringhals unit 2 are significantly higher than for the two other containments.

Table 7
Predicted prestress losses due to elastic shortening.

Unit	Vertical	Horizontal		
		Mean	Upper	Lower
Forsmark 1	1.3%	1.6%	0.8%	2.3%
Forsmark 2	1.7%	0.7%	0.3%	1.0%
Forsmark 3	1.3%	1.4%	1.3%	1.5%
Ringhals 2	1.9%	2.6%	–	–
Ringhals 3	1.9%	2.6%	–	–
Ringhals 4	1.9%	2.6%	–	–

Table 8
Predicted prestress losses due to relaxation.

Unit	Vertical	Horizontal		
		Mean	Upper	Lower
Forsmark 1	1.7%	1.0%	1.4%	0.7%
Forsmark 2	1.6%	1.1%	1.5%	0.8%
Forsmark 3	1.8%	1.7%	2.2%	1.3%
Ringhals 2	1.8%	1.7%	–	–
Ringhals 3	1.7%	1.6%	–	–
Ringhals 4	1.7%	1.6%	–	–

According to Anderson (2005), two factors can explain the higher losses: the type of cement and the early start of operation. Slow-hardening cement was used in all containments except for Ringhals unit 2, where normal hardening cement was used. This affects the creep of the concrete to some extent. The other factor affecting prestress losses is that the time between tensioning and the start of operation was approximately 1 year compared to the other containments, where the start of operation was 4–5 years after the initial tensioning. Since the temperature in the containment increases from some 20 °C to approximately 50 °C at the start of operation, the increased temperature at startup influences shrinkage, creep and relaxation. From the results it is clear that the models are unable to predict the losses in this containment. For all the other containments in this study the temperature was also increased at the start of operation. However, this increase occurred at a much higher concrete age and thus at more advantageous concrete properties, i.e. at a higher degree of hydration, which probably reduces the effect of the increase in temperature. In this study one additional factor affecting both the measured and calculated losses was found. The time between the initial tensioning and the latest measurement of tendon forces at Ringhals unit 2 was longer compared to the other containments. Thus the prestress losses have developed during a longer period of time.

Because of the above-mentioned effects in Ringhals unit 2 and Forsmark unit 2, respectively, the results from these containments have been disregarded when drawing the conclusions.

The prestress losses due to elastic shortening of the concrete are presented in Table 7. The difference between containments in elastic shortening is due to that the stress level in the concrete differs between the containments. The stresses in the concrete also vary within the containment, depending on the direction of the tendons. The mean losses due to elastic shortening are also strongly influenced by the order in which the measured tendons initially were tensioned.

The mean prestress losses due to relaxation shown in Table 8 are similar for all containments, except for the horizontal tendons at Forsmark. The deviation depends on the temperature effect on relaxation and for units 1 and 2 also on the initial stresses in the tendons, which were lower for the tendons at these units. According to the results in Tables 7 and 8 approximately one-third of the calculated prestress losses originate from elastic shortening of the concrete and relaxation of the tendons, thus the major part of the losses is due to shrinkage and creep.

Author's personal copy

This study shows that there is a need for improving existing prediction models. Two important parameters lacking in the models can be indentified, namely: reinforcement ratio and ambient temperature: the reinforcement ratio in the structure is a parameter which, as is shown in Oh et al. (1995), significantly reduces the strains due to creep and shrinkage and is thus a parameter that should be considered when developing a prediction model. The influence of temperature on prestress losses is a parameter which has been omitted in all of the prediction models, except for model B3 for which an improvement, Bazant and Kim (1992), has been published that deals with the temperature effect on creep. This improvement was, however, not used in this study because it would increase the losses predicted by the model and thus affect the accuracy. The ambient temperature is a factor which has a major influence on creep, but also on shrinkage and relaxation. This parameter is probably excluded from the models because most structures are subjected to normal temperatures, i.e. around 20 °C. This is the temperature at which the most tests, on which the models are based, are performed at and thus calibrated for. In this study, the temperature effect on prestress losses was indirectly accounted for in the prediction of shrinkage by calculating the development of drying at different temperatures and for relaxation by basing the prediction on results from relaxation tests.

7. Conclusions

- The prediction models were evaluated using unique data on long-term prestress losses measured on actual structures, which are hard to obtain.
- The accuracy of the prediction models was increased by 0.5–1.2 percentage points of prestress losses by estimating the time development of shrinkage from actual drying data measured inside the reactor building.
- In most cases, the losses predicted by the models overestimate the measured loss of prestress. The deviation between measured and calculated losses can be due to the high reinforcement ratio in the containments, tests in the literature have shown that the use of reinforcement reduces both creep and shrinkage of concrete. Other probable explanations for this deviation can be found in the procedure used for developing the models, but there are also uncertainties attached to the measuring procedure. Generally, there is a better agreement between measured and calculated losses in the vertical direction, which probably is due to the influence of friction and force redistribution along the horizontal tendons.
- The variation between the prestress losses estimated by the models is quite significant, for some containments the difference is up to 4.5 percentage points of prestress losses. It was found that the difference between the models mainly depends on differences in the prediction of creep.
- The results from the prediction models indicate that creep is the phenomenon with the biggest contribution to the total prestress losses, depending on the model, some 35–60% of the losses is due to creep.
- The variation in the prediction of shrinkage between the models was less than that for creep predictions, depending on the model, 15–35% of the losses is due to shrinkage. Comparisons between the time development of shrinkage calculated by the models and the development based on drying data reveals that all of the models underestimate the development of shrinkage, except for ACI 209 which significantly overestimates the development.
- The predictions by CEB/FIP Model code 1999 and ACI 209, were closest to the measured results for the main part of the containments. These were also the models which predicted the lowest losses due to creep.

References

ACI Committee 209, 1992. Prediction of Creep, Shrinkage and Temperature Effects in Concrete Structures, ACI 209R-92. American Concrete Institute, Detroit, MI.
Anderson, P., 2005. Thirty years of measured prestress at Swedish nuclear reactor containments. Nuclear Engineering and Design 235, 2323–2336.
Bazant, Z.P., Kim, J.-K., 1992. Improved prediction model for time-dependent deformations of concrete. Part 4. Temperature effects. Materials and Structures 25, 84–94.
Bazant, Z.P., Murphy, W.P., 1995. Creep and shrinkage prediction model for analysis and design of concrete structures – Model B3. Materials and Structures 28, 357–365.
CEB Bulletin d'Ínformation no. 199, 1991. Evaluation of the Time Dependent Properties of Concrete. Comite European du Beton/Federation Internationale de la Precontrainte, Lausanne, Switzerland.
CEB-FIP Bulletin 1, 1999. Structural Concrete, Textbook on Behaviour, Design and Performance – Updated Knowledge on the CEB/FIP Model Code 1990. The International Federation for Structural Concrete, Lausanne, Switzerland.
Eurocode 2: Design of concrete structures, 2005. European standard, prEN 1992-1-1. European Committee for Standardization.
Furr, H.L., 1967. Creep tests of two-way prestressed concrete. ACI Journal (64-29), 288–294.
Gardner, N.J., Lockman, M.J., 2001. Design provisions for drying shrinkage and creep of normal strength concrete. Canadian Journal for Civil Engineering 98 (March–April (2)), 159–167.
Jordaan, I.J., Illston, J.M., 1969. The creep of sealed concrete under multi-axial compressive stresses. Magazine of Concrete Research 21 (69), 195–203.
Lanig, N., Stöckl, S., Kupfer, H., 1991. Versuche zum Kriechen und zur Restfestigkeit von Beton bei mehrachsiger Beanspruchung. Beuth Verlag, Berlin (in German).
Nilsson, L.-O., Johansson, P., 2006. Climatic conditions at the surfaces of concrete containments – examples for two BWR and PWR reactors. In: NUCPERF 2006 – EFC Event No. 284: Workshop on: Corrosion and Long Term Performance of Concrete in NPP and Waste Facilities, 27-360 March 2006, Cadarache, France.
Nilsson, L.-O., Johansson, P., 2009. Changes in Reactor Containments – Climatic Conditions and Drying of Concrete Walls (in Swedish), ELFORSK Report 09:100. ELFORSK, Stockholm, Sweden.
Oh, B.H., Cha, S.W., Um, J.Y., Lim, D.H., 1995. Effects of reinforcement and humidity on the creep and shrinkage behaviour of high-strength concrete members. In: Creep and Shrinkage of Concrete, Proceedings of the Fifth International RILEM Symposium, pp. 517–522.
Regulatory Guide 1.35, 1990. In-service Inspection of Ungrouted Tendons in Prestressed Concrete Containments. U.S. Nuclear Regulatory Commission (NRC).
Roth, T., 2004. Lifetime Issues Concerning Prestressing Steel in Concrete Structures. Licentiate Thesis. Royal Institute of Technology, Stockholm, Sweden.

Paper III

NDT&E International 50 (2012) 36–41

Contents lists available at SciVerse ScienceDirect

NDT&E International

journal homepage: www.elsevier.com/locate/ndteint

Acoustoelastic effects on the resonance frequencies of prestressed concrete beams—Short-term measurements

Peter Lundqvist [a,*], Nils Rydén [b]

[a] Division of Structural Engineering, Lund University, PO Box 118, SE-22100, Lund, Sweden
[b] Division of Engineering Geology, Lund University, Lund, Sweden

ARTICLE INFO

Article history:
Received 19 October 2011
Received in revised form
17 April 2012
Accepted 26 April 2012
Available online 5 May 2012

Keywords:
Prestressed concrete
Resonance frequency
Acoustoelasticity

ABSTRACT

In this study resonant acoustic spectroscopy was applied during static loading and unloading of three prestressed concrete beams in the context of acoustoelasticity. At each load step multiple modes of vibration were measured using an accelerometer and a small impact source. It was found that the measured resonance frequencies increased with increasing compressive stress in a manner which can be predicted using a non-linear finite element model based on Murnaghan's third order elastic theory. Previous results from experimental studies on concrete bridges indicate that measured structural resonance frequencies increase with increasing prestress forces. These results have been difficult to explain theoretically and the results from this study can possibly provide a new theoretical basis for the observed stress dependency of the resonance frequencies of concrete structures. Furthermore, the results indicate that a change in the state of stress in a concrete structure can be detected or monitored by measuring one or several resonance frequencies.

© 2012 Elsevier Ltd. All rights reserved.

1. Introduction

Today, no method exists for determining the state of stress in a concrete structure and a method where the state of stress can be assessed non-destructively would have several potential applications. One example is prestressed concrete structures where the safety and function of the structure depend on the induced compressive stresses in the concrete and where various long term effects, i.e. creep and shrinkage of concrete and relaxation of the prestressing steel, causes the stresses in the concrete to decrease over time.

In several previous studies [1–3] the potential influence of stress on the resonance frequencies of prestressed concrete structures has been investigated. An increasing resonance frequency with increasing compressive stress have been experimentally observed [1,2] However this observed behavior has up until now been explained using linear elastic theory which predicts a decrease in resonance frequency with increased compressive stress and has thus been the subject of debate [4].

In this study, a different approach for explaining the stress dependency of the resonance frequencies of concrete structures has been used, namely the theory of acoustoelasticity. Recent studies where ultrasonic measurements [5–7], have been applied during uniaxial loading have shown a strong acoustoelastic effect in concrete. According to the theory of acoustoelasticity, the modulus of elasticity of a material is stress dependent and increases with applied compressive stress. Since the resonance frequency of a body, among other factors such as mass and geometry, depends on the modulus of elasticity of the material, the resonance frequency is thus stress dependent. This means that, at least theoretically, the change in state of stress in a concrete structure may be estimated by measuring one or several resonance frequencies. Furthermore, in a recent study [8] the influence on the wave speeds by the change in the state of stress was determined using coda wave interferometry for a concrete bridge during the construction phase. These results indicate that this nonlinear response of concrete may be determined under more complicated conditions than those in a laboratory and that the acoustoelastic approach may possibly be used for practical applications in the field. Monitoring resonance frequencies in concrete structures is already performed in many structural health monitoring applications and can be practically performed with high accuracy using only passive noise as a source [11]. To the authors knowledge the analysis of resonance frequencies in prestressed concrete structures have not been studied in the context of acoustoelasticity before. Measurements of the resonance frequencies may have some practical advantages on prestressed concrete structures since they are easier to measure and generally sense a larger global volume of the structure compared to local ultrasonic measurements.

In the experimental work performed in this study, resonant acoustic spectroscopy, RAS, was used to measure the resonance

* Corresponding author. Tel.: +46 46 2229882.
E-mail address: peter.lundqvist@kstr.lth.se (P. Lundqvist).

0963-8695/$ - see front matter © 2012 Elsevier Ltd. All rights reserved.
http://dx.doi.org/10.1016/j.ndteint.2012.04.010

frequencies of three concrete beams during the post-tensioning. The post-tensioning was performed in steps for both loading and unloading and RAS measurements were performed at each load step. The behavior of the beams was also modeled using a non-linear finite element model [9] based on Murnaghan's [10] third order elastic theory.

2. Theory

2.1. Resonance frequency

Theoretically every mechanical system or body has an infinite number of resonance frequencies at which the vibrations in the system increase significantly. The resonance frequencies of a homogenous, elastic material are a function of the mass and geometry of the solid, elastic constants and the boundary conditions. Thus measuring the resonance frequency of a body during constant ambient conditions, the modulus of elasticity and Poisson's ratio of the material can be determined. This technique is widely used in many fields of engineering [11] and is normally called resonant ultrasonic spectroscopy (RUS) or resonant acoustic spectroscopy (RAS).

2.2. Acoustoelasticity

Acoustoelasticity concerns the influence of stress on acoustic wave velocities in non-linear elastic materials, normally the increase in wave velocity due to compressive stress [6]. The variation of the wave velocities is due to the change in modulus of elasticity in a material under stress. Acoustoelasticity has been studied for several different materials, for example rocks and for various types of metals [12,13]. In 1953, Hughes and Kelly [14] derived expressions for the wave speeds in a stressed solid using Murnaghan's theory of finite deformations [10]. Based on these expressions and by using coda wave interferometry, Payan et al. [5] calculated Murnaghan's third order elastic constants, l, m and n for a cylindrical concrete sample. Murnaghan's constants can be related to the non-linear acoustoelastic constants L_{ij}, which relates the relative change in wave speed to the relative change in axial strain [14] or stress [15]. The index i refers to the direction of the propagating wave and the index j to the direction of polarization. Normally, an orthonormal basis with directions 1, 2 and 3 is used, where the uniaxial loading is in the 1 direction. For example, L_{11}, is then the wave speed for a compressional wave propagating in the direction of loading. This is usually the wave direction and polarization showing the greatest stress dependency. Assuming small deformations the definition of L_{ij} is

$$L_{ij} = \frac{dV_{ij}/V_{ij}^0}{d\sigma} \tag{1}$$

where dV_{ij} is the change in wave speed for a wave propagating in the i direction, polarized in the j direction. V_{ij}^0 is the wave speed in the unstressed state, m/s. $d\sigma$ is the change in stress in the direction of loading. A third order non-linear stress–strain relationship, where the nonlinearity parameter, β, describes the stress dependency of the modulus of elasticity can be written as [5]:

$$\sigma_c = E_c\varepsilon_c(1+\beta\varepsilon_c) \tag{2}$$

where σ_c is the concrete stress, MPa. E_c is the modulus of elasticity of concrete, GPa. ε_c is the concrete strain, β is the nonlinearity parameter. β can be expressed using the second and third order elastic constants.

$$\beta = \frac{3}{2} + \frac{(l+2m)}{\lambda+2\mu} \tag{3}$$

where l, m is two of Murnaghan's third order elastic constants (l, m, n), GPa. λ, μ is Lame's second order elastic constants, GPa.

Payan et al. [5] calculated a β value of -157 for concrete, since the influence of the parameter β depends on the square of the strain, according to Eq. (2), the acoustoelastic effect in concrete is very small.

Due to the stress dependency of the modulus of elasticity the resonance frequency should also be stress dependent, according to the acoustoelastic theory. Most resonance modes are directly proportional to the speed of stress waves which implies that relative changes in resonance frequencies should follow the same general stress dependent behavior. The acoustoelastic constant, L, would then be described similarly as in Eq. (1) by substituting the wave speed with the resonance frequency.

3. Experimental details

3.1. Description of tested beams

In total, four beams were constructed, each 3 m long with a square cross section of 350×350 mm^2. The tendon, placed straight in the center of the cross section, is of the type VSL (Vorspann System Losinger) which consists of 5 individual strands, each with a diameter of 15 mm. Each strand consists of 7 wires with a diameter of 5 mm. The anchorage system, VSL Type E, consists of a square bearing plate with split holding rings and a circular anchor head with openings for passage of the wires, see Fig. 1. Three of the beams were prestressed, the fourth beam was left unloaded and used as a reference. The concrete quality was C35/45, i.e. characteristic cylinder and cube strength of 35 and 45 MPa, respectively, with a water–cement ratio of 0.4. At a concrete age of 28 day the mean compressive strength was determined on 150 mm concrete cubes, cast simultaneously as the beams, to 63.4 MPa. The density of the concrete was determined to 2350 kg/m^3.

3.2. Measurements

The resonance frequencies of the beams were measured during the post-tensioning process, which was performed in steps of approximately 100 kN up to 950 kN, where 100 kN corresponds

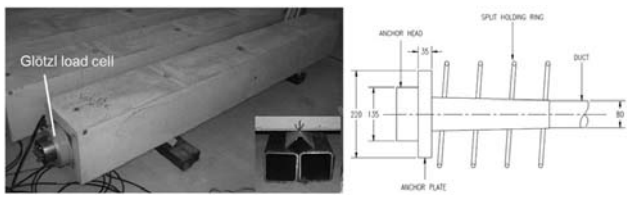

Fig. 1. Details of the beams and the supports, the picture to the right shows the details of the anchorage for the VSL post-tensioning system.

to approximately 1 MPa of concrete stress. The prestressing force was then reduced back to zero load in similar steps, see Fig. 4. During the entire procedure, the prestress force was measured using Glötzl load cells (KK 1000A 105 DK 4) placed between the anchor head and the anchor plate, see Fig. 1. A hydraulic fluid in the load cell records the applied pressure and the signal is converted to an electric signal using a piezoelectric converter, the accuracy of the load cells is 0.5%. The resonance frequencies of the beams were measured at each step of both the loading and un-loading. The hydraulic jack, weighing approximately 60 kg, used for post-tensioning was attached to one end of the beams, see Fig. 2 for details. To avoid any possible prestress dependent effects on the boundary conditions of the beams, the hydraulic jack was suspended by chains from an overhead crane and thus not rigidly connected to anything else. At each load step two different modes of vibration were examined; torsional and longitudinal. The resonance frequency was measured 20 times for each load step and mode of vibration and the final result was taken as the mean value of the 20 measurements.

To record the resonance frequencies when the beams vibrated, a piezoelectric accelerometer (PCB Model 353B33, 100 mV/g) and data acquisition system (NI USB-4432) was used. The resonance frequency of the accelerometer is higher than 22 kHz and the measured response is linear within 5% from 1–4000 Hz. The accelerometer was attached magnetically to thin washers glued onto the surface of the beams, which ensured a good mechanical contact between accelerometer and beam. The coupling resonance frequency of the accelerometer (~10 kHz) using this method is well above the measured resonance frequencies of the concrete beams. The beams were excited using an impact hammer (PCB Model 086D05) and the accelerometer was attached at the opposite end of the impact point, see Fig. 3. Both the impact hammer and accelerometer were connected to a signal conditioner (PCB Model 480B21) from which the output signal was sent to the digital data acquisition system. The data acquisition system was connected to a laptop computer which recorded the signal. The data sampling rate was 100 kHz with a recording time of 1 s per impact.

The longitudinal mode was excited by striking the bearing plate with the hammer while the accelerometer was attached to the bearing plate at the other end of the beam. The torsional mode was excited by striking the beam at the upper corner of the long side of the beam, with the accelerometer placed in the opposite corner on the same side, see Fig. 3.

Fig. 2. Attachment of the hydraulic jack to the end of one of the beams during the post-tensioning process.

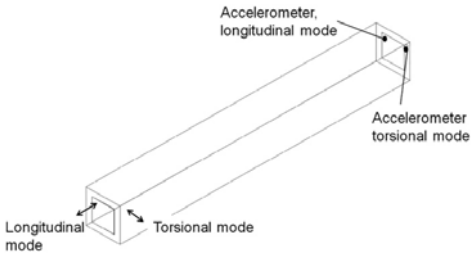

Fig. 3. Impact points (arrows) and the positions of the accelerometer for exciting the different modes of vibration.

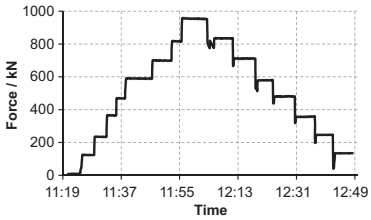

Fig. 4. Loading steps for the post-tensioning of beam number 1.

For each recorded signal the amplitude spectrum was obtained using the Discrete Fourier Transform, DFT. Fig. 5 shows an example of amplitude spectra from all 20 impacts in one of the measurements of the torsional mode on beam number 2. Fig. 5a shows the amplitude spectra from the force tsransducer on the impact hammer. The impulse contact time is about 350 μs generating input energy up to about 5000 Hz. Fig. 5b shows the corresponding response from the accelerometer at the opposite end of the beam. In order to determine the resonance frequencies accurately, the DFT was applied in two steps using a finer frequency interval in the second step around the resonance frequency peak of interest.

During the measurements each beam rested on two triangular steel supports placed 672 mm, i.e. 0.224 times the length of the beam, from each end of the beam, see Fig. 1. These positions were chosen to minimize the effects of the support conditions and are close to the nodal points of the fundamental flexural, first higher torsional and first higher longitudinal mode.

4. Finite element modeling

The influence of applied static stress on the resonance frequencies of the beams were modeled using a nonlinear finite element software [9]. The application of the prestressing force was modeled by applying a distributed load in the longitudinal direction on the edge boundaries of the beam, corresponding to the anchor heads, see Fig. 6, and performing a non-linear static analysis, based on second (i.e. Lame's constants) and third order (i.e. Murnaghan's constants) elastic constants. This was followed by a dynamic resonance frequency analysis, using the static stress field as a new linearization point for the dynamic calculations. As a first approximation the values of Murnaghan's constants were taken from the work performed in [5]. The steel supports were modeled as simply supported edges and to provide numerical stability in the calculations the movements in the z-direction on

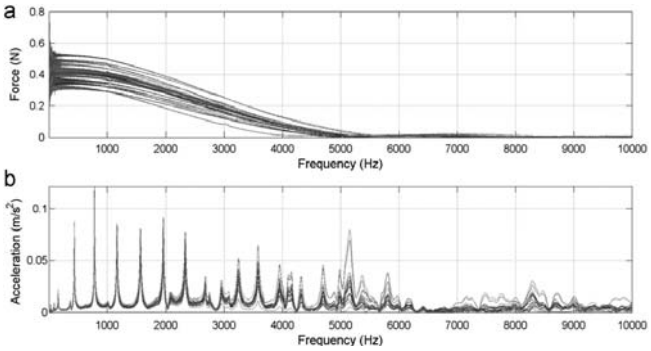

Fig. 5. (a) Input amplitude spectra from the 20 hammer impacts. (b) Resulting output amplitude spectra for the torsional mode for beam number 2.

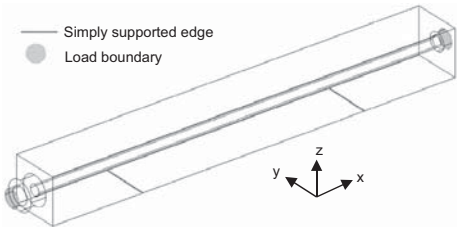

Fig. 6. Finite element model of the beams.

Table 1
Input data for the finite element modeling.

Parameter	*l*	*m*	*n*
Murnaghan's constants from [5],GPa	−3007	−2283	−1813
Murnaghan's constants from this study, GPa	−5040	−4150	−3340
Dynamic modulus of elasticity, GPa		39.0	
Poisson's ratio		0.21	

these edges were constrained to zero displacement. The dynamic modulus of elasticity was used in the dynamic resonance frequency analysis and was estimated to 39 GPa from the dynamic measurements on the same beams performed prior to the post-tensioning, i.e. in the unstressed state. The input data for the calculations are presented in Table 1. In the model 24 193 tetrahedral second order elements with a maximum size of 0.282 m were used, the total number of degrees of freedom were 109 683. Convergence checks with smaller element size and greater number of degrees of freedom showed that the chosen values were sufficient, i.e. the computed resonance frequencies were independent of the size of the elements. In addition, the analysis was performed iteratively for several different new values of the Murnaghan constants in order to investigate which values that would match the new measurements in this study.

5. Results and discussion

Several resonant frequencies from all three beams have been analyzed. Results from both the finite element modeling and the measurements for one torsional mode and one longitudinal mode are presented below. The twenty measurements which were performed on each load step and mode of vibration were in good agreement, the coefficient of variation (COV) ranged between 0.002% and 0.25% and between 0.001% and 0.1% for the longitudinal and torsional mode, respectively. It should be noted that our measured COV of 0.001% is in the same range as the relative resolution presented in [15] using diffuse ultrasound and a more sophisticated signal processing technique compared to the simple DFT used in this study. The measured resonance frequencies of the beams in the unstressed state and the coefficient of variation from the measurements are given in Table 2. The corresponding values of the initial (unstressed state) resonance frequencies from the finite element model were 801.0 Hz and 1300.4 Hz for the first higher torsional mode and the first higher longitudinal mode, respectively. Part of the difference between the measurements and modeling is probably due to the influence of the hydraulic jack, which was not included in the finite element model.

Figs. 7 and 8, show the measured resonance frequencies plotted against the measured compressive concrete stress. The stress dependency of the resonance frequencies is obvious in

Table 2
Resonance frequencies in the unstressed state.

Beam #	Torsional 2 (Hz)	COV (%)	Longitudinal 2 (Hz)	COV (%)
1	778.6	0.001	1331.7	0.06
2	775.1	0.001	1311.1	0.04
3	780.9	0.001	1307.0	0.02

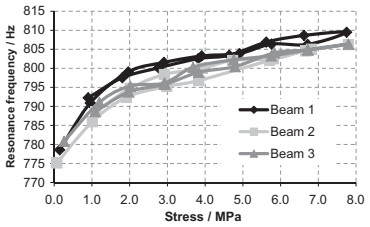

Fig. 7. First higher torsional mode (Torsional 2) resonance frequency from all the beams versus applied compressive stress in the concrete.

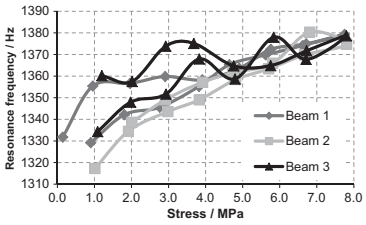

Fig. 8. First higher longitudinal mode (Longitudinal 2) resonance frequency from all the beams versus applied compressive stress in the concrete.

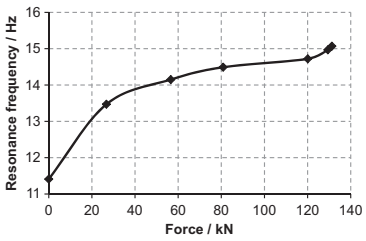

Fig. 9. Previously unexplained increasing frequency of the fundamental flexural mode of vibration from the resonance frequency measurements performed in [1].

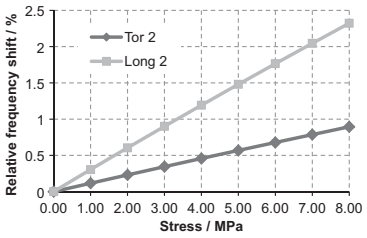

Fig. 10. Results from the finite element modeling as the predicted relative shift in frequency with the compressive stress, based on the values of the Murnaghan's constants obtained from [5].

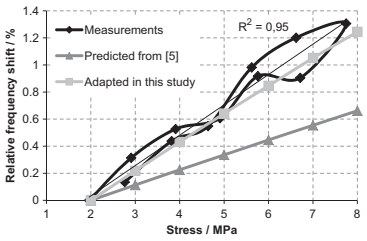

Fig. 11. Measured relative frequency shift with applied compressive stress for the first higher torsional mode resonance frequency for beam 1. The R^2 value concerns the fit for the regression line adapted to the results from the measurements. The adapted FEM curve shows our best estimate of the Murnaghan constants (Table 1).

these figures. Furthermore, it was found that the resonance frequencies increase with the applied compressive stress for all modes of vibration, i.e. not only for those presented in Figs. 7 and 8. It should also be noted that the more scattered results for the first higher longitudinal mode probably is due to the influence of the hydraulic jack, which affects this mode to a greater extent than the torsional.

According to the acoustoelastic theory the increase in resonance frequency should be linear with the applied stress. However, this is not the case for compressive stresses lower than approximately 2 MPa. Similar behavior was found in [1], where the resonance frequencies of a prestressed concrete beam, with a centrally placed tendon, were measured at different stress levels, the result from one of these measurements is shown in Fig. 9 as a comparison. It should be noted that this previously unexplained increasing resonant frequency with compressive stress [1,4] is very similar to the measured behavior in this present study. In addition, the similar initial non-linear increase has also been found on the speed of ultrasonic waves in various types of rocks subjected to confining pressures [12,16]. One possible explanation to the initial greater increase in frequency is that the presence of micro cracks in the concrete softens the material and that these micro cracks gradually close as the compressive stress increase. Furthermore, from Figs. 7 and 8 it is clear that this behavior is most prominent for the torsional mode, where the initial increase up to 2 MPa is significantly greater than the increase from 2 to 8 MPa. In [7] the same trend was found for ultrasonic shear waves polarized perpendicular to the uniaxial stress direction. For the longitudinal mode the initial increase is much smaller which is also in agreement with recent results in [7].

The result from the finite element modeling based on the values of the Murnaghan's constants obtained from [5] is shown in Fig. 10, where the relative shift in frequency is plotted against the compressive stress for the first higher torsional mode and the first higher longitudinal mode. The slope of the curves corresponds to the acoustoelastic constant L, which in this case describes the relative change in resonance frequency with compressive stress for each specific mode. It is clear that the longitudinal mode shows the greatest sensitivity for compressive stress, which is expected since this mode should have similar behavior as compressional waves propagating in the direction of loading. Compressional waves propagating in the direction of loading are those which have shown the greatest stress dependency [17]. Due to the applied static stress the length of the beams will be reduced, which affects the resonance frequencies of the beams. It should be noted that this effect is directly proportional to the applied stress and approximately two orders of magnitude smaller than the acoustoelastic effect. The change in resonance frequency due to the shortening of the beams is approximately 0.05%, compared to the total increase which is between 1.3 and 3.5% for the different modes of vibration.

In Figs. 11 and 12, the measured relative frequency shift for the first higher torsional mode for beam 1 and the first higher longitudinal mode for beam 2 is compared to the predicted results from the non-linear analysis, using both the values of the Murnaghan constants from [5] and the new adjusted constants matching measurements in this study (see Table 1). The initial nonlinearity in the measurements, which is inconsistent with the acoustoelastic theory, has been omitted in the comparison. From a manual iterative analysis it was found that the behavior of the beams corresponds relatively well to the following values of the Murnaghan constants: $l=-5040$ GPa, $m=-4150$ GPa, $n=-3340$ GPa. However, it should be noted that to obtain a unique set of Murnaghan's constants at least three different acoustoelastic constants, based on measurements of either wave velocities in

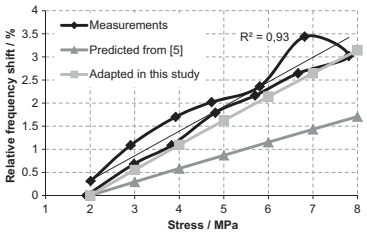

Fig. 12. Measured relative frequency shift with applied compressive stress for the first higher longitudinal mode resonance frequency for beam 2. The R^2 value concerns the fit for the regression line adapted to the results from the measurements. The adapted FEM curve shows our best estimate of the Murnaghan constants (Table 1).

three different directions [13] or three different modes of vibration, are required and that the values obtained in this study only are the result of a manual iteration and do not necessarily represent a true material behavior. The predicted relative frequency shift, using the Murnaghan constants from [5], also agrees quite well with the measurements in this study. In addition, the relative frequency shifts from the measurements are very close to being linear with R^2-values above 0.93 for the adapted regression lines. The difference between the measurements and the finite element modeling with the measured values of the Murnaghan constants from [5] is probably due to the chosen values of the constants. To the authors' knowledge, the values of the Murnaghan's constants obtained from [5] are the only ones which have been published for concrete. The constants were determined on a concrete with a slightly higher compressive strength and stiffness (compressive strength of 76.6 MPa, modulus of elasticity of 42.4 GPa and Poisson's ratio of 0.21) and thus probably not directly applicable for the concrete used in this study. Furthermore, it seems reasonable that the amount of elastic non-linearity should decrease with increasing modulus and strength.

The results from both the modeling and the measurements indicate that the stress dependency of the resonance frequencies of concrete structures can be explained by the acoustoelastic theory. This also indicates that the change in the state of stress in a simple concrete structure may be estimated by measuring the resonance frequencies of the structure.

6. Conclusions

The results from this study indicate that the observed stress dependency of the resonance frequencies of concrete structures can be described by the acoustoelastic theory. These results can possibly provide a new theoretical basis for the previously observed and debated results from prestressed concrete bridges [4], where the stress dependency was described using a linear elastic approach. The experimental measurements and the numerical non-linear analysis performed in this study show that the acoustoelastic effect in concrete is detectable and can be measured using structural resonance frequencies. The modulus of elasticity of the concrete and hence the resonance frequencies increases with applied compressive stress. However, the acoustoelastic effect is relatively small in concrete, for the stress levels applied in this study, approximately 13% of the ultimate compressive strength, the increase in resonance frequencies was about 1.3% and 3.5% for the torsional and longitudinal mode, respectively. As is well known to the research community in this field, the resonance frequencies of a concrete structure can be determined with high accuracy, more than sufficient to capture the acoustoelastic effect. In this study the largest coefficient of variation from 20 averages of measured resonance frequencies were 0.06% and in many measurements as low as 0.01%, which correspond to a change in stress of approximately 6.4 kPa. Results indicate that a change in the state of stress in a simple concrete structure may be detectable by measuring or monitoring one or several resonance frequencies as already performed in many structural health monitoring systems [11]. In order to detect small and slow variations in stress it is likely that the influence of temperature and moisture must also be taken into account which is a subject for future studies.

Acknowledgments

The authors gratefully acknowledge the help with the post-tensioning of the beams, which was performed by the Swedish construction company Skanska. The work presented in this study was funded by ELFORSK, the Swedish Electrical Utilities R&D Company, with contributions from Vattenfall, EON, Fortum, Skellefteå Kraft and Karlstad Energi the power producing companies owning and operating the Swedish nuclear power plants, the Swedish Radiation Safety Authority and TVO, Teollisuuden Voima Oyj in Finland.

References

[1] Saiidi M, Douglas B, Feng S. Prestress force effect on vibration frequency of concrete bridges. J Struct Eng 1994;120:2233–41.
[2] Lu ZR, Law SS. Identification of prestress force from measured structural responses. Mech Syst Signal Process 2006;20:2186–99.
[3] Hamed E, Frostig Y. Natural frequencies of bonded and unbonded prestressed beams—prestress force effects. J Sound Vib 2006;295:28–39.
[4] Dall'Asta A, Dezi L, Deák G, Jain SK, Goel SC. Discussion on Prestress force effect on vibration frequency of concrete bridges. J Struct Eng 1996;122:458–60.
[5] Payan C, Garnier V, Moysan J, Johnson PA. Determination of third order elastic constants in a complex solid applying coda wave interferometry. Appl Phys Lett 2009;94 1:011904-1: 011904-3.
[6] Wiggenhauser H, Feldmann R, Shokouhi P. Stress dependency of sonic velocity in concrete under uniaxial load. In: Proceedings of the transportation research board 87th annual meeting. Washington DC, USA; 2008.
[7] Lillamand I, Chaix JF, Ploix MA, Garnier V. Acoustoelastic effect in concrete material under uni-axial compressive loading. NDT&E Int 2010;43:655–60.
[8] Stähler SC, Sens-Schönfelder C, Niederleithinger E. Monitoring stress changes in a concrete bridge with coda wave interferometry. J Acoust Soc Am 2011;129(4):1945–52.
[9] Comsol multiphysics, User's Guide. Version 3.5a. COMSOL AB, November 2008.
[10] Murnaghan FD. Finite deformation of an elastic solid. New York: John Wiley and Sons, Inc.; 1951.
[11] Fan W, Qiao P. Vibration-based damage identification methods: a review and comparative study. Struct Health Monit 2010;10(1):83–111.
[12] Huang X, Burns DR, Toksöz MN. The effect of stresses on the sound velocity in rocks: theory of acoustoelasticity and experimental measurements. Consortium report, Earth resources laboratory. Cambridge, MA, USA.: Massachusetts Institute of Technology; 2001.
[13] Egle DM, Bray DE. Measurement of acoustoelastic and third-order elastic constants for rail steel. J Acoust Soc Am 1976;60(3):741–4.
[14] Hughes DS, Kelly JL. Second-order elastic deformation of solids. Phys Rev 1953;92(5):1145–9.
[15] Larose E, Hall S. Monitoring stress related velocity variations in concrete with a 2×10^{-5} relative resolution using diffuse ultrasound (L). J Acoust Soc Am 2009;125(4):1853–6.
[16] Sayers CM, Van Munster JG, King MS. Stress-induced ultrasonic anisotropy in Berea sandstone. Int J Rock Mech Mining Sci Geomech 1990;27(5):429–36.
[17] Rydén N, Lundqvist P, Thelandersson S. Acoustoelastic effects on the natural frequencies of prestressed concrete beams. QNDE 2010, San Diego, California; 18–23 July 2010.

Paper IV

Acoustoelastic Effects on the Resonance Frequencies of Prestressed Concrete Beams – Long-Term Measurements

About the authors
Peter Lundqvist[1], MSc, Div. of Structural Engineering, Lund University, Lund, Sweden.
Nils Rydén, PhD, Div. of Engineering Geology, Lund University, Lund, Sweden.

Abstract

Today, no method exists for determining the state of stress and/or small changes in the state of stress in a concrete structure and such a method would be very useful, for example for prestressed concrete structures where the function and safety of the structure depend on the compressive stresses in the concrete. In a previous study it was shown that the resonance frequencies of three prestressed concrete beams were stress dependent according to the theory of acoustoelasticity. In this study, resonance frequency measurements were performed on the same beams, for approximately 17 months, in an attempt to monitor the prestress losses. It was found that it is possible to measure the resonance frequencies continuously over a longer period of time with good accuracy and reliability and that after correcting for the development of the modulus of elasticity with time, the change in resonance frequencies correlates with changes in tendon forces. The results also show that resonance frequencies are affected by the ambient temperature and relative humidity.

Keywords: Concrete, Resonance frequency, Acoustoelasticity, Prestress losses, Non-destructive testing.

[1] Corresponding author, Structural Engineering, Lund University, P.O. Box 118, SE-22100, Lund, Sweden. Tel. +46 46 2229882, E-mail address: peter.lundqvist@kstr.lth.se.

1. Introduction

No method exists for determining the state of stress in a concrete structure and such a method would be very useful, for example for prestressed concrete structures where the function and safety of the structure depend on the applied compressive stresses in the concrete. Due to long term effects, i.e. creep and shrinkage of concrete and relaxation of the prestressing steel the prestress forces decrease with time. To be able to measure or at least estimate the prestress losses would therefore be of great value, especially in structures with bonded tendons where the ducts are injected with cement grout, which makes direct measurements of the tendon forces impossible.

Results from studies where ultrasonic measurements during uniaxial loading were performed have demonstrated a strong acoustoelastic effect in concrete, see e.g. [1] and [2]. According to the theory of acoustoelasticity the modulus of elasticity of concrete depends on the stress in the concrete and the modulus increases with concrete compressive stress [1]. The resonance frequency of a structure depends on the geometry and mass of the structure, modulus of elasticity of the material and the boundary conditions and should therefore also be stress dependent. In addition, a recent study on a concrete bridge during the construction phase [3] showed that it is possible to determine the influence on the wave speeds by the change in the state of stress by using coda wave interferometry. These results indicate that this nonlinear response of concrete may be determined under more complicated conditions than those in a laboratory and that the acoustoelastic approach may possibly be used for practical applications in the field In a previous study [4], resonant acoustic spectroscopy (RAS) was used to measure the resonance frequencies of three prestressed concrete beams during the post-tensioning process. It was found that the resonance frequencies of the beams depended on the applied compressive stress and for all modes of vibration the resonance frequencies increased with the applied compressive stress. These results agree with the theory of acoustoelasticity and can be predicted using a non-linear finite element model of the beams, based on Murnaghan's theory of finite deformations [5].

Based on the findings in the previous study, continuous measurements during approximately 17 months were performed on the same beams in an attempt to monitor the prestress losses in the beams. The results from these long-term measurements are presented in this paper.

2. Theory

2.1. Resonance frequency

Every mechanical system or body has several resonance frequencies at which the vibrations in the system increase significantly without any increase in the applied force. The resonance frequencies of a body with homogenous, elastic material depend on the geometry and mass of the body, elastic constants and boundary conditions. This means that by measuring the resonance frequency during constant ambient conditions, the modulus of elasticity and Poisson´s ratio of the material can be determined. This technique is frequently used in many engineering fields and is normally referred to as resonant acoustic spectroscopy (RAS) or resonant ultrasonic spectroscopy (RUS) [6].

2.2. Acoustoelasticity

The acoustoelastic theory describes the influence of stress on acoustic wave velocities in non-linear elastic materials, normally the increase in wave velocity due to compressive stress [2]. This stress dependency is due to the change in modulus of elasticity in a material under stress. Acoustoelastic effects have been studied for a wide variety of materials, for example for metals and various types of rocks [7]. Based on Murnaghan's theory five different elastic constants are required to describe a

non-linear acoustoelastic material satisfactorily; Lame's constants λ and μ and Murnaghan's third order elastic constants *l, m* and *n* [6].Using a non-linearity parameter β, which takes the stress dependency of the modulus of elasticity into account, a non-linear stress-strain relationship can be written as:

$$\sigma_c = E_c\varepsilon_c(1 + \beta\varepsilon_c) \quad (1)$$

Where:
σ_c = concrete stress
E_c = Modulus of elasticity of concrete
ε_c = concrete strain
β = non-linear parameter taking the acoustoelastic effect into account

β can be expressed as follows using Lame's and Murnaghan's elastic constants:

$$\beta = \frac{3}{2} + \frac{(l + 2m)}{\lambda + 2\mu} \quad (2)$$

Where:
l, m = Murnaghan's third order elastic constants, GPa
λ, μ = Lame's elastic constants, GPa

Another important parameter is the acoustoelastic constant L_{ij} [1], which gives the relation between the relative change in wave speed (or, as in this case, the relative change in resonance frequency) versus the strain or stress in the material. For wave speeds, the index *i* refers to the direction of the propagating wave and index *j* to the direction of polarization. An orthonormal base is normally used with the directions 1, 2 and 3, where direction 1 usually is the direction of loading. L_{ij} is defined as follows:

$$L_{ij} = \frac{dV_{ij}/V_{ij}^0}{d\sigma} \quad (3)$$

Where:
dV_{ij} = the change in wave speed for a wave propagating in the i direction, polarized in the j direction.
V^0_{ij} = wave speed in the unstressed state, m/s
$d\sigma$ = the change in stress in the direction of loading, MPa

3. Experimental details

3.1. Description of test beams

A total of four beams were manufactured, each 3 meters long with a square cross section of 350 x 350 mm^2, see figure 1 for details. The tendon, which was placed straight in the center of the cross section, was of the type VSL (Vorspann System Losinger) consisting of 5 strands, each with a diameter of 15 mm. Three of the beams were prestressed and the fourth beam was used as a reference, the initial post-tensioning force was approximately 820 kN. The concrete quality was C35/45, i.e. characteristic cylinder and cubic strength of 35 MPa and 45 MPa, respectively, with a water-cement ratio of 0.4. At the age of 28 days the mean compressive strength of the concrete was determined for 150 mm cubes to 63.4 MPa.

3.2. Measurements

The beams were excited using an impact hammer (PCB Model 086D05) and the resonance frequency was obtained by connecting a piezoelectric accelerometer (PCB Model 353B33, 100mV/g) to the beams. The resonance frequency of the accelerometer is higher than 22 kHz and the measured response is linear within 5% from 1-4000 Hz. The accelerometer was attached to the beam on the opposite side of the impact point. To ensure a good mechanical contact, thin metal washers were glued to the surface of the beams and the accelerometer was attached magnetically to these washers, it should be noted that the coupling resonance frequency of the accelerometer (~10 kHz) using this method is well above the measured resonance frequencies of the concrete beams. In total, three different modes of vibration were examined; longitudinal, flexural and torsional, the excitation points for each mode are shown in figure 2. Both the impact hammer and accelerometer were connected to a data acquisition system (NI USB-4432). The data sampling rate was 100 kHz with a recording time of 1 second. For each mode of vibration, the resonance frequency was measured 20 times and the final value was taken as the mean value of these measurements. In order to analyze the signal Discrete Fourier Transform was used to determine the resonance frequencies.

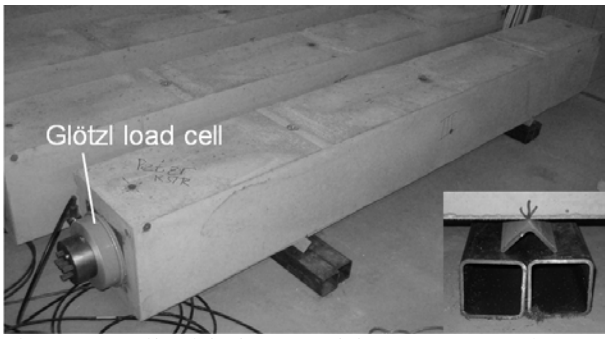

Figure 1. Details of the beams and the arrangement of supports.

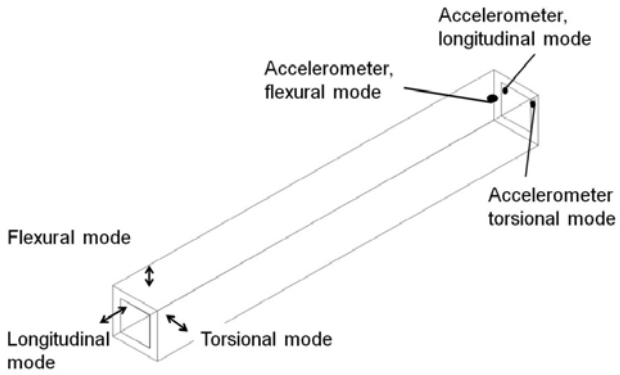

Figure 2. Impact points (arrows) and accelerometer positions for the different modes of vibration.

The measurements were performed during approximately 17 months on all four beams, including the unstressed reference beam. To minimize the effects of the ambient climate the beams were stored in a climate chamber with a constant climate of some 20°C and approximately 60 % relative humidity (RH). The prestress forces in the beams were measured continuously, with one measurement every hour by load cells (Glötzl model KK 1000 A 105) attached between the bearing plate and anchor head at one end of each beam, see figure 1. A hydraulic fluid in the load cell

records the applied pressure and the signal is converted to an electric signal using a piezoelectric converter. The accuracy of the load cells is 0.5 %.

Figure 3 shows an example of amplitude spectra from all 20 impacts in one of the measurements of the longitudinal mode from beam number 1. The top figure in figure 3 shows the amplitude spectra from the force transducer on the impact hammer, the impulse contact time is about 350 μs generating input energy up to about 5000 Hz. In the bottom figure the corresponding response from the accelerometer at the opposite end of the beam is shown. The DFT was applied in two steps using a finer frequency interval in the second step around the resonance frequency peak of interest, in order to determine the resonance frequencies accurately. It should be noted that, although the manual hammer impacts generate slightly different amplitudes, the measured resonance frequencies, i.e. the peaks in figure 4b, are very repeatable, see table 2.

During the study, the beams rested on two triangular steel supports placed 672 mm from each end of the beam, see figure 1. This placement of the supports coincides with the nodal points of the first flexural mode and is also close to the nodal points of the second longitudinal and second torsional mode.

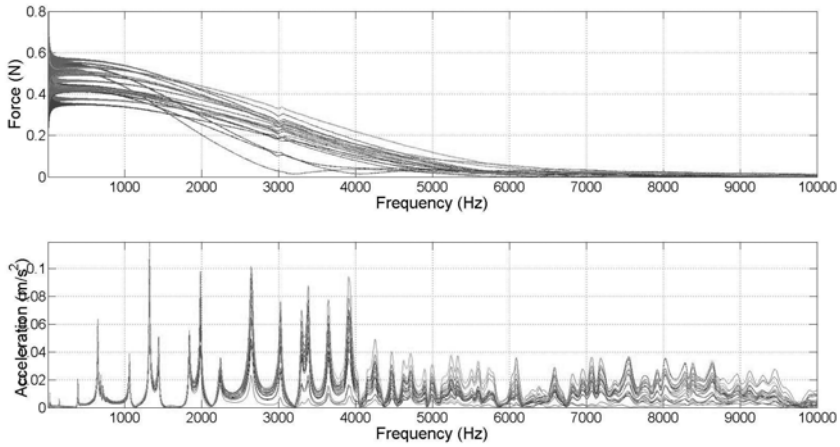

Figure 3. Examples of the input amplitude spectra from the 20 impact points (top)
Resulting output amplitude spectra for the longitudinal mode for beam number 1 (bottom)

4. Results and Discussion

The results from the measurements of the tendon forces, using the Glötzl load cells, are shown in figure 4 and table 1. As can be seen from the results, the relative prestress losses were almost identical in all the beams, about 12 % corresponding to a decrease in concrete stress of approximately 0.86 MPa.

Table 1. Results from the monitoring of the tendon forces.

Beam #	Original tendon force / kN	Loss of tendon force kN	Relative loss %	Decrease in concrete stress / MPa
1	817.6	99.6	12.2	0.85
2	848.5	102.3	12.1	0.87
3	830.1	100.9	12.2	0.86

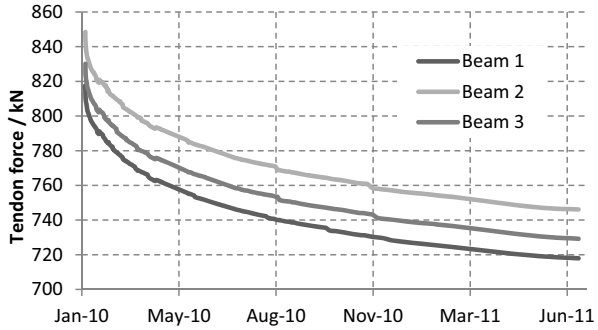

Figure 4. Tendon forces in the beams registered by the Glötzl load cells.

The resonance frequencies for the beams directly after the post-tensioning are presented in table 2 along with the standard deviation, calculated from the twenty measurements performed for each mode of vibration. The slightly greater resonance frequencies for the reference beam was probably due to the additional weight, approximately 50 kg, of the tendons, anchor heads and Glötzl load cells which were attached to the post-tensioned beams. The standard deviations for all the measurements conducted during the study were of the same order of magnitude as those in table 2. This shows that the method used in this study for determining the resonance frequencies of the beams can be used for long-term measurements with high accuracy and repeatability. In addition, the measured COV of 0.002 %, which corresponds to a change in concrete stress of approximately 3 kPa, is in the same range as the relative resolution presented in [8] using diffuse ultrasound and a more sophisticated signal processing technique compared to the simple DFT used in this study.

Table 2. Resonance frequencies of the beams directly after post-tensioning

Beam #	Flexural 1 / Hz	Std. dev / Hz	Torsional 2 / Hz	Std. dev / Hz	Longitudinal 2 / Hz	Std. dev / Hz
1	142.7	0.003	777.2	0.01	1303.2	0.04
2	143.7	0.007	775.2	0.04	1305.2	0.05
3	142.0	0.002	774.0	0.01	1297.9	0.02
4*	147.3	0.005	779.5	0.007	1318.3	0.05

*Reference beam.

The results from the resonance frequency measurements are shown in figures 5 to 6. As can be seen from the results, the resonance frequencies increase with decreasing tendon force, which is in contradiction with the acoustoelastic theory. However, the resonance frequencies of the reference

beam also change with time, mostly because the modulus of elasticity of the concrete increases with time due to the cement reactions in the concrete. Factors influencing the initial unstable response of the beams will be discussed later in the paper. According to measurements performed in [9], the increase of the dynamic modulus of elasticity of concrete due to the hydration of the cement was approximately 17 and 25 percent after one and three years, respectively. The decrease in modulus of elasticity due to the acoustoelastic effect is smaller than the increase due to the cement reactions which thus cancels the acoustoelastic effect. As an example, for the short-term measurements performed in the previous study, the maximum frequency shift was about 3.5 % for 8 MPa change of concrete stress [4]. The decrease in concrete stress in this study was approximately 0.86 MPa, which means that the acoustoelastic effect on the resonance frequencies is significantly smaller. However, by subtracting the resonance frequencies for the reference beam from those of the prestressed beams, the long term effects of the cement reactions can be accounted for. The results of this operation are displayed in figures 7 to 8, which shows clearly that the difference in resonance frequencies decrease with time.

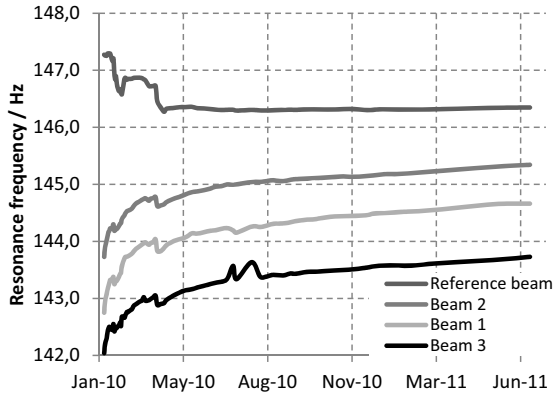

Figure 5. Results from the long-term measurements for the fundamental flexural mode.

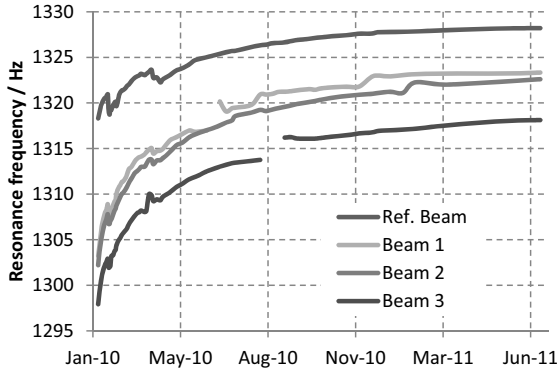

Figure 6. Results from the long-term measurements for the first higher longitudinal mode.

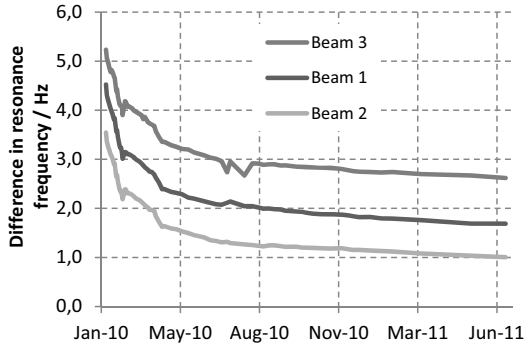

Figure 7. Difference in resonance frequency between the prestressed beams and the reference beam for the fundamental flexural mode.

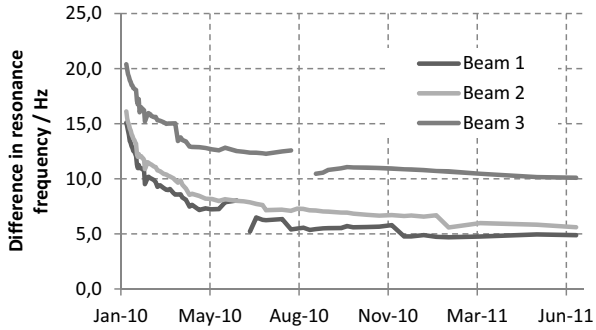

Figure 8. Difference in resonance frequency between the prestressed beams and the reference beam for the first higher longitudinal mode.

The curves of the decreasing differences in resonance frequencies in figures 8 and 9 when compared to the curves of the decreasing tendon forces in figure 2, show the same general behavior with high initial losses and a slowly decreasing rate of the losses.

According to the theory of acoustoelasticity, the relative frequency shift increases linearly with the applied stress. In figures 9 and 10, the results from the measurements for the first higher longitudinal and fundamental flexural mode are presented as the relative frequency shift versus the stress in the concrete. The relative frequency shift is here defined as the difference in resonance frequency, shown in figures 7 and 8, divided by the resonance frequency in the unstressed state. The slope of the curves corresponds to the acoustoelastic constant L_{ij}. The relative frequency shifts decrease approximately linearly with the prestress losses, however, there is a slight tendency that the slope of the curves, i.e. $L_{ij,}$ change over time. This could indicate that the Murnaghan constants also develop over time along with the cement reactions in the concrete, i.e. they may depend on the degree of hydration. The rate of cement reactions decreases with time and thus its influence on the resonance frequencies of the beams, which could explain the flattening out of the curves. Two previous studies [10] and [11] have shown that the stress dependency, i.e. the non-linear parameter $\beta,$ increase with the induced damage in the concrete, considering this it seems reasonable that the stress dependency would decrease with the development of the modulus of elasticity. This can possibly be another explanation to the change in the slopes over time. Despite the change of the slopes with time, regression lines were adapted to the curves in figures 9 and 10 and the fits were good, with R^2 values above 0.90. The slopes in figures 9 and 10, i.e. the acoustoelastic constant L_{ij},

were approximately twice as large as those obtained from the short-term measurements performed on the same beams, see [4].

Several factors probably contribute to the initial unstable behavior of the beams. First of all, the hydration of the cement which causes the modulus of elasticity of the concrete to increase will, as stated above, have the highest influence in the early stage and then decrease with time. A second factor which probably also contributes to the initial unstable behavior is that prior to the post-tensioning the beams were stored in approximately 17°C and under sealed conditions, i.e. 100 % RH. After the post-tensioning they were placed in the controlled climate and the change in the temperature may affect the resonance frequencies. For example, from measurements performed in [12] it was calculated that the relative change of acoustic velocities in concrete was 0.15 % per °C. Furthermore, from figure 11, where the logged temperature and RH in the climate chamber are shown, small initial fluctuations in the ambient climate can be seen, which also may contribute to the initial unstable behavior.

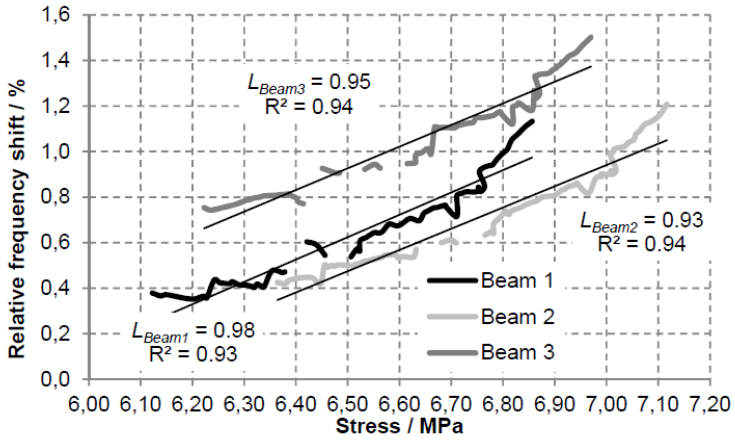

Figure 9. Relative frequency shift plotted against the stress in the concrete for the first higher longitudinal mode.

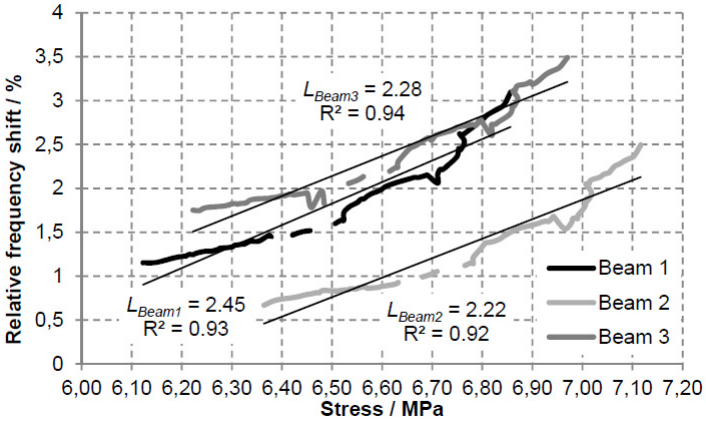

Figure 10. Relative frequency shift plotted against the stress in the concrete for the fundamental flexural mode.

Due to problems in the climate control system, the influence of changes in the ambient climate on the resonance frequencies of the beams was, unintentionally, investigated. Three major failures, the 15th and 25th of February and 7th of April, occurred which can be seen in figure 12. The first failure caused the temperature to drop from 20°C to 15°C (the RH was constant at 60 %). The two other failures only caused changes in RH, during the second failure the RH was increased to 85 % and the third failure caused a decrease of the RH from 60 to 45 %. The changes in the ambient climate all caused a decrease of the resonance frequencies of the beams, which can be seen in figures 6 and 7. From this figure it can also be seen that it is not until after the last failure, when the climate in the chamber is stabilized, that the increase of the resonance frequencies is stabilized. The effect of the changes in the climate is more evident in figures 10 and 11, where the failures can be seen as temporary drops in the relative frequency shift for both the first higher longitudinal and fundamental flexural mode, e.g. at concrete stresses of 6.87 MPa, 6.82 MPa and 6.67 MPa for beam 3. Corresponding temporary drops can be seen for beams 1 and 2. However, the small fluctuations in RH which can be seen later in the climate plot do not seem to have any effects on the behavior of the beams.

The results in figures 9 and 10 along with figure 11 show that changes in both RH and temperature affect the resonance frequencies of the beams. Furthermore, the results also indicate that the ambient climate affects the acoustoelastic behavior of concrete, i.e. that the relative frequency shifts in figures 9 and 10, are sensitive to changes in the ambient climate.

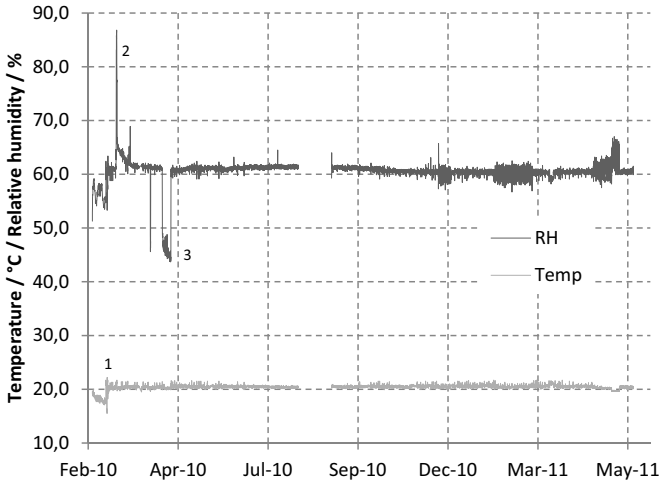

Figure 11. Data for the ambient climate in which the beams were placed during the measurements, the upper line shows the RH and the lower the temperature. (The numbers refer to the failures in the climate control system).

In figure 12, the relative frequency shift for the first higher longitudinal mode is plotted against the stress in the concrete for the time after the initial phase of two months, i.e. when the resonance frequencies are stabilized. In this case, the slopes of the curves agree quite well with those from the short-term measurements, where the slope was 0.53 for the first higher longitudinal mode for beam 2. This shows that the relative frequency shifts in the beams are similar for the short- and long-term measurements under stable environmental conditions.

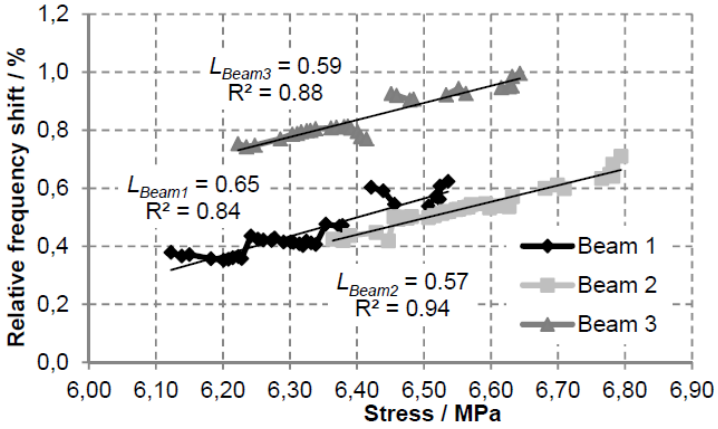

Figure 12. The relative frequency shift plotted against the stress in the concrete for the first higher longitudinal mode, after the ambient climate was stabilized.

The results show that the change in the resonance frequencies follows the loss of the tendon forces, which indicates that by monitoring the development of the mechanical properties of the concrete, as in this case using a reference structure, and the ambient climate, i.e. temperature and relative humidity, changes in the state of stress in a simple concrete structure can be detected over time by measuring the resonance frequencies. In addition, changes in the state of stress in existing concrete structures would probably be more easily detectable since the hydration of the concrete significantly decreases with age, which means that the influence of the development of the modulus of elasticity on the resonance frequencies is significantly reduced or could for very old concrete even be eliminated. Considering that the development of the modulus of elasticity caused some uncertainties in this study, more stable results would probably have been obtained if the post-tensioning of the beams would have been performed at a higher concrete age.

5. Conclusions

The following can be concluded from this study:

The results from this study show that resonance frequencies of a simple prestressed concrete structure can be measured continuously during a longer period of time with good accuracy and reliability and also that the ambient climate, i.e. both the temperature and RH influence the resonance frequencies of a concrete structure. The results also indicate that the non-linear acoustoelastic behavior of concrete depends on the degree of hydration and the ambient climate, which means that the Murnaghan constants change over time along with the cement reactions of the concrete. Further, the resonance frequencies of the beams changed with the prestress losses and by correcting for the development of the modulus of elasticity with time, the decrease in the resonance frequencies follows the loss of tendon forces. It was also found that the relative frequency shifts for the long-term measurements are similar to those obtained from short-term measurements [4]. Finally, the results indicate that by monitoring the ambient climate and the development of the mechanical properties of the concrete, changes in the state of stress in a simple concrete structure can be detected by measuring the resonance frequencies.

Acknowledgements

The authors gratefully acknowledge the help with the post-tensioning of the beams, which was performed by the Swedish construction company Skanska. The work presented in this study was funded by ELFORSK, the Swedish Electrical Utilities R&D Company, with contributions from Vattenfall, EON, Fortum, Skellefteå Kraft and Karlstad Energi the power producing companies owning and operating the Swedish nuclear power plants, the Swedish Radiation Safety Authority and TVO, Teollisuuden Voima Oyj in Finland.

References

[1] Payan C, Garnier V, Moysan J, Johnson PA. Determination of third order elastic constants in a complex solid applying coda wave interferometry, Applied Physics Letters 94 2009;1:011904-1: 011904-3.
[2] Lillamand I, Chaix JF, Ploix MA, Garnier V. Acoustoelastic effect in concrete material under uni-axial compressive loading. NDT&E International 2010;43:655-660.
[3] Stähler SC, Sens-Schönfelder C, Niederleithinger E. Monitoring stress changes in a concrete bridge with coda wave interferometry. Journal of the Acoustical Society of America 2011;129(4):1945-1952.
[4] Lundqvist P, Rydén N. Acoustoelastic effects on resonance frequencies of prestressed concrete beams - Short-term measurements. NDT&E International 2012;50:36-41
[5] Murnaghan FD. Finite deformation of an elastic solid. New York:John Wiley and Sons, Inc. 1951.
[6] Fan W, Qiao P. Vibration-based damage identification methods: a review and comparative study. Structural Health Monitoring 2010;10(1):83-111.
[7] Huang X, Burns DR, Toksöz MN. The effect of stresses on the sound velocity in rocks: Theory of Acoustoelasticity and experimental measurements. Consortium Report, Earth resources laboratory, Massachusetts Institute of Technology, Cambridge, MA, USA. 2001.
[8] Larose E, Hall S. Monitoring stress related velocity variations in concrete with a $2x10^{-5}$ relative resolution using diffuse ultrasound (L). Journal of the Acoustical Society of America 2009;125(4):1853-1856.
[9] Klieger P. Long-time study of cement performance in concrete. Journal of the American Concrete Institute 1957;54 (6): 481-504.
[10] Schurr D.P, Kim J-Y, Sabra K.G, Jacobs L.J. Damage detection in concrete using coda wave interferometry. NDT&E International, 2011;44:728-735.
[11] Shokouhi P, Zoëga A, Wiggenhauser H. Nondestructive evaluation of stress-induced damage in concrete, Advances in Civil Engineering, Vol. 2010, article ID 740189, 9 pages.
[12] Larose E, de Rosny J, Margerin L, Anache D, Gouedard P, Campillo M, van Tiggelen B. Observation of multiple scattering of kHz vibrations in a concrete structure and application to monitoring weak changes. Physical Review E 2006;73.

Paper V

Thermal effects on long term loss in prestressed concrete

About the authors

Peter Lundqvist[1], MSc, Div. of Structural Engineering, Lund University, Lund, Sweden.

Abstract

Unlike most civil engineering structures, prestressed nuclear reactor containments are subjected to a constant elevated temperature of approximately 40°C. The purpose of this study was to investigate the influence of this climate on prestress losses, thus, eight prestressed concrete beams were constructed of which six were subjected to similar climatic conditions as those inside reactor containments during a period of almost 3 years. The remaining two were subjected to a normal climate of the order 20°C. Five of the beams were grouted and in the remaining three load cells were used to monitor the decrease of tendon forces with time. At the end of the study the remaining tendon forces in all the beams were determined using the so-called crack re-opening method. The results showed that the prestress losses in the beams subjected to the elevated temperature were approximately 25 % greater than those subjected to normal temperature. It was also found that the remaining tendon forces obtained from the crack re-opening tests, when interpreted according to previously used methods described in the literature, tend to underestimate the tendon forces. However, by using a simple finite element model of the testing procedure the accuracy of determining the tendon forces was greatly increased.

Keywords: Prestressed concrete, concrete beams, prestress losses, bonded tendons, creep, shrinkage, relaxation.

---

[1] Corresponding author, Structural Engineering, Lund University, P.O. Box 118, SE-22100, Lund, Sweden. Tel. +46 46 2229882, E-mail address: peter.lundqvist@kstr.lth.se.

1. Introduction

Prestressed concrete is applied for a wide variety of structures, in for example, nuclear power plants the reactor containment is normally a prestressed concrete structure enclosing the reactor vessel and designed to prevent any radioactive discharge in the event of a severe accident. The safety and integrity of the containment depend on the compressive stresses in the concrete induced by the prestressing tendons and one major problem in these structures is that the tendon forces decrease over time due to long-term deformation in the concrete, i.e. creep and shrinkage, and relaxation in the steel tendons. Several factors influence the creep and shrinkage behavior of concrete, for example the stress levels, duration of the load, the composition of the concrete, ambient temperature and humidity. The most important factors which influence the relaxation of the steel are the stress levels, duration of the load and the temperature [1].

The majority of studies on creep of concrete do not include the temperature as a parameter and studies performed for the temperature range 30 to 100°C are quite few. In a reactor containment, the internal temperature may vary between 30 and 50°C [2], depending on the design of containment. In a previous study, it was found that the creep strains in concrete subjected to 40°C is almost twice as those for concrete subjected to 20°C [3]. In another study on the prestress losses in Swedish reactor containments it was found that rate of the prestress losses increased at the start of operation of the reactors, i.e. when the temperature was increased from some 20°C to the operating temperature of approximately 45°C [4]. This increase was attributed to the temperature effect on creep of concrete, but a part of it can probably also be attributed to the increase in relaxation due to the raise in temperature.

The purpose of the study presented in this paper was to investigate the influence of the temperature levels of a reactor containment on the prestress losses in eight prestressed concrete beams during a period of approximately 3 years.

2. Description of the beams

In total, eight concrete beams were constructed, each with a square cross-section of 350 x 350 mm^2 and a length of 3 m. The post-tensioning system consisted of one tendon placed in the center of the cross-section. Each tendon in turn consists of five strands, each with a diameter of 15 mm and the strands consist of seven wires, each with a diameter of 5 mm. The same anchorage system were used at both the passive and active end and consists of a square bearing plate with attached split holding rings and a circular hole for passage of the strands. All the beams were post-tensioned at a concrete age of 6 months, with an initial post-tensioning force of approximately 950 kN. To be able to measure the tendon forces load cells were placed between the bearing plate and the anchor head at the passive end of each beam, see figure 1. For five of the beams the ducts were injected with cement grout, the remaining three were left ungrouted thus making it possible to measure the tendon forces continuously with the load cells. Prior to the posttensioning the beams were sealed by plastic foil and it was not until after the posttensioning that drying of the beams was allowed to start.

The concrete used was of the quality C35/45, which means that the characteristic cylinder and cube strength of the concrete are 35 MPa and 45 MPa, respectively. The water-cement ratio of the concrete was 0.4. The mean compressive strength of the concrete was measured on cubes cast simultaneously with the beams to 55.6 MPa at a concrete age of 28 days.

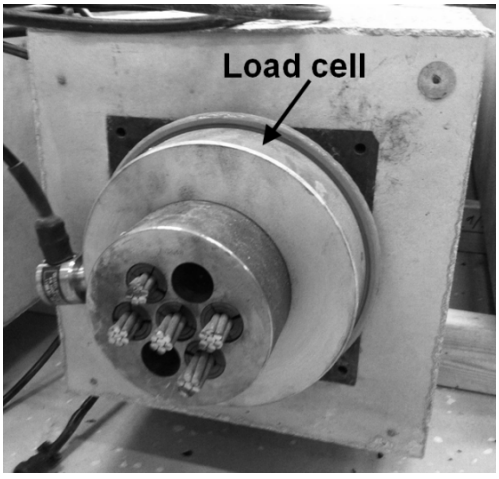

Figure 1. The load cell placed between the anchor head and the bearing plate.

3. Measurements

To be able to investigate the influence of an elevated temperature on prestress losses six of the beams were placed in a climate chamber with mean temperature 42°C and mean relative humidity 18 % for a period of approximately 33 months. Three of the beams, number 1, 2 and 3, were placed in the climate chamber 2 months after the posttensioning and the other three, number 4, 5 and 6, after additionally 3 months. The two remaining beams, number 7 and 8, were used as references and subjected to a normal indoor climate, i.e. approximately 21°C and 40 % relative humidity.

Beams number 3, 6 and 8 were ungrouted and the tendon forces were measured continuously in these beams using the load cells. The details of the climate in which the beams were stored is given in table 1. In order to reduce any uncertainties in the measurements, the load cells were calibrated both before and after the study.

Table 1. Mean value and coefficient of variation for temperature and relative humidity.

Beam #	Mean temp. / °C	Range / °C	COV / %	Mean RH / %	Range / %	COV / %	Temperature increased after
1, 2, 3	42	39–46	12	18	12-30	58	2 months
4, 5, 6	42	39-46	12	18	12-30	58	5 months
7, 8	21	18-26	12	40	27-55	20	Never

4. Testing procedure

In order to determine the remaining tendon forces in the beams with bonded tendons at the end of the study the so-called crack re-opening method were used. This method has been used in several previous studies to determine the remaining tendon forces in prestressed concrete beams, [5], [6], [7] and [8]. To assess the accuracy of the method the remaining tendon forces were first determined for the beams with unbonded tendons, where the tendon forces were known from the load cells. The beams were subjected to a three point bending test, see figure 2, and were loaded in deflection control with increments of 0.02 mm per second. The load was first increased until the first open flexural crack appeared at the bottom edge of the beam, the crack was then marked and the beam unloaded. One LVDT (Linear Variable Displacement Transducer) gauge was mounted across the crack in order to determine the load required to re-open the crack, the so-called decompression load. The beam was then loaded again until the crack was reopened and to be able to determine the decompression load more accurately, the procedure was repeated three times. An additional LVDT-gauge was mounted below the beam recording the deflection during the entire test.

Figure 2. Test setup for determining the crack re-opening load.

5. Interpretation of the decompression load

As can be seen in figure 3, a significant change of the slope in the vertical load versus relative displacement (obtained from the LVDT gauge at the bottom edge of the beam) diagram occurred after the crack re-opened. In several previous studies [5], [6], [7] and [8], the crack re-opening load, also referred to as the decompression load (indicated in figure 3 as the estimated intersection point), was determined by intersecting the two slopes in the vertical load versus relative displacement diagram. Since the stress at the bottom fiber of the beams is zero at the decompression load, the remaining tendon forces can be calculated using Navier`s formula. The calculation of the remaining tendon force for a beam with centrically placed tendon is shown in equation 1.

$$0 = \frac{P}{A_c} - \frac{M_F + M_S}{S} \qquad (1)$$

Where:

P = remaining tendon force, N

A_c = cross-section area of beam, m^2

M_F = applied moment from the testing machine, Nm

M_S = moment due to selfweight of the beam, Nm

S = section modulus of the beam, m^3

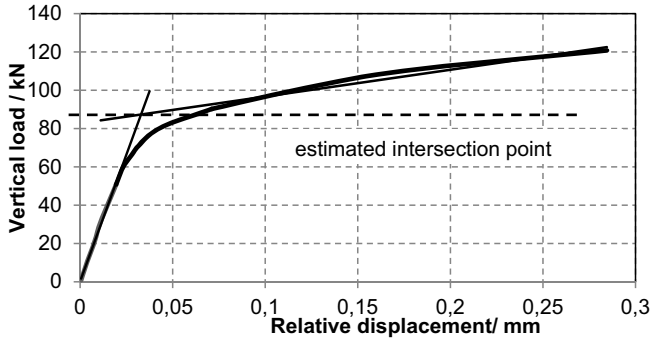

Figure 3. Vertical load versus relative displacement diagram for beam number 3.

However, the results from the load cells on the beams with unbonded tendons showed that the procedure for interpreting the decompression load as the intersection point shown in figure 3 will result in an overestimation of the remaining tendon force. In addition, a finite element modeling of the test procedure gave similar result. The test beam was described by a two-dimensional plane stress model. In order to model the crack the beam was divided into two parts connected at midspan using a contact interaction element, which simulates the presence of an existing crack by only transferring compressive forces. Loads were applied in three steps, in the first step the posttensioning force was applied as a pressure of 7.4 MPa, corresponding to a posttensioning force of 906 kN, at both ends of the beam and in the second step, the selfweight of the beam was added as an external load of 2.9 kN/m. Finally, in the third step which was divided into 100 increments, a vertical load of 140 kN was applied as a point load at the midpoint of the beam. The LVDT gauge was modeled by attaching two small rectangular elements 50 mm apart at each side of the crack and during each increment in the third step the relative displacement was taken as the distance between the center of the end faces of these two rectangular elements. The FE model is shown in figure 4.

The vertical load versus relative displacement diagram was produced by plotting the vertical load applied at midspan versus the relative displacement between the elements symbolizing the LVDT gauge for each increment of the third step in the FE-model, see figure 5. The intersection point of the two slopes was determined as follows: for the first part of the slope a regression line was adopted between the points corresponding to a load of 0 and 50 kN, respectively. The relative displacement (after application of the vertical load from the testing machine) at a load of 50 kN was 0.017 mm. For the second part of the curve a regression line was adopted between the end of the curve, corresponding to a relative displacement of 0.26 mm, and the point which corresponds to a crack displacement of 0.09 mm, i.e. for a span of the relative displacement which is ten times greater than the value at a load of 50 kN, see figure 5. The intersection point of the two regression lines corresponds to a load of 101 kN, which gives a calculated post-tensioning force of 1360 kN, which in turn is considerably greater than the 906 kN that was applied in the simulation. Moreover, the finite element analysis showed that the stress becomes zero at the bottom edge of the beam for a vertical load of approximately 71 kN. This load corresponds to the point on the vertical load versus crack-width diagram where the curve initially deviates from the linear behavior and is approximately 42 % lower than the load at the intersection point of the regression lines.

The decompression loads from the testing of the beams were evaluated based on the results from the FE-modeling. The regression lines were adopted for the two slopes in the curves using the same procedure as for the FE-model and the decompression load was estimated by dividing the load at the intersection point of the regression lines with a factor of 1.42, i.e. the difference between the true decompression load and the estimated intersection point in the FE-analysis. It should be noted that this procedure was first adopted on the beams with unbonded tendons, where the tendon forces were known from the reading of the load cells, in order to verify the accuracy of the method. Furthermore, the deflection of the beams were plotted versus the applied vertical load as an additional investigation since the deflection should increase after the crack is re-opened due to the reduced cross-section of the beam.

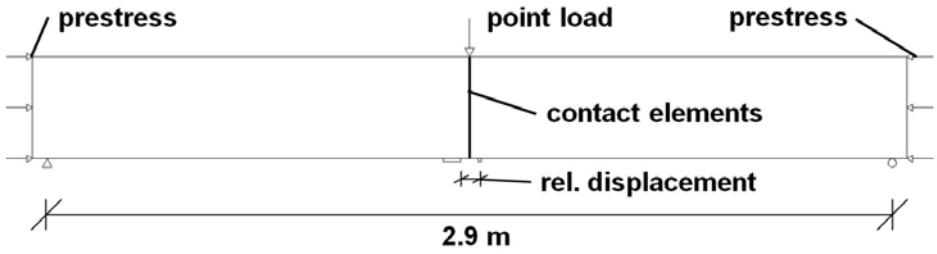

Figure 4. Details of the FE-model.

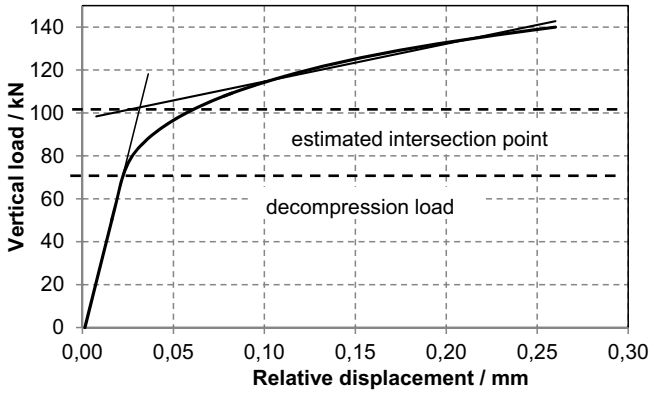

Figure 5. Vertical load versus crack width diagram from the FE analysis.

6. Results and Discussion

The results from the measurements with the load cells on the ungrouted beams are presented in table 2 and figure 6. The results from the crack re-opening tests are shown in table 3 where the decompression load is presented as the mean value along with the range of the three load cycles for each beam, the remaining tendon forces are calculated from the decompression load using equation 1. As can be seen from the results in table 3 the calculated prestress losses for the beams with unbonded tendons are in relatively good agreement with those obtained from the load cells, which shows that the procedure used for estimating the decompression load should give reasonable results for the prestress losses in the beams with bonded tendons. It should be noted that the variation in the initial tendon forces between the beams, i.e. the force directly after post-tensioning and anchorage, is due to different slip in the wedges in the anchor head when the force was transferred from the hydraulic jack. Note that the initial prestress after anchorage was recorded by the load cells for all beams.

Table 2. The results from measurements with the load cells.

Beam #	Temperature increased to 42°C	Initial tendon force / kN	Final tendon force / kN	Prestress loss / %
3	2 months	915	777	15,0
6	5 months	957	811	15,3
8	Indoor climate	980	868	11,4

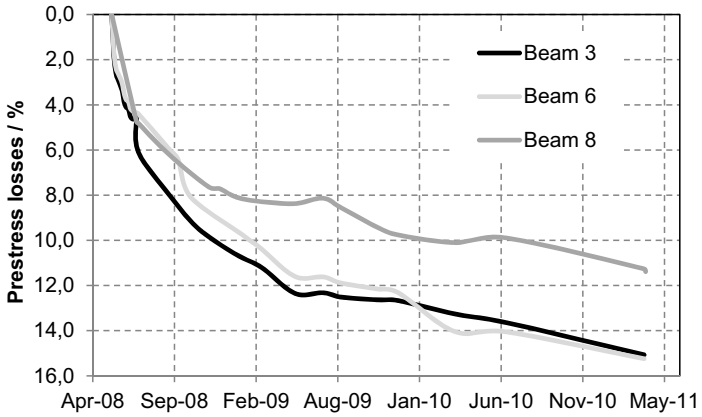

Figure 6. Results from the measurements of the tendon forces with the load cells. Beams 3 and 6 were subjected to the elevated temperature 2 and 5 months after the post-tensioning, respectively and beam 8 was subjected to normal indoor climate. Note that the vertical lines mark the end of the month displayed below the line.

Table 3. The results from the crack re-opening tests. Note that for the beams 1 to 3 the temperature was increased two months after the post-tensioning, for beams 4 to 6 five months after the post-tensioning and that beams 7 to 8 were subjected to normal indoor climate.

Beam #	**Initial tendon force / kN**	**Decompression load / kN**		**Remaining tendon force / kN**	**Prestress Losses / %**	**Measured loss / %**
		Mean	**Range**			
1	943	64	63-65	821	13.0	-
2	943	63	62-65	803	14.9	-
3	915	60	60-61	776	15.2	15.0
4	958	69	68-70	809	15.6	-
5	950	73	72-73	808	14.9	-
6	957	63	59-68	804	16.0	15.3
7	940	64	63-65	824	12.3	-
8	980	68	67-68	872	11.0	11.4

The results show that the prestress losses in the beams stored in the climate chamber were approximately 25 % greater than those for the reference beams, which could be expected considering the temperature effect on both creep and relaxation. The increase of the temperature also affects the shrinkage of the concrete since elevated temperature increases the drying of the concrete due to the reduced ambient relative humidity. In addition, the drying rate of the concrete is also increased due to the elevated temperature, which also will influence the drying-creep of the concrete. The initial effect of the elevation of the temperature can clearly be seen in figure 6 for beams 3 and 6, which were placed in the climate chamber in July and October of 2008, respectively. This increase in the rate of the prestress losses at the elevation of the temperature is similar to that found for some of the Swedish nuclear reactor containments [4]. In addition, the results in table 3 showed no significant difference in the prestress losses for the beams with unbonded tendons compared to those with bonded tendons.

The losses were somewhat greater in beam number 6 than beam number 3, which is opposite to what should have been expected since beam number 3 was subjected to the elevated temperature three months earlier. This is probably due to the higher initial tendon force in beam number 6 and that the effect of the three months longer period of elevated temperature for beam 6 is quite small considering that the duration of the study was almost three years. In addition, beam number 6 also experienced losses during these three months in the normal indoor climate.

Compared to prestress losses measured in other structures, for example nuclear reactor containments [4] and old bridge girders [6], [7], the losses in the beams are relatively high considering the short time during which they have developed. Apart from the influence of the elevated temperature, which the nuclear reactor containments also are subjected to, this can probably be due to the size of the beams, i.e. the low volume to surface ratio, which causes the drying creep and shrinkage to develop much faster than for larger structures.

Unfortunately, no method for directly determining the remaining tendon forces in prestressed concrete beams with bonded tendons exists. The crack re-opening method is the most frequently used for this purpose in the literature and is also a simple method based on beam theory. However, as the results from this study show, the drawback with this method is the difficulty associated with determining the load at which the existing crack re-opens accurately,

i.e. when the stress in the bottom fiber of the beam equals zero. To the knowledge of the author, this is the only study where the tendon forces have been measured directly during the testing procedure and where the testing method has been evaluated using a FE-analysis. After the correction of the decompression loads the prestress losses determined from the testing were in relatively good agreement with the results from the load cells. Considering that the decompression loads in table 3 are 42 % lower than those obtained when interpreted as the estimated intersection point of the regression lines, this shows that the normal procedure for estimating the decompression load as, for example, in [5], [6], [7] and [8], tends to overestimate the effective tendon forces. The results show that to accurately determine the decompression load using the crack re-opening method, it should be interpreted as the point where the slope in the vertical load versus crack width diagram deviates from its initial linear behavior and that this point is very difficult to determine accurately without a finite element analysis of the procedure. Similar results were found when estimating the decompression load from the vertical load versus deflection diagram as the point where the slope of the curve decreases (the deviation point in figure 7), see figure 7 where the applied vertical load is plotted against the deflection of the beam is shown for the FE-analysis, as can be seen the decompression load is impossible to determine visually from the test results.

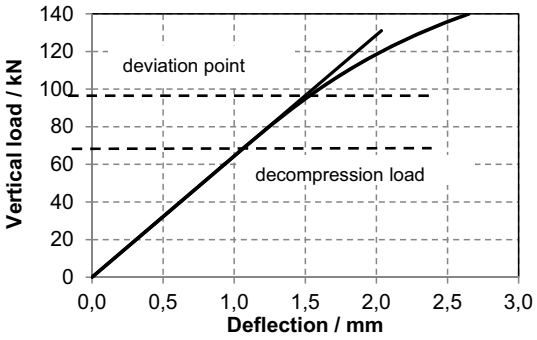

Figure 7. Vertical load versus deflection diagram from the FE-analysis.

7. Conclusions

The following can be concluded from this study.

- Elevating the ambient temperature from 20°C to approximately 40°C, increased the prestress losses in the test beams by approximately 25 % compared to the losses in beams that was stored in 20°C.
- The rate of the prestress losses was increased for a longer period of time for the beams subjected to the elevated temperature, which is in agreement with results from measurements in the Swedish nuclear reactor containments [4].
- Currently, no method exists for directly determining the remaining tendon force in an prestressed concrete beam with bonded tendons. In this study, the remaining tendon forces were evaluated using the crack re-opening method and the results show that the tendon forces will be overestimated when using the normal procedure described in the literature. To accurately determine the decompression load using the crack re-opening method, the decompression load should be interpreted as the point where the slope in the vertical load versus crack width diagram deviates from its initial linear behavior. This point is very difficult to determine visually from the test data and the interpretation of the decompression load can be improved significantly by simple finite element modeling of the testing procedure.
- The results showed no significant difference between the prestress losses in beams with bonded and unbonded tendons, respectively.

8. Acknowledgement

The author gratefully acknowledges the help and assistance from the Swedish construction company Skanska with the post-tensioning of the beams. The work presented in this study was funded by ELFORSK, the Swedish Electrical Utilities R&D Company, with contributions from Vattenfall, EON, Fortum, Skellefteå Kraft and Karlstad Energi the power producing companies owning and operating the Swedish nuclear power plants, the Swedish Radiation Safety Authority and TVO, Teollisuuden Voima Oyj in Finland.

9. References

[1] Leonhardt, F. Spannbeton für die praxis. Berlin: Wilhelm Ernst & Son; 1961.

[2] Johansson, P. & Nilsson, L-O. Climatic conditions at the surfaces of concrete containments – examples for two BWR and PWR reactors. The 19th International Conference on Structural Mechanics in Reactor Technology (SMiRT 19), August 12-17 2007, Toronto, Canada

[3] Gross H. High temperature creep of concrete, *Nuclear Engineering and Design 1975;* 32(1): 129-174.

[4] Anderson, P. Thirty years of measured prestress at Swedish nuclear reactor containments. *Nuclear Engineering and Design* 2005; 235(21):2323-2336.

[5] Lundqvist, P., Rihiimäki, J. Testing of five 30-year-old prestressed concrete beams. *PCI Journal* 2010: 55(4):50-58.

[6] Saiidi, S., Labia Y., Douglas, B. Full-Scale Testing and Analysis of 20-Year-Old Pretensioned Concrete Box Girders. *ACI Structural Journal* 1997: 94(5): 471-482.

[7] Halsey, J.T., Miller, R. Destructive testing of two forty-year-old prestressed concrete bridge beams. *PCI Journal* 1996: 41(5):85-93.

[8] Eder, R.W., Miller, R. A., Baseheart, T. M., Swanson, J. A. Testing of two 50-year old precast post-tensioned concrete bridge girders. *PCI Journal* 2005: 50(3): 90-95.